NASA Technical Memorandum 104606, Vol.

Technical Report Series on Global Modeling and Data Assimilation

Max J. Suarez, Editor
Goddard Space Flight Center
Greenbelt, Maryland

Volume

The GMAO CGCMv1: Climatology and Interannual Variability

Sonya K. Miller
Science Applications International Corporation,

Michele M. Rienecker
NASA - Goddard Space Flight Center,

Max J. Suarez
NASA - Goddard Space Flight Center,

Philip J. Pegion
Science Applications International Corporation,

Julio Bacmeister
Goddard Earth Sciences and Technology Center, University of Maryland - Baltimore County,

Global Modeling and Assimilation Office,
Goddard Space Flight Center,
Greenbelt, Maryland

Goddard Space Flight Center
Greenbelt, Maryland
2005

Abstract

This technical report details the annual climatology, seasonal means, and interannual variability of version 1 of the coupled general circulation model developed at the GMAO, CGCMv1. The results of a 156-year free coupled experiment show that the model has skill in reproducing the long term climatology and major modes of variability.

Contents

List of Figures **vii**

1 Introduction **1**

2 Description of the model **1**

3 Description of the integration **4**

4 Validation data sets **5**

5 Organization **5**

6 Annual means and biases **6**

7 Seasonal means **6**

8 Interannual variability **7**

9 Model Comparison **7**

10 Summary **8**

11 References **9**

List of Figures

ANNUAL MEAN CLIMATOLOGY **13**

1 Sea surface temperature (°C).Top: observations from Reynolds and Smith (1994); Middle: model; Bottom: annual mean SST bias. Contour interval is 1°C. 14

2 Sea surface salinity.Top: observations from the 2001 World Ocean Atlas (Conkright et al.) ; Middle: model; Bottom: annual mean SSS bias. Contour interval is 0.4. 15

3a Mixed layer depth from model climatology (m).Contour interval is 10 m. . . 16

3b Mixed layer depth from GMAO ocean analysis (m).Contour interval is 10 m. 17

4 Annual mean sea surface temperature and wind stress in the Equatorial Pacific.Top: SST, Bottom: τ_x. Solid black line: observations; dotted line: results from an AMIP-style run using the NSIPP-1 AGCM; dashed line: model; dashed blue line: model with 1° atmospheric resolution. 18

5a Annual mean profile at the Equator in the Pacific Ocean.Top: temperature (°C); Middle: salinity; Bottom: zonal current (m s^{-1}). Model cross-section from 130°E to 90°W. Contour intervals are 1°C for temperature, 0.1 for salinity, and 0.1 m s^{-1} for zonal current. 19

5b Annual mean profile at the Equator in the Pacific Ocean.Top: Temperature (°C), Middle: Salinity, Bottom: Zonal Current (m s^{-1}). Temperature and salinity data from World Ocean Atlas. Zonal current data from GMAO ocean analysis. Cross-section extends from 130°E to 90°W. Contour intervals are 1°C for temperature, 0.1 for salinity, and 0.1 m s^{-1} for zonal current. 20

6a Annual mean profile at 165°E in the tropics.Top: Temperature (°C), Middle: Salinity, Bottom: Zonal Current (m s^{-1}). Model cross-section from 20°S to 20°N. Contour intervals are 1°C for temperature, 0.1 for salinity, and 0.1 m s^{-1} for zonal current. 21

6b Annual mean profile at 165°E in the tropics.Top: Temperature (°C), Middle: Salinity, Bottom: Zonal Current (m s^{-1}). Temperature and salinity data from World Ocean Atlas. Zonal current data from GMAO Analysis. Cross-section extends from 20°S to 20°N. Contour intervals are 1°C for temperature, 0.1 for salinity, and 0.1 m s^{-1} for zonal current. 22

7a Annual mean profile at 155°W in the tropics.Top: Temperature (°C), Middle: Salinity, Bottom: Zonal Current (m s^{-1}). Model cross-section from 20°S to 20°N. Contour intervals are 1°C for temperature, 0.1 for salinity, and 0.1 m s^{-1} for zonal current. 23

7b Annual mean profile at 155°W in the tropics.Top: Temperature (°C), Middle: Salinity, Bottom: Zonal Current (m s^{-1}). Temperature and salinity data from World Ocean Atlas. Zonal current data from GMAO Analysis. Cross-section extends from 20°S to 20°N. Contour intervals are 1°C for temperature, 0.1 for salinity, and 0.1 m s^{-1} for zonal current. 24

8a Annual mean profile at 140°W in the tropics.Top: Temperature (°C), Middle: Salinity, Bottom: Zonal Current (m s^{-1}). Model cross-section from 20°S to 20°N. Contour intervals are 1°C for temperature, 0.1 for salinity, and 0.1 m s^{-1} for zonal current. 25

8b Annual mean profile at 140°W in the tropics.Top: Temperature (°C), Middle: Salinity, Bottom: Zonal Current (m s^{-1}). Temperature and salinity data from World Ocean Atlas. Zonal current data from GMAO Analysis. Cross-section extends from 20°S to 20°N. Contour intervals are 1°C for temperature, 0.1 for salinity, and 0.1 m s^{-1} for zonal current. 26

9a Annual mean profile at 110°W in the tropics.Top: Temperature (°C), Middle: Salinity, Bottom: Zonal Current (m s^{-1}). Model cross-section from 20°S to 20°N. Contour intervals are 1°C for temperature, 0.1 for salinity, and 0.1 m s^{-1} for zonal current. 27

9b Annual mean profile at 110°W in the tropics.Top: Temperature (°C), Middle: Salinity, Bottom: Zonal Current (m s^{-1}). Temperature and salinity data from World Ocean Atlas. Zonal current data from GMAO Analysis. Cross-section extends from 20°S to 20°N. Contour intervals are 1°C for temperature, 0.1 for salinity, and 0.1 m s^{-1} for zonal current. 28

10a Ice Fraction in the Antarctic Ocean.Top: July, Bottom: January. Contour interval is 5% 29

10b Ice Fraction in the Antarctic Ocean.Observations from ISCCP ice cover climatology. Top: July, Bottom: January. 30

11a Ice Fraction in the Arctic Ocean.Top: July, Bottom: January. Contour interval is 5% 31

11b Ice Fraction in the Arctic Ocean.Observations from ISCCP ice cover climatology. Top: July, Bottom: January. Contour interval is 5% 32

SEASONAL MEAN CLIMATOLOGY **33**

12a Zonal wind at 200 mb (m s^{-1}). Upper panels: model; Lower panels: observations; Left panels: December-January-February mean; Right panels: June-July-August mean. Contour interval is 8 m s^{-1}. 34

12b Zonal wind at 200 mb (m s^{-1}). Upper panels: model; Lower panels: observations; Left panels: March-April-May mean; Right panels: September-October-November mean. Contour interval is 8 m s^{-1}. 35

13a Eddy geopotential height at 200 mb (m). Upper panels: model; Lower panels: observations; Left panels: December-January-February mean; Right panels: June-July-August mean. Contour interval is 40 m. 36

13b Eddy geopotential height at 200 mb (m). Upper panels: model; Lower panels: observations; Left panels: March-April-May mean; Right panels: September-October-November mean. Contour interval is 40 m. 37

14a Sea level pressure (mb). Upper panels: model; Lower panels: observations; Left panels: December-January-February mean; Right panels: June-July-August mean. Contour interval is 5 mb. 38

14b Sea level pressure (mb). Upper panels: model; Lower panels: observations; Left panels: March-April-May mean; Right panels: September-October-November mean. Contour interval is 5 mb. 39

15a Total precipitation (mm day^{-1}).Upper panels: model; Lower panels: observations; Left panels: December-January-February mean; Right panels: June-July-August mean. Contour interval is 1 mm day^{-1}. 40

15b Total precipitation (mm day^{-1}).Upper panels: model; Lower panels: observations; Left panels: March-April-May mean; Right panels: September-October-November mean. Contour interval is 1 mm day^{-1}. 41

16a Net surface water flux, expressed as evaporation minus precipitation (mm day^{-1}).Upper panels: model; Lower panels: observations; Left panels: December-January-February mean; Right panels: June-July-August mean. Contour interval is 1 mm day^{-1}. 42

16b Net surface water flux, expressed as evaporation minus precipitation (mm day^{-1}).Upper panels: model; Lower panels: observations; Left panels: March-April-May mean; Right panels: September-October-November mean. Contour interval is 1 mm day^{-1}. 43

17a Net surface heat flux (W m^{-2}). Positive values indicate a net upward flux. Upper panels: model; Lower panels: observations; Left panels: December-January-February mean; Right panels: June-July-August mean. Contour interval is 30 W m^{-2}. 44

17b Net surface heat flux (W m^{-2}). Positive values indicate a net upward flux. Upper panels: model; Lower panels: observations; Left panels: March-April-May mean; Right panels: September-October-November mean. Contour interval is 30 W m^{-2}. 45

18a Outgoing longwave radiation (W m^{-2}).Upper panels: model; Lower panels: observations; Left panels: December-January-February mean; Right panels: June-July-August mean. Contour interval is 20 W m^{-2}. 46

18b Outgoing longwave radiation (W m^{-2}).Upper panels: model; Lower panels: observations; Left panels: March-April-May mean; Right panels: September-October-November mean. Contour interval is 20 W m^{-2}. 47

19a Net cloud radiative forcing (W m^{-2}).Upper panels: model; Lower panels: observations; Left panels: December-January-February mean; Right panels: June-July-August mean. Contour interval is 20 W m^{-2}. 48

19b Net cloud radiative forcing (W m^{-2}).Upper panels: model; Lower panels: observations; Left panels: March-April-May mean; Right panels: September-October-November mean. Contour interval is 20 W m^{-2}. 49

20a Net shortwave radiation at surface (W m^{-2}). Positive values indicate upward flux. Upper panels: model; Lower panels: observations; Left panels: December-January-February mean; Right panels: June-July-August mean. Contour interval is 20 W m^{-2}. 50

20b Net shortwave radiation at surface (W m^{-2}). Positive values indicate upward flux. Upper panels: model; Lower panels: observations; Left panels: March-April-May mean; Right panels: September-October-November mean. Contour interval is 20 W m^{-2}. 51

21a Zonal wind stress (N m^{-2}). Upper panels: model; Lower panels: observations; Left panels: December-January-February mean; Right panels: June-July-August mean. Contour interval is 0.03 N m^{-2}. 52

21b Zonal wind stress (N m^{-2}). Upper panels: model; Lower panels: observations; Left panels: March-April-May mean; Right panels: September-October-November mean. Contour interval is 0.03 N m^{-2}. 53

22a Meridional wind stress (N m^{-2}). Upper panels: model; Lower panels: observations; Left panels: December-January-February mean; Right panels: June-July-August mean. Contour interval is 0.02 N m^{-2}. 54

22b Meridional wind stress (N m^{-2}). Upper panels: model; Lower panels: observations; Left panels: March-April-May mean; Right panels: September-October-November mean. Contour interval is 0.02 N m^{-2}. 55

23a Sea surface temperature (°C). Upper panels: model; Lower panels: observations; Left panels: December-January-February mean; Right panels: June-July-August mean. Contour interval is 2°C. 56

23b Sea surface temperature (°C). Upper panels: model; Lower panels: observations; Left panels: March-April-May mean; Right panels: September-October-November mean. Contour interval is 2°C. 57

24a Sea surface salinity.Upper panels: model; Lower panels: observations; Left panels: December-January-February mean; Right panels: June-July-August mean. Contour interval is 0.4. 58

24b Sea surface salinity.Upper panels: model; Lower panels: observations; Left panels: March-April-May mean; Right panels: September-October-November mean. Contour interval is 0.4. 59

25a Sea surface height (m).Upper panels: model; Lower panels: observations; Left panels: December-January-February mean; Right panels: June-July-August mean. Contour interval is 12.5 m. 60

25b Sea surface height (m).Upper panels: model; Lower panels: observations; Left panels: March-April-May mean; Right panels: September-October-November mean. Contour interval is 12.5 m. 61

26a Zonal surface current (m s^{-1}). Upper panels: model; Lower panels: observations; Left panels: December-January-February mean; Right panels: June-July-August mean. Contour interval is 0.1 m s^{-1}. 62

26b Zonal surface current (m s^{-1}). Upper panels: model; Lower panels: observations; Left panels: March-April-May mean; Right panels: September-October-November mean. Contour interval is 0.1 m s^{-1}. 63

27a Meridional surface current (m s^{-1}). Upper panels: model; Lower panels: observations; Left panels: December-January-February mean; Right panels: June-July-August mean. Contour interval is 0.02 m s^{-1}. 64

27b Meridional surface current (m s^{-1}). Upper panels: model; Lower panels: observations; Left panels: March-April-May mean; Right panels: September-October-November mean. Contour interval is 0.02 m s^{-1}. 65

28a Salinity at 300m depth. Upper panels: model; Lower panels: observations; Left panels: December-January-February mean; Right panels: June-July-August mean. Contour interval is 0.2 66

28b Salinity at 300m depth. Upper panels: model; Lower panels: observations; Left panels: March-April-May mean; Right panels: September-October-November mean. Contour interval is 0.2 67

29a Temperature at 300m depth (°C). Upper panels: model; Lower panels: observations; Left panels: December-January-February mean; Right panels: June-July-August mean. Contour interval is 1°C. 68

29b Temperature at 300m depth (°C). Upper panels: model; Lower panels: observations; Left panels: March-April-May mean; Right panels: September-October-November mean. Contour interval is 1°C. 69

30 Seasonal anomaly in the Equatorial Pacific (averaged 2°S to 2°N).Upper panels: sea surface temperature; Lower panels: zonal wind stress; Left panels: Observations; Middle left panels: results from NSIPP-1 AMIP experiment; Middle right: model; Right panels: model with 1° atmosphere. Contour interval for SST is 0.5 °C. Contour interval for zonal wind stress is 0.005 N m^{-2}. 70

INTERANNUAL VARIABILITY **71**

31 Standard deviation of sea surface temperature (°C).Top: Model, Bottom: Observations from Hadley Centre. 72

32 Interannual anomaly of sea surface temperature (SST) across the Equatorial Pacific.Hovmuller diagram of SST anomaly for 100 years of the experiment. Years progress from bottom to top and left to right. 73

33 Interannual anomaly of zonal wind stress across the Equatorial Pacific.Hovmuller diagram of zonal wind stress anomaly for 100 years of the model experiment. Years progress from bottom to top and left to right. 74

34 Interannual anomaly of depth of the 20°C isotherm across the Equatorial Pacific.Hovmuller diagram of the interannual anomaly of an estimate of thermocline depth for 100 years of the model experiment. Years progress from bottom to top and left to right. 75

35 NINO3 Sea Surface Temperature Index.Black line: model; Orange line: SST data from the Hadley Centre. The NINO3 index box extends from 5°S to 5°N and from 90°W to 150°W. 76

36a Pointwise correlation of NINO3 index and sea surface temperature. 77

36b Pointwise correlation of NINO3 index and sea surface temperature.. SST data and NINO3 index from Hadley Centre. 78

37a Pointwise correlation of NINO3 index and 200mb geopotential height. . . . 79

37b Pointwise correlation of NINO3 index and 200mb geopotential height.Sea surface temperature data from Hadley Centre. Data for 200mb geopotential height from NCEP reanalysis. 80

38 Empirical orthogonal function (EOF) of model sea surface temperature.Only the first four rotated EOFs are shown. The associated principal component timeseries is plotted below each EOF. 81

39 North Pacific Index of normalized sea level pressure anomaly.Black line: Raw North Pacific Index (NPI) from model; Red: NPI filtered by a weighted seven point moving average; Blue: Filtered NPI from observations from 1901-2003, adapted from Trenberth and Hurrell (1994). NPI normalized by standard deviations of 1.9 mb (model) and 2.2 mb (data). NPI consists of a weighted average of northern winter sea level pressure anomaly in the area of 30°N to 65°N and 160°E to 140°W. 82

40 Indian Ocean dipole of sea surface temperature anomaly.Black line: model; Orange line: SST data from the Hadley Centre. The Indian Ocean dipole is defined as the difference between the SSTA over a western region and eastern region. The western region extends from the Equator to 10°N and from 90°E to 110°E. The eastern region extends from 10°S to 10°N and from 50°E to 70°E. 83

41 Atlantic Ocean dipole of sea surface temperature anomaly.Black line: model; Orange line: SST data from the Hadley Centre. The Atlantic Ocean dipole is defined as the difference between the SSTA over a northern region and southern region. The northern region extends from the 50°N to 20°N and from 60°W to 30°W. The southern region extends from 20°S to the Equator and from 30°W to 10°E. 84

42a North Atlantic Oscillation.First EOF of the annual mean SLP anomaly over the Atlantic sector (20°N to 80°N and 90°W to 40°E). This EOF represents 40.5% of the total variance in SLP anomaly in this sector. The associated principal component time series is plotted below the EOF pattern. 85

42b North Atlantic Oscillation from observations.First EOF of the annual mean SLP anomaly over the Atlantic sector (20°N to 80°N and 90°W to 40°E). This EOF represents 33.87% of the total variance in SLP anomaly in this sector. The associated principal component time series is shaded below the EOF pattern; the thick black line represents the NAO index as computed from the station data in Iceland and the Azores. These two stations are represented by black dots on the upper plot. Figure from Hurrell (1995). . 86

MODEL COMPARISON **87**

43 Sea surface temperature (°C).Top: difference in bias between the regular CGCMv1 and the 1° CGCM (0.5°C contour interval); Middle: annual mean SST bias for the 1 ° CGCM (1.0°C contour interval); Bottom: annual mean SST bias for CGCMv1 (1.0°C contour interval). 88

44 Standard deviation of sea surface temperature (°C).Top: 1° CGCM, Bottom: observations from Hadley Centre. 89

45 Interannual anomaly of Equatorial Pacific sea surface temperature (SST).Hovmuller diagram of SST anomaly for 87 years of the 1° CGCM. Years progress from bottom to top and left to right. 90

46 NINO3 Sea Surface Temperature Index.Black line: 1 ° CGCM; Orange line: SST data from the Hadley Centre. The NINO3 index box extends from 5°S to 5°N and from 90°W to 150°W. 91

47 Pointwise correlation of NINO3 index and sea surface temperature. 92

48 Pointwise correlation of NINO3 index and 200mb geopotential height. . . . 93

49 Empirical orthogonal function (EOF) of model sea surface temperature.Only the first four rotated EOFs are shown. The associated principal component timeseries is plotted below each EOF. 94

50 Ice Fraction in the Antarctic Ocean from an experiment with more realistic abyssal temperature and salinity values in the Antarctic.Top: July, Bottom: January. 95

1 Introduction

The Global Modeling and Assimilation Office (GMAO) is tasked to develop state-of-the-art global models of the Earth system together with data assimilation systems to enhance the understanding of climate and climate variability. As part of this goal, a coupled general circulation model is used to predict El Nino/Southern Oscillation (ENSO) and the resulting teleconnections. When used with the assimilation of data, this model can demonstrate the utility of remotely-sensed observations through experimental prediction.

This report presents the climate characteristics and interannual variability of version 1 of the GMAO Coupled General Circulation Model (CGCMv1). The analysis and figures contained in this report are long term means and estimates of variability from a single 157-year run with CGCMv1. Some results from other experiments with this model are shown to illustrate improvements possible with changes to resolution and other parameters. The results from hindcast and forecast studies with this model will be presented in a subsequent report.

Section 2 describes the GMAO CGCMv1. Sections 3 and 4 describe the model integration and validation data, respectively. Section 5 gives an overview of the organization of the atlas. The results are discussed in Sections 6–9.

2 Description of the model

The GMAO CGCMv1 employs the Goddard Earth Modeling System (GEMS) to couple the atmospheric, ocean and land surface models. The model components used for CGCMv1 are the NSIPP-1 Atmospheric General Circulation Model (AGCM), the Poseidon v4 Ocean General Circulation Model (OGCM), and the Mosaic Land Surface Model (LSM). A thermodynamic sea-ice model is included. The component models were developed and tested separately, and only minor tuning was required for coupling.

The AGCM

The NSIPP-1 AGCM has a finite-difference, primitive equations dynamical core (Suarez and Takacs, 1995) that allows arbitrary horizontal and vertical resolution. It uses a finite-difference C-grid, on latitude-longitude coordinates, in the horizontal and a generalized sigma coordinate in the vertical. The vertical coordinate used in CGCMv1 is a standard σ-coordinate (σ = pressure/surface pressure) and vertical differencing follows Arakawa and Suarez (1983). The momentum equations use a fourth-order version of the enstrophy conserving scheme of Sadourny (1975). The horizontal advection schemes for potential temperature, moisture, and other tracers are fourth-order (Takacs and Suarez, 1996). Vertical tracer advection is accomplished using space-centered second-order differences. An eighth-order Shapiro filter is used to dissipate small horizontal scales in all prognostic fields except surface pressure. A polar Fourier filter is applied poleward of 45° latitude to the time tendencies of all prognostic variables.

The parameterizations of solar and infrared radiative heating rates are those of Chou and Suarez (1994 and 1999). From the moist physics parameterization, the GCM estimates a

cloud fraction at each level. For the solar radiation calculation, the GCM levels are then grouped into three regions which are identified with high ($\sigma < 0.56$), middle ($0.56 < \sigma < 0.77$), and low ($\sigma > 0.77$) clouds. Within each of these regions, clouds are assumed to be maximally overlapped and the cloud fractions are scaled using a scheme that depends on solar zenith angle and optical thickness. This leaves us with a single cloud fraction in each of the three regions. The overlapping between these region is treated "exactly" by assuming random overlapping and combining the results of full transfer calculations for the eight possible cases.

The boundary layer scheme in the model is a simple K-scheme that calculates turbulent diffusivities for heat and momentum based on Monin-Obukhov similarity theory (Louis et al. , 1982). The implementation for the coupled model uses a mixing length of 20m, a value that results in better simulations of oceanic wind stresses along the equator without seriously degrading other aspects of the simulation. Gravity-wave drag is parameterized according to Zhou et al. (1996). As discussed in Takacs and Suarez (1996), the inclusion of gravity wave drag in this model produces a remarkable improvement in the simulation of the zonal flow even at the fairly low resolutions used in climate modeling.

Penetrative convection originating in the boundary layer is parameterized using the Relaxed Arakawa-Schubert (RAS) scheme (Moorthi and Suarez, 1992). RAS uses a sequence of simple linearly entraining plumes (cloud types) that originate and detrain at specified model levels. In the coupled model, all convection originates from the relatively thin, lowest layer ($\Delta\sigma = 0.015$), and can detrain into any layer above. Thus, we are allowing RAS to act as a parameterization of both deep and shallow convection. Re-evaporation of convective rainfall is included and is based on the formulation of Sud and Molod (1988).

Large-scale cloudiness is determined using a simple relative humidity-based diagnostic scheme such as that of Slingo (1987). However, even with a high-threshold relative humidity, the scheme produces excessive cloudiness over subtropical oceans. Thus, a second "destruction" step is invoked that uses the magnitude of subsidence drying produced by RAS to destroy a fraction of the large-scale clouds produced by the relative humidity diagnostic.

The AGCM performance is documented in the Technical Memoranda of Bacmeister et al. (2000) and Pegion et al. (2000). Further details and performance of the model used in the CGCMv1 are given in Bacmeister and Suarez (2002).

The LSM

The AGCM is coupled to the Mosaic Land Surface Model (LSM) of Koster and Suarez (1996), a well-established soil-vegetation-atmosphere transfer (SVAT) model originally derived from SiB. The Mosaic LSM computes area-averaged energy and water fluxes from the land surface in response to meteorological forcing. The model allows explicit vegetation control over the computed surface energy and water balances, with environmental stresses (high temperatures, dry soil, etc.) acting to increase canopy resistance and thus decrease transpiration. The scheme includes a canopy interception reservoir and three soil reservoirs: a thin layer near the surface, a middle layer that encompasses the remainder of the root zone, and a lower "recharge" layer for long term storage. Bare soil evaporation, transpiration, and interception loss occur in parallel, and runoff occurs both as overland flow during precipitation events and as ground water drainage out of the recharge layer. A complete

snow budget is included. The model was originally derived from the SiB model of Sellers et al. (1996) and still maintains certain SiB formulations, particularly those for canopy resistance.

The model's main innovation is its attempt to account for subgrid variability in surface characteristics through the "mosaic" approach. A grid square area containing several different vegetation regimes is divided into relatively homogeneous sub-regions ("tiles" of the mosaic), each containing a single vegetation or bare soil type. Observed vegetation distributions are used to determine the partitioning. A separate energy balance is calculated for each tile, and each tile maintains its own prognostic soil moisture contents and temperatures.

A general description of the model is given in Koster and Suarez (1992), and a detailed description of the model's heat and energy balances is given in Koster and Suarez (1996). The model performance is documented in the PILPS analyses (e.g., Wood et al. , 1998).

The OGCM

The ocean GCM, Poseidon V4 (Schopf and Loughe, 1995; updated to include prognostic salinity as in Yang et al. , 1999), is designed with generalized horizontal and vertical coordinates including an embedded turbulent surface mixed layer parameterized according to Kraus-Turner and implemented following Sterl and Kattenberg (1994). The interior layers are treated in a quasi-isopycnal fashion in which layers do not vanish at outcrops, but retain a thin minimum thickness at all grid points. Exchanges between layers are such as to tend to maintain the target densities on a specified timescale. Horizontal mixing within the model is implemented with high order Shapiro filtering. Vertical mixing and diffusion are parameterized using a Richardson number dependent scheme of Pacanowski and Philander, enhanced for layers within the mixed layer and within the water column where the inferred density profile is gravitationally unstable. Shortwave radiation penetrates below the ocean surface, with penetration depth provided from a SeaWiFS climatology of kpar. The is a reduced gravity model with the abyss at rest. The abyss is an infinite reservoir of heat and salt, with spatially varying potential temperature and salinity derived from the World Ocean Atlas (Levitus et al. , 1994). A thermodynamic sea-ice model, following Hakkinen and Mellor (1992) is included, with heat and freshwater exchange to the first layer of the ocean model. The equations are solved implicitly.

Coupling

The land/ocean mask for the coupled model is defined on the ocean's latitude-longitude grid, so each grid box is either all ocean or all land. The atmosphere to ocean couplers interpolate from the atmospheric grid to the mass point of the underlying ocean boxes using bilinear interpolation (e.g., Vintzileos and Sadourny, 1997). In the ocean to atmosphere coupling, interpolation consists of averaging together the underlying ocean grid boxes. Fluxes are exchanged on a daily basis. The coupling between the land and the atmosphere is handled in a similar fashion; fluxes are exchanged during every atmospheric time step. The CGCM runs without any flux correction.

The ocean model controls the evolution of all non-land surfaces, i.e., open ocean, shallow seas and sea ice. Inland lakes are treated by the atmosphere as land surfaces.

The ocean domain extends from Antarctica to 72°N. There is a 10°-wide buffer zone at the northern boundary in which the temperature, salinity and layer thickness are relaxed to climatological fields derived from the World Ocean Atlas (Levitus et al. , 1994). From the northern boundary to the North Pole, a slab ocean "mixed layer" model, with sea-ice enabled, is used merely for heat exchange with the atmosphere. This approach is also used for shallow seas and the continental shelves.

3 Description of the integration

For this experiment, the atmospheric model component is integrated at a resolution of 2° latitude by 2.5° longitude, using 34 sigma layers as specified in Table 1.

Table 1: Sigma surfaces separating the 34 layers of the model.

L	σ	L	σ	L	σ	L	σ	L	σ
1	0.000	2	0.005	3	0.010	4	0.015	5	0.025
6	0.050	7	0.075	8	0.100	9	0.125	10	0.150
11	0.175	12	0.200	13	0.225	14	0.275	15	0.325
16	0.375	17	0.425	18	0.500	19	0.625	20	0.700
21	0.750	22	0.775	23	0.800	24	0.825	25	0.850
26	0.865	27	0.880	28	0.895	29	0.910	30	0.925
31	0.940	32	0.955	33	0.970	34	0.985	35	1.000

The ocean model component has a resolution of $\frac{1}{3}$° latitude by $\frac{5}{8}$° longitude. The ocean has 27 quasi-isopycnal layers with a specified abyssal layer below the lowest active layer. The temperature and salinity of the abyssal layer are determined based on values in the World Ocean Atlas (Levitus et al. , 1994) with buoyancy values slightly greater than 0. Regions in the high latitudes are extremely sensitive to the values set in the the abyssal layer.

The land surface is fully interactive and consists of 15,832 tiles distributed over the atmospheric grid boxes that contain a non-zero land fraction. The tiles represent six different vegetation types, as well as land ice, bare soil, desert, and lakes. Lakes are treated as a freely evaporating surface (i.e., no surface, only aerodynamic, resistance) with a heat capacity equivalent to 2 meters of water.

The atmosphere and land surface are spun up separately from the ocean. The model components drift to their own climatology when forced with various observations. The surface salinity is constrained by a 2-year relaxation to observed surface salinity from the World Ocean Atlas (Levitus et al. , 1994).

The main experiment discussed here is a single 157-year free coupled system run. In general, the first 20 years were discarded as spin-up prior to any analysis. Two other runs are also presented. One run has a horizontal resolution of 1° latitude by 1.25° longitude in the atmospheric component. Another uses more realistic values for abyssal layer temperature and salinity in the Antarctic Ocean south of 60°S.

4 Validation data sets

Several data sets are used for comparison to model fields. In general, we use monthly averages and monthly climatologies. For sea surface temperature (SST) climatology, we use the data from Reynolds and Smith (1994). For time series comparisons, we use reconstructed SSTs from the Hadley Centre Global dataset (Rayner et al. , 2003). We use 1961-1990 to construct the climatology for these data. Sea surface salinity data are taken from the World Ocean Atlas (Levitus et al. , 1994, updated in Conkright et al. , 2002). The tropical Pacific drifting buoy climatology (Reverdin et al. , 1994) is used as a comparison for surface currents.

For surface heat fluxes, we use data from the Southampton Oceanography Centre (SOC) Air-Sea Flux Climatology (Josey et al. , 1998). Precipitation data is from the Global Precipitation Climatology Project (GPCP, Huffman 1997). Freshwater fluxes are calculated from this precipitation climatology combined with evaporation from the NCEP/NCAR Reanalysis (Kalnay et al. , 1994). Surface wind stress data are derived from the Special Sensor Microwave Imager (SSM/I) winds obtained from Atlas et al. (1996).

Temperature and salinity profiles from the ocean are obtained from the World Ocean Atlas (Levitus et al. , 1994, Conkright et al. , 2002). The GMAO Ocean Data Assimilation (ODAS) Analysis (Sun et al. , 2005) is used as a comparison for zonal current profiles and mixed layer depth. We use the dynamic height field from the 1994 World Ocean Atlas (Levitus et al.) as a comparison to sea surface height.

Ice fraction climatology is obtained from the International Satellite Cloud Cover Project (ISCCP, Prigent et al. , 2002).

Upper air fields are compared with the 1980-1999 climatology from NCEP/NCAR Reanalysis (Kalnay et al. , 1994). Values for the atmospheric radiation fields are compared with a five-year period (1985-1989) from the Earth Radiation Budget Experiment (ERBE, more information at http://asd-www.larc.nasa.gov/erbe/ASDerbe.html).

The North Pacific Index data is adapted from Trenberth and Hurrell (1994). Updated data can be found on at http://www.cgd.ucar.edu/ jhurrell/np.html.

Finally, some comparisons are made to a NSIPP-1 atmospheric model experiment forced by observed SSTs. This AMIP-style run and the resulting climatology are described in Bacmeister et al. (2000).

5 Organization

Section 6 discusses the annual means and bias of surface fields. Section 7 discusses seasonal means, and Section 8 presents some discussion of interannual variability. Comparisons with other models and other experiments is documented in section 9.

6 Annual means and biases

The annual mean bias in SST in the tropics is small, except for the far eastern Pacific. However, significant biases remain in the mid and high latitudes. Some of the high latitude bias may be due to sensitivity to the abyssal layer temperature and salinity definition. Other sources of the SST bias may include problems with surface stresses and surface fluxes from the atmosphere.

The SSS bias is somewhat mitigated by the weak relaxation to climatological SSS values. The inflow of fresh water from river runoff is not included in this model, which can explain regions of high salinity bias near the mouths of several major rivers.

Concentrating on the tropical Pacific Ocean, the annual mean bias in SST and zonal wind stress (τ_x) is more apparent. The central and western part of the equatorial region has slightly stronger wind stresses and slightly cooler SSTs. The simulation of τ_x improves east of 100°W, but now the SSTs are warmer than observations.

Crossections show problems with the simulation of the upper ocean as seen in the temperature, salinity, and zonal current profiles in the equatorial Pacific. The currents are too strong and too deep, and the temperature profile in the eastern Equatorial Pacific is disconnected from the surface. The salinity profile in the western Pacific shows a lack of a fresh water tongue in the warm pool.

Other crossections show more problems in the off-equatorial regions in the Pacific. The thermocline gradients are too tight compared to observations. The salinity gradients are also too tight, and the saltiest water extends too far north. The currents are too strong and closer to the surface.

The bias in the southern ocean is large in most of the fields. This bias shows up in the ice fraction around Antarctica. There is no permanent ice field, and several areas never grow ice on average. Additional experiments with this model have shown that the surface temperature, salinity, and ice fraction in this region are sensitive to the definition of the abyssal layer.

7 Seasonal means

Overall, the model reproduces the seasonality of most fields quite reasonably. The major biases are year-round occurrences, although the amplitude of the bias may change by season.

In precipitation, a double Intertropical Convergence Zone (ITCZ) tends to show up during all seasons, although it is weakest in the June-July-August (JJA) mean. The problems with the double ITCZ are more apparent in the net water flux (calculated from evaporation minus precipitation). In addition, the outgoing longwave radiation (OLR) fields show some tendency toward a double ITCZ.

The deformation of the northern subtropical gyres is present during all seasons in sea

surface height, temperature and salinity at depth, and SST. There is also some indication that problems with the net surface heat flux and net water flux in the mid-latitudes may contribute to this bias.

The surface currents are too strong during all seasons, especially during September-October-November (SON).

8 Interannual variability

The standard deviation of SSTs in the model is too strong around 100°W in the tropical Pacific Ocean, and the Hadley Centre SST variability is less narrow and more closely tied to the South American coast. Some regions in the mid-latitudes also exhibit more variability than observed.

The CGCMv1 internal variability includes ENSO warm and cold events in the tropical Pacific; however, the amplitude and periodicity of these events are problematic. The events are too weak in amplitude, with the maximum anomaly rarely above 2.5C. Only the strongest events reach the west coast of South America. Also, the return period of the ENSO events is too biennial.

The first four rotated Empirical Orthogonal Functions (REOFs) of SST show the major modes of interannual variability. The first EOF is the El Nino-Southern Oscillation (ENSO) signal in the model. The pattern is too narrow when compared to observed, and there is little correlation of the ENSO pattern to signals in other regions. The overall amplitude is somewhat weak, and the frequency of the ENSO event is too biennial.

There is some evidence of other oscillations in the coupled model. EOFs of the sea level pressure (SLP) in the North Atlantic reveal a signature similar to that observed for the North Atlantic Oscillation (NAO). In addition, calculations of the North Pacific Index compare favorably with a decadal signal in the EOFs of SST.

Observed teleconnections from these oscillations can be found in the model output. The 200mb northern winter response to ENSO is similar to the observed signal, although the teleconnection is not as strong. Unfortunately, the expected response to the NAO and NPI signal is not as clear.

9 Model Comparison

CGCMv1 has been run for 100 years at a higher resolution. In this experiment, the atmospheric grid has a resolution of 1° latitude by 1.25° longitude. The number of tiles in the LSM has increased to 55,495. All other parameters remain the same.

The results from this experiment shows that the representation of the tropical Pacific Ocean, specifically the far eastern region, is cooler. The overall bias east of 90°W is less. The phasing of the seasonal cycle of temperature and wind stress improves, although the amplitude

of the seasonal cycle in the central equatorial Pacific is reduced. The amplitude and frequency of the ENSO events in the higher resolution model has improved, and the ENSO events are more likely extend to the South American coastline. However, the ENSO signal is still too narrow with respect to observations.

In a third experiment, the abyssal temperature and salinity values south of 60°S are reset to values more representative of deep source water values for the Antarctic. This run is shorter, and it shows improvement over the original run. Specifically, the ice fractions and ocean temperatures in this region have less bias when compared to climatology.

10 Summary

11 References

Arakawa, A., and M. J. Suarez, 1983: Vertical differencing of the primitive equations in sigma coordinates. *Mon. Weather Rev.,* **111**, 34-45.

Atlas, R., R. Hoffman, S. Bloom, J. Jusem, and J. Ardizzone, 1996: A Multi-year Global Surface Wind Velocity Data Set Using SSM/I Wind Observations. *Bull. Amer. Meteor. Soc.*, **77**, 869-882.

Bacmeister, J. T., and M. J. Suarez, 2002: Wind stress simulations and the equatorial momentum budget in an AGCM. *J. Atmos. Sci.*, **59**, 3051-3073.

Bacmeister, J., P. J. Pegion, S. D. Schubert, and Max J. Suarez, 2000: Atlas of seasonal means simulated by the NSIPP-1 atmospheric GCM, *NASA/TM-2000-104606, Vol. 17*, 194pp.

Chou, M.-D. and M. Suarez, 1994: An efficient thermal infrared radiation parameterization for use in general circulation models. *NASA/TM-104606, Vol. 10*, 84pp.

Chou, M.-D. and M. J. Suarez, 1999: A solar radiation parameterization for atmospheric studies. *NASA/TM-104606, Vol. 11*, 40pp.

Conkright, M. E., R. A. Locarini, H. E. Garcia, T. D. O'Brien, T. P. Boyer, C. Stephens, and J. I. Antonov, 2002: World Ocean Atlas 2001. *National Oceanographic Data Center, Silver Spring, MD*, 17 pp.

Hakkinen, S., and G. L. Mellor, 1992: Modeling the seasonal variability of a coupled Arctic ice-ocean system. *J. Geophys. Res.*, **97**, 20285-20304.

Huffman, G. J., 1997: Estimates of root-mean-square random error contained in finite sets of estimated precipitation. *J. Appl. Meteor.*, **36**, 1191-1201.

Josey, S. A., E. C. Kent and P. K. Taylor, 1998: The Southampton Oceanography Centre (SOC) Ocean - Atmosphere Heat, Momentum and Freshwater Flux Atlas. *Southampton Oceanography Centre Report No. 6*, 30 pp.

Kalnay, E., M. Kanamitsu, R. Kistler, W. Collins, D. Deaven, J. Derber, L. Gandin, S. Sara, G. White, J. Woollen, Y. Zhu, M. Chelliah, W. Ebisuzaki, W. Higgins, J. Janowiak, K. C. Mo, C. Ropelewski, J. Wang, A Leetma, R. Renolds, R Jenne, 1995: The NMC/NCAR Reanalysis Project. *Bull. Amer. Meteor. Soc.*, **77**, 437-471.

Koster, R., and M. Suarez, 1992: Modeling the land surface boundary in climate models as a composite of independent vegetation stands. *J. Geophys. Res.*, **97**, 2697-2715.

Koster, R. and M. Suarez, 1996: Energy and Water Balance Calculations in the Mosaic LSM, *NASA/TM-104606, Vol. 9*.

Levitus, S., R. Burgett, T. Boyer, 1994: World Ocean Atlas 1994, Vol. 3: Salinity. *NOAA Atlas NESDIS 3, U.S. Gov. Printing Office, Wash., D.C.*, 99 pp.

Louis, J., M. Tiedtke, and J. Geleyn, 1982: A short history of the PBL parameterization at ECMWF. *Proc. ECMWF Workshop on Planetary Boundary Layer Parameterization*, Reading, United Kingdom, ECMWF, 59-80.

Moorthi, S. and M. Suarez, 1992: Relaxed Arakawa-Schubert: a parameterization of moist convection for general circulation models. *Mon. Weather Rev.,* **120,** 978-1002.

Pegion, P. J., S. D. Schubert, and M. J. Suarez, 2000: An assessment of predictability of northern winter seasonal means with the NSIPP-1 AGCM. *NASA/TM-2000-104606, Vol. 18*, 110pp.

Prigent, C., F. Aires, and W.B. Rossow, 2002: ISCCP reference?

Rayner, N. A., D. E. Parker, E. B. Horton, C. K. Folland, L. V. Alexander, D. P. Rowell, E. C. Kent, and A. Kaplan, 2003: Global analyses of sea surface temperature, sea ice and night marine air temperature since the late nineteenth century. *J. Geophys. Res.*, **108**, 4407.

Reverdin, G., C. Frankignoul, E. Kestenare, and M. J. McPhaden, 1994: Seasonal variability in the surface currents of the Equatorial Pacific. *J. Geophys. Res.*, **99**, 20323-20344.

Reynolds, W. R. and T. M. Smith, 1994: Improved global sea surface temperature analyses using optimum interpolation. *J. Climate*, **7**, 929-948.

Sadourny, R., 1975: The dynamics of finite difference models of the shallow water equations. *J. Atmos. Sci.*, **32**, 680-689.

Schopf, P. S., and A. Loughe, 1995: A reduced-gravity isopycnal model: Hindcast of El Niño. *Mon. Wea. Rev.*, **123**, 2839-2863.

Sellers, P. J., Y. Mintz, Y. C. Sud, and A. Dalcher, 1986: A simple biosphere model (SiB) for use within general circulation models. *J. Atmos. Sci.*, **43**, 505-531.

Slingo, J. M., 1987: The development and verification of a cloud precipitation scheme for the ECMWF model. *Quart. J. Royal Met. Soc.*, **113**, 899-927.

Sterl, A., and A. Kattenberg, 1994: Embedding a mixed layer model into an ocean general circulation model of the Atlantic: The importance of surface mixing for heat flux and temperature. *J. Geophys. Res.*, **99**, 14139-14157.

Suarez, M. J. and L. L. Takacs, 1995: Documentation of the Aries/GEOS dynamical core Version 2, *NASA/TM-104606, Vol. 5*, 58pp.

Sud, Y., and A. Molod, 1988: The roles of dry convection, cloud-radiation feedback processes, and the influence of recent improvements in the parameterization in the GLA GCM. *Mon. Wea. Rev.*, **116**, 2366-2387.

Sun, C., and several others, 2005: Intercomparison of global ocean data assimilation systems in ODASI experiments. *In Progress.*

Takacs, L. L.and M. J. Suarez, 1996: Dynamical aspects of climate simulations using the GEOS GCM, *NASA/TM-104606, Vol. 10*, 56pp.

Trenberth, K. E. and J. W. Hurrell, 1994: Decadal atmosphere-ocean variation in the Pacific. *Climate Dyn.*, **9**, 303-319.

Vintzileos, A., M. M. Rienecker, M. J. Suarez, S. K. Miller, P. J. Pegion, and J. T. Bacmeister, 2003: Simulation of the El Nino-Southern Oscillation phenomenon with NASA's Seasonal-to-Interannual Prediction Project coupled general circulation model. *CLIVAR Exchanges*, **8**, 25-27.

Vintzileos, A. and R. Sadourny, 1997: A general interface between an atmopsheric general circulation model and underlying ocean and land surface models: Delocalized physics scheme. *Mon. Wea. Rev.*, **125**, 926-941.

Wood, E. F., and 28 others, 1998: The project for the inercomparison of land surface parameterization schemes (PILPS): Phase 2(c) Red Arkansas River basin experiment, 1, Experiment description and summary intercomparisons. *J. Global and Planetary Change*, **19**, 115-135.

Yang, S., K. Lau, and P. Schopf, 1999: Sensitivity of the tropical Pacific Ocean to precipitation induced freshwater flux. *Clim. Dyn.*, **15**, 737-750.

Zhou, J., Y. C. Sud, and K. M. Lau, 1996: Impact of orographically induced gravity wave drag in the GLA GCM. *Q. Journ. Roy. Meteorol. Soc.*, **122**, 903-927.

ANNUAL MEAN CLIMATOLOGY

Sea Surface Temperature

Sea Surface Salinity

Mixed Layer Depth

Equatorial Surface Temperature and Wind Stress

Subsurface Temperature, Salinity, and Zonal Current in the Tropical Pacific Ocean

Antarctic Ocean Ice Fraction

Arctic Ocean Ice Fraction

Annual Mean Sea Surface Temperature

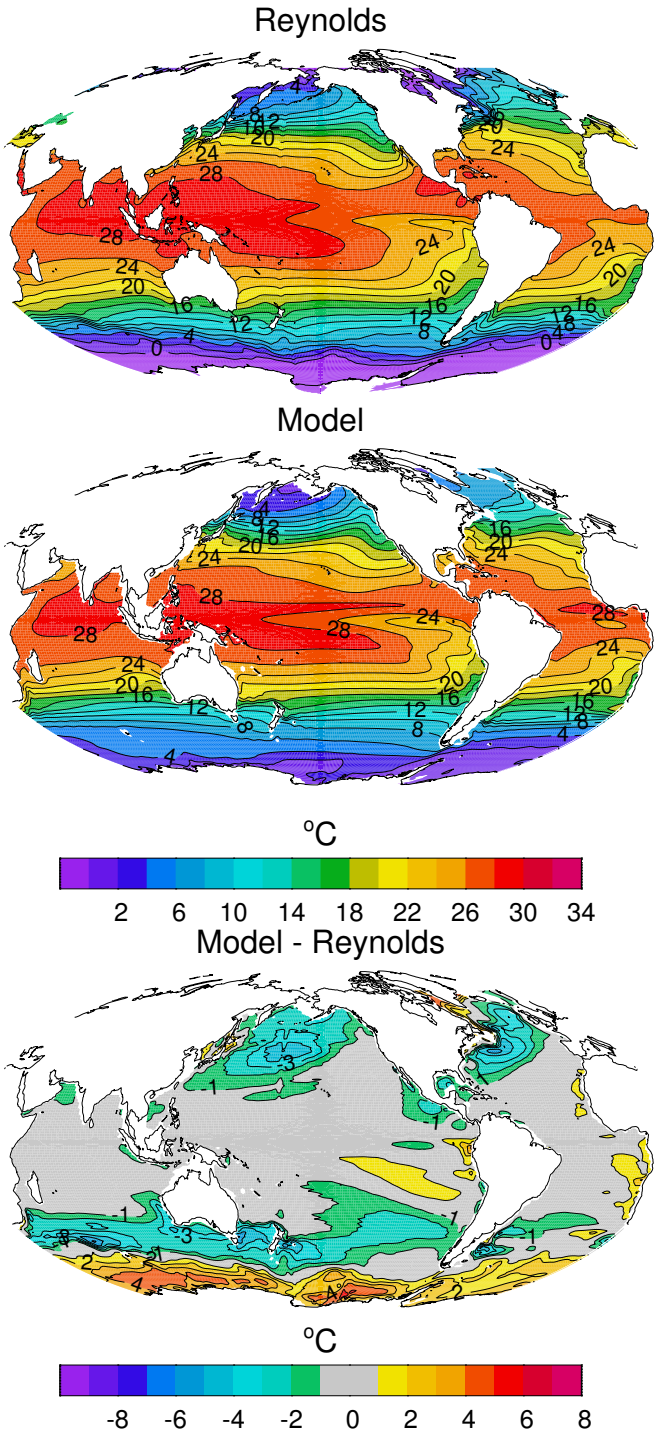

Figure 1: Sea surface temperature (°C).Top: observations from Reynolds and Smith (1994); Middle: model; Bottom: annual mean SST bias. Contour interval is 1°C.

Annual Mean Sea Surface Salinity

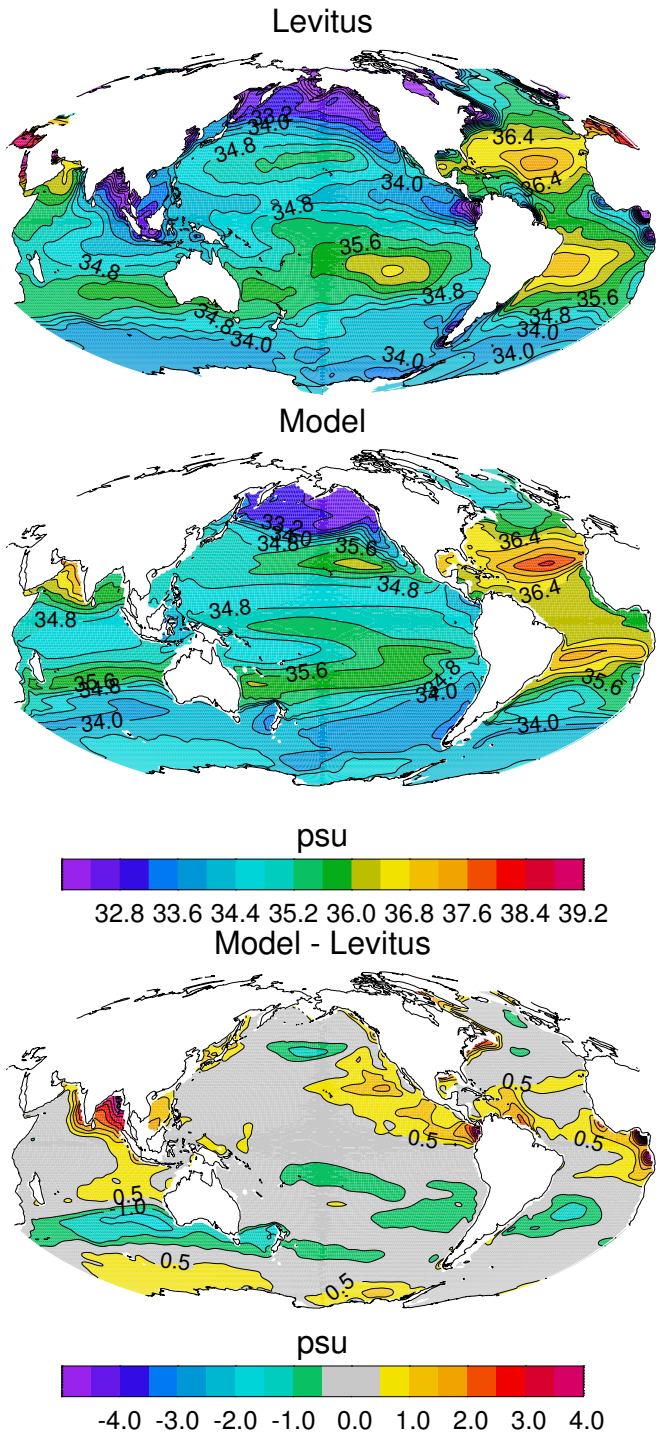

Figure 2: Sea surface salinity.Top: observations from the 2001 World Ocean Atlas (Conkright et al.) ; Middle: model; Bottom: annual mean SSS bias. Contour interval is 0.4.

Annual Mean Mixed Layer Depth Climatology

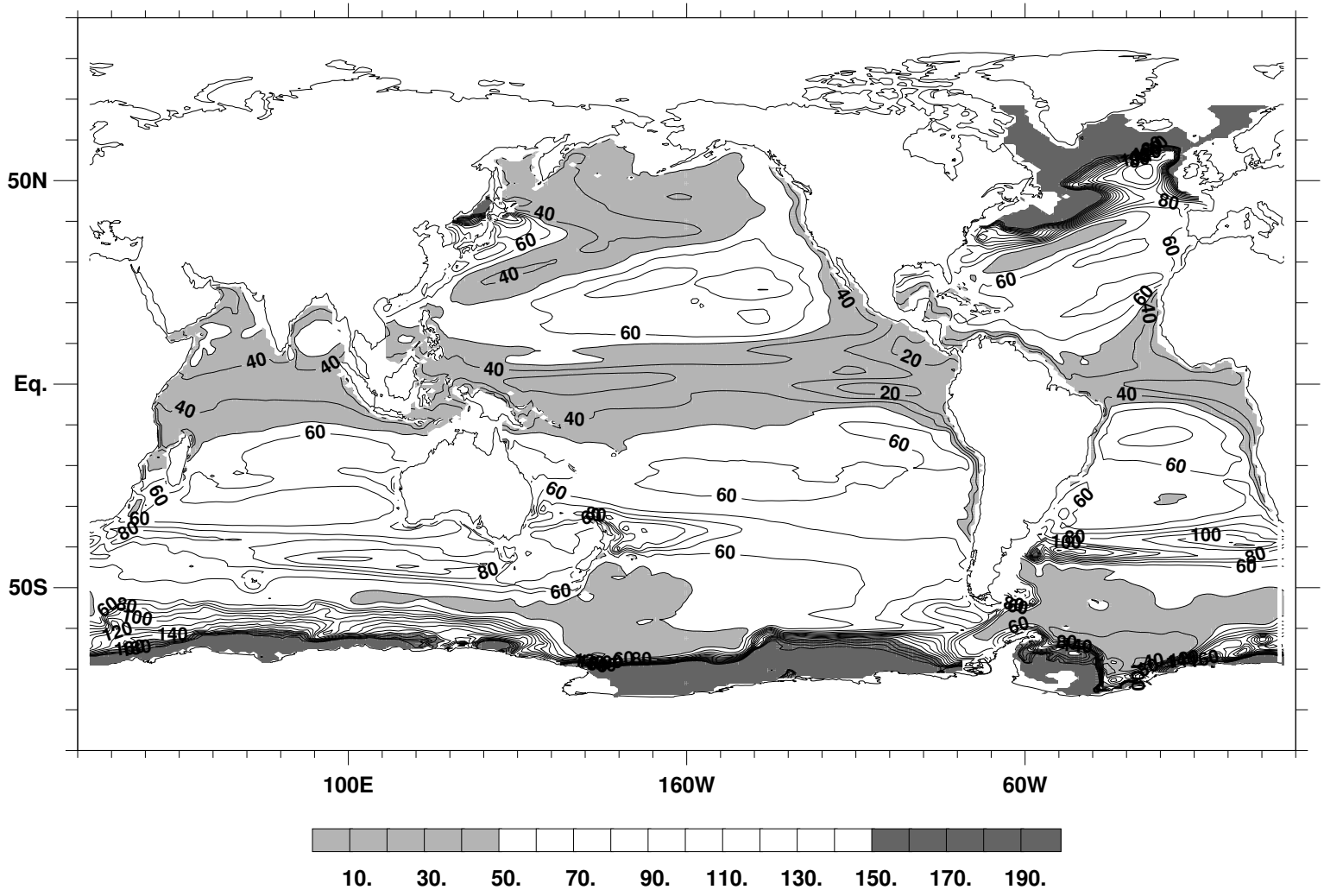

Figure 3a: Mixed layer depth from model climatology (m).Contour interval is 10 m.

Annual Mean Mixed Layer Depth Climatology from GMAO Ocean Analysis

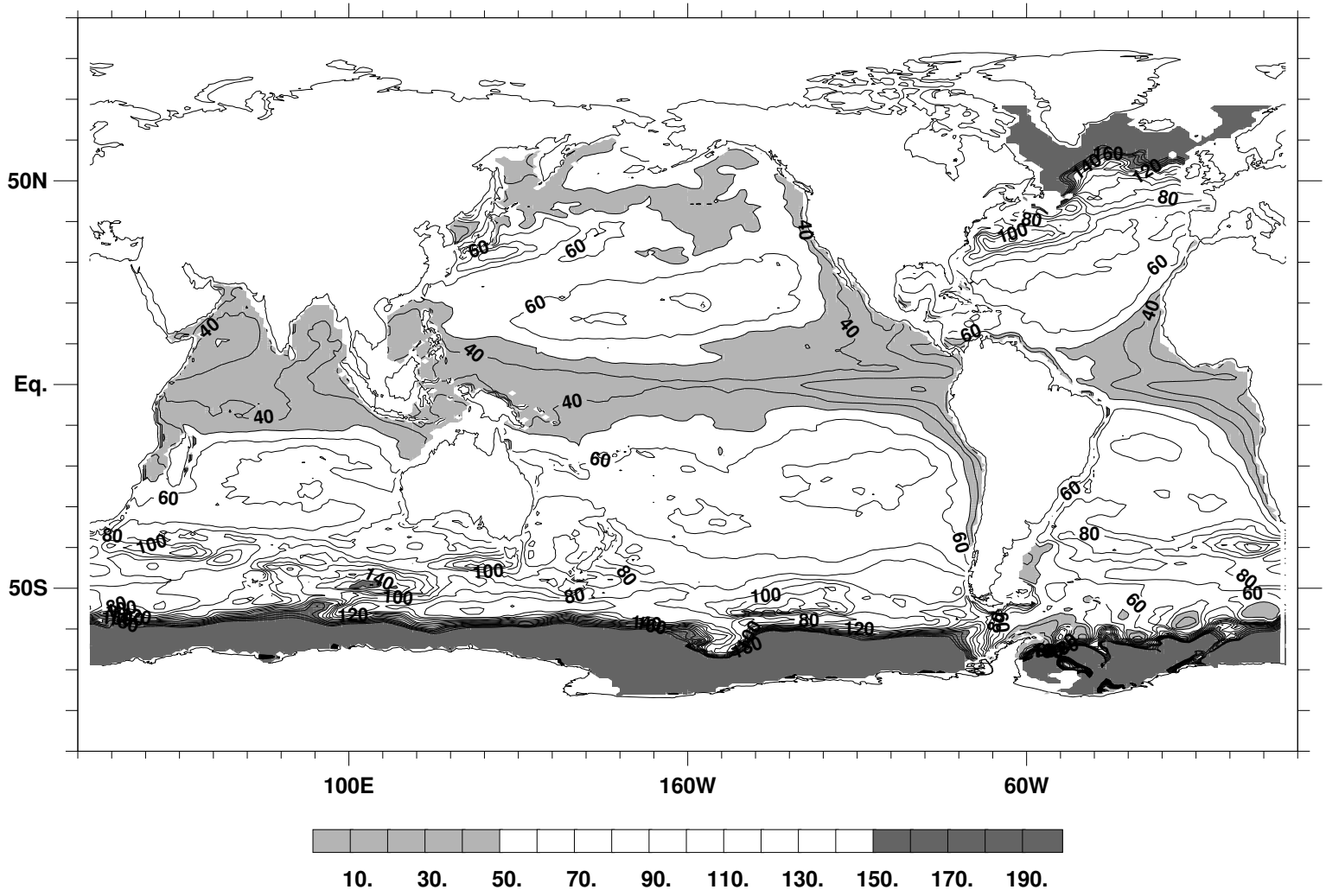

Figure 3b: Mixed layer depth from GMAO ocean analysis (m).Contour interval is 10 m.

Annual Mean in the Equatorial Pacific

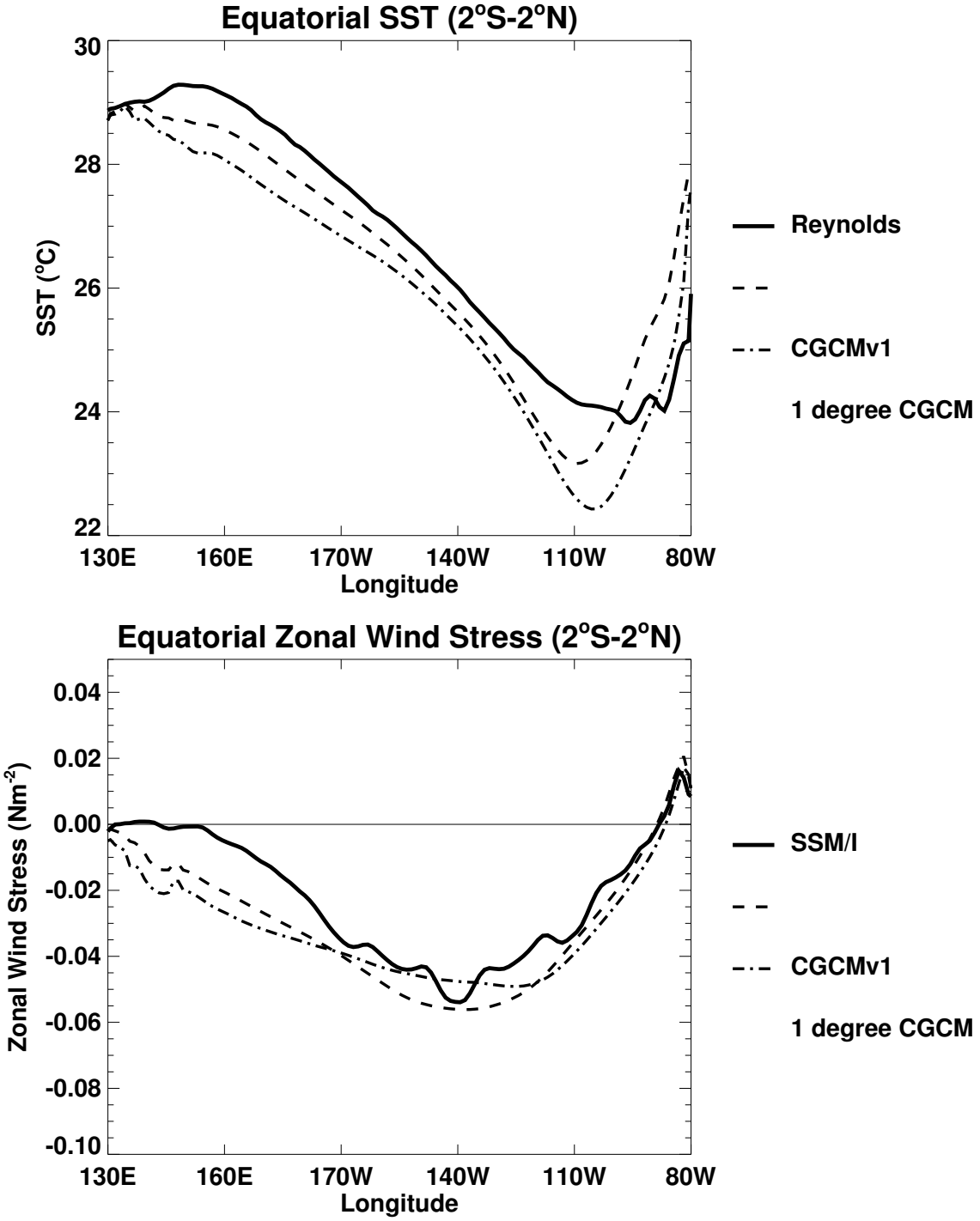

Figure 4: Annual mean sea surface temperature and wind stress in the Equatorial Pacific.Top: SST, Bottom: τ_x. Solid black line: observations; dotted line: results from an AMIP-style run using the NSIPP-1 AGCM; dashed line: model; dashed blue line: model with 1° atmospheric resolution.

Annual Mean at the Equator from CGCM

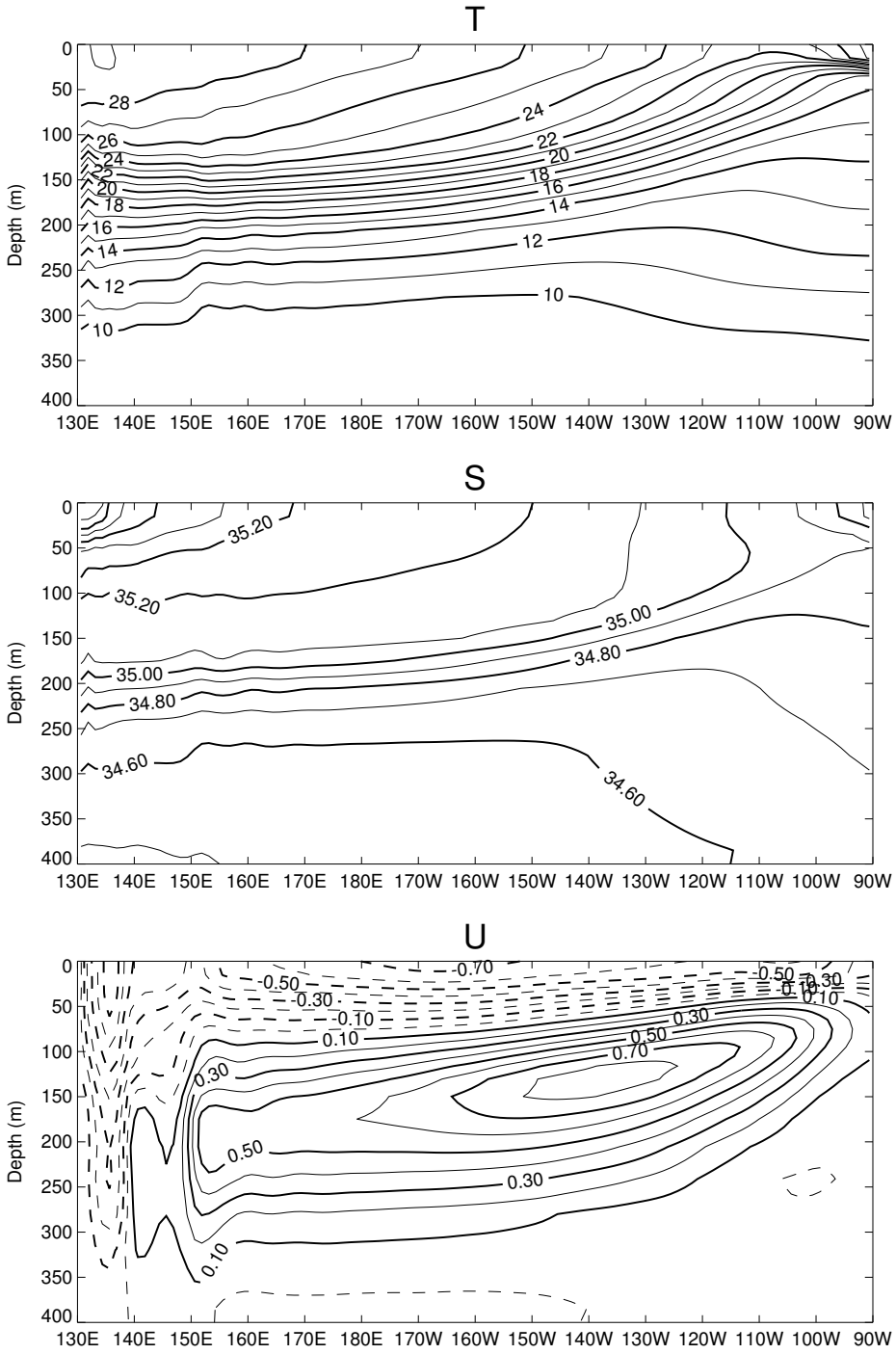

Figure 5a: Annual mean profile at the Equator in the Pacific Ocean.Top: temperature (°C); Middle: salinity; Bottom: zonal current (m s^{-1}). Model cross-section from 130°E to 90°W. Contour intervals are 1°C for temperature, 0.1 for salinity, and 0.1 m s^{-1} for zonal current.

Observed Annual Mean at the Equator

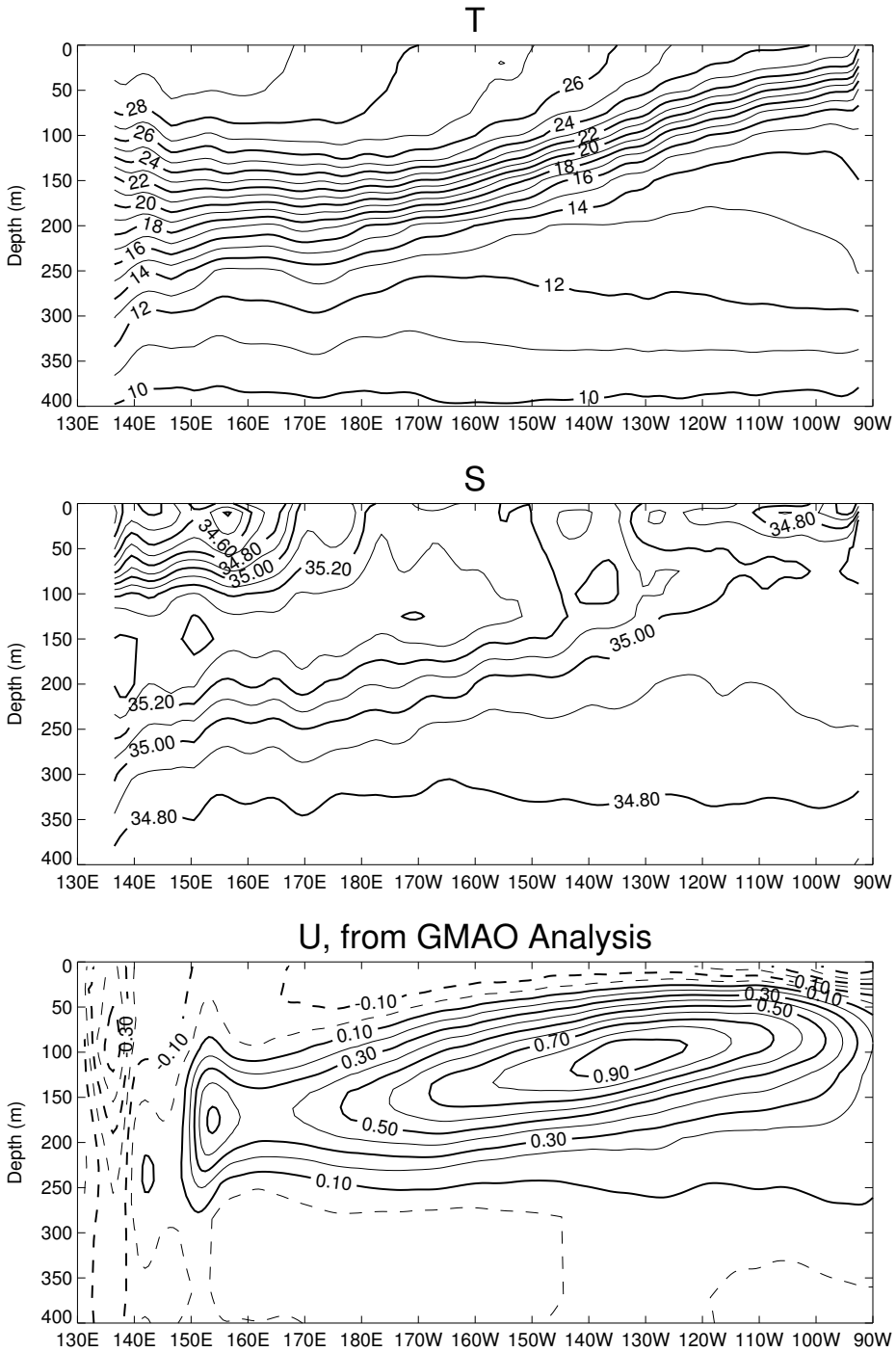

Figure 5b: Annual mean profile at the Equator in the Pacific Ocean.Top: Temperature (°C), Middle: Salinity, Bottom: Zonal Current (m s^{-1}). Temperature and salinity data from World Ocean Atlas. Zonal current data from GMAO ocean analysis. Cross-section extends from 130°E to 90°W. Contour intervals are 1°C for temperature, 0.1 for salinity, and 0.1 m s^{-1} for zonal current.

Annual Mean at 165°E from Model

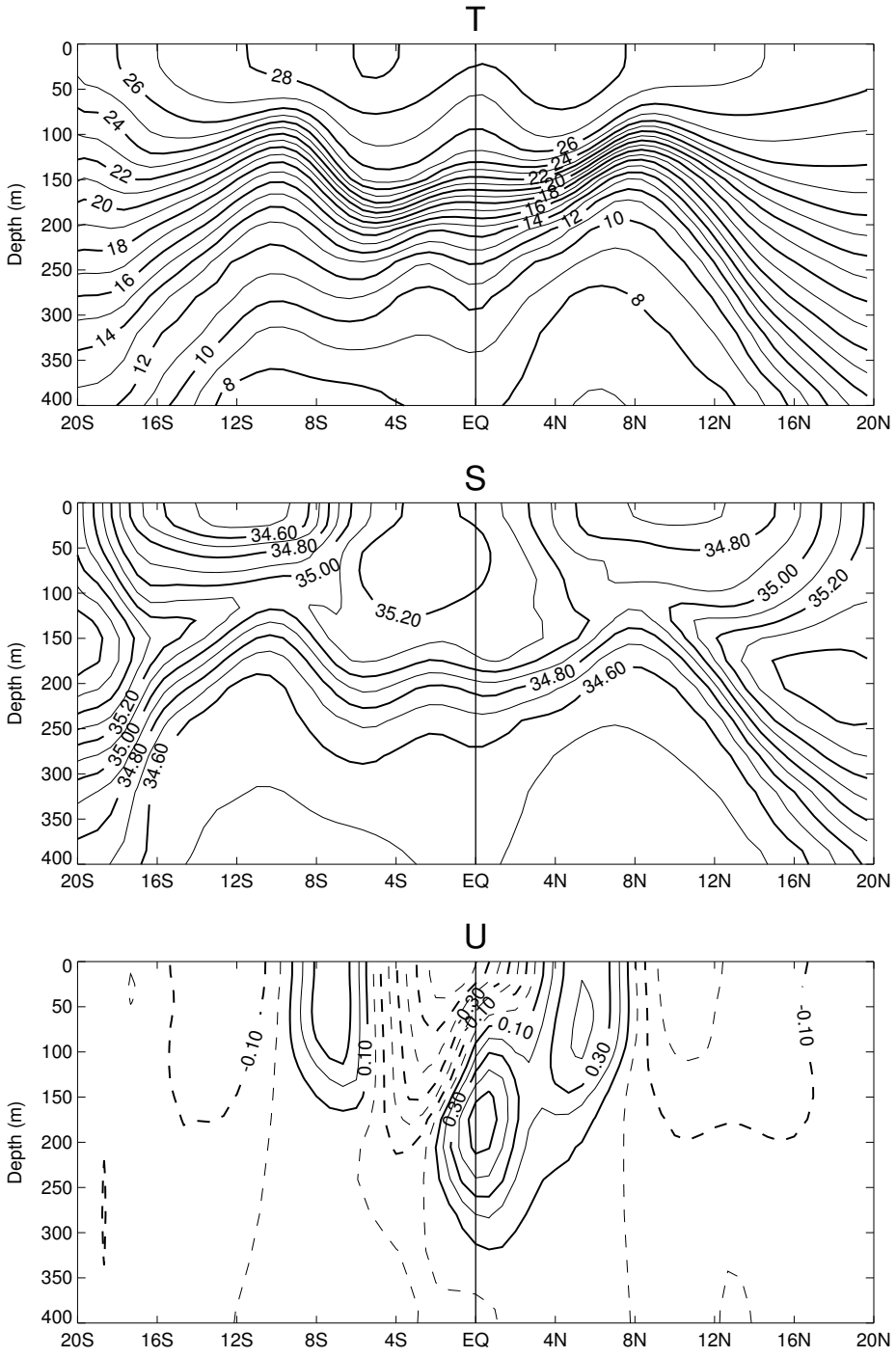

Figure 6a: Annual mean profile at 165°E in the tropics.Top: Temperature (°C), Middle: Salinity, Bottom: Zonal Current (m s^{-1}). Model cross-section from 20°S to 20°N. Contour intervals are 1°C for temperature, 0.1 for salinity, and 0.1 m s^{-1} for zonal current.

Annual Mean at 165°E from Observations

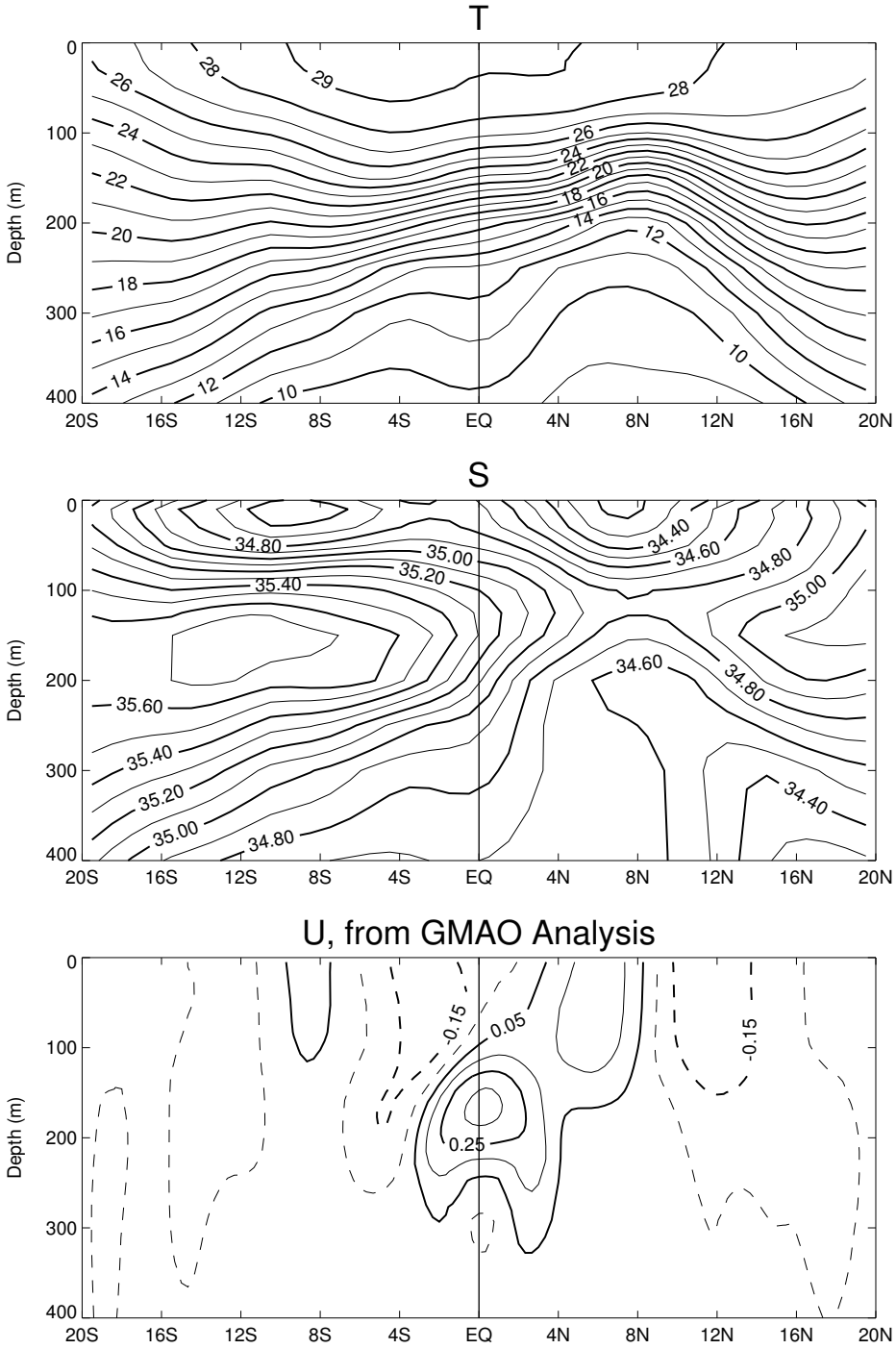

Figure 6b: Annual mean profile at 165°E in the tropics.Top: Temperature (°C), Middle: Salinity, Bottom: Zonal Current (m s^{-1}). Temperature and salinity data from World Ocean Atlas. Zonal current data from GMAO Analysis. Cross-section extends from 20°S to 20°N. Contour intervals are 1°C for temperature, 0.1 for salinity, and 0.1 m s^{-1} for zonal current.

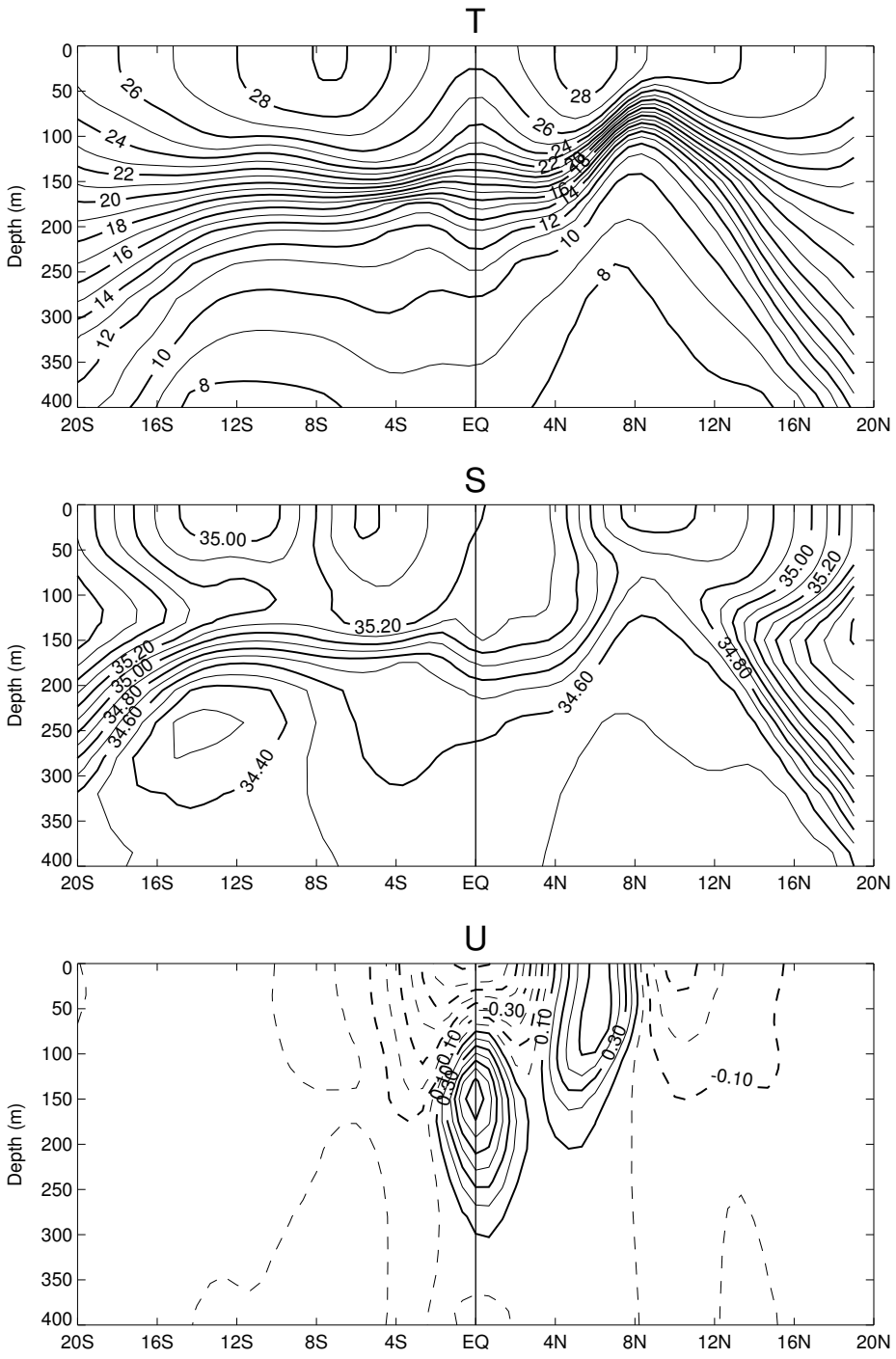

Figure 7a: Annual mean profile at 155°W in the tropics.Top: Temperature (°C), Middle: Salinity, Bottom: Zonal Current (m s^{-1}). Model cross-section from 20°S to 20°N. Contour intervals are 1°C for temperature, 0.1 for salinity, and 0.1 m s^{-1} for zonal current.

Annual Mean at 155°W from Observations

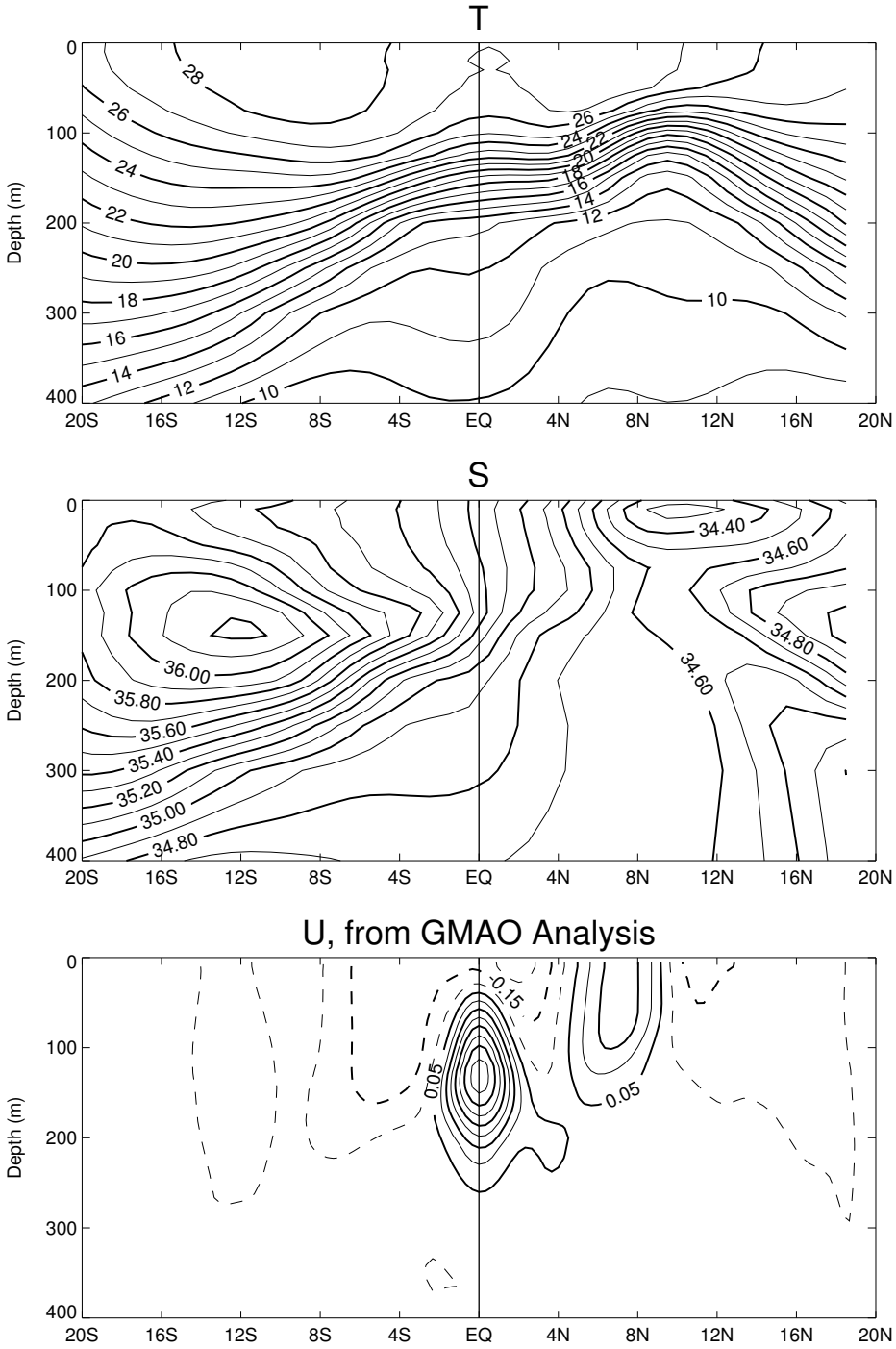

Figure 7b: Annual mean profile at 155°W in the tropics.Top: Temperature (°C), Middle: Salinity, Bottom: Zonal Current (m s^{-1}). Temperature and salinity data from World Ocean Atlas. Zonal current data from GMAO Analysis. Cross-section extends from 20°S to 20°N. Contour intervals are 1°C for temperature, 0.1 for salinity, and 0.1 m s^{-1} for zonal current.

Annual Mean at 140°W from Model

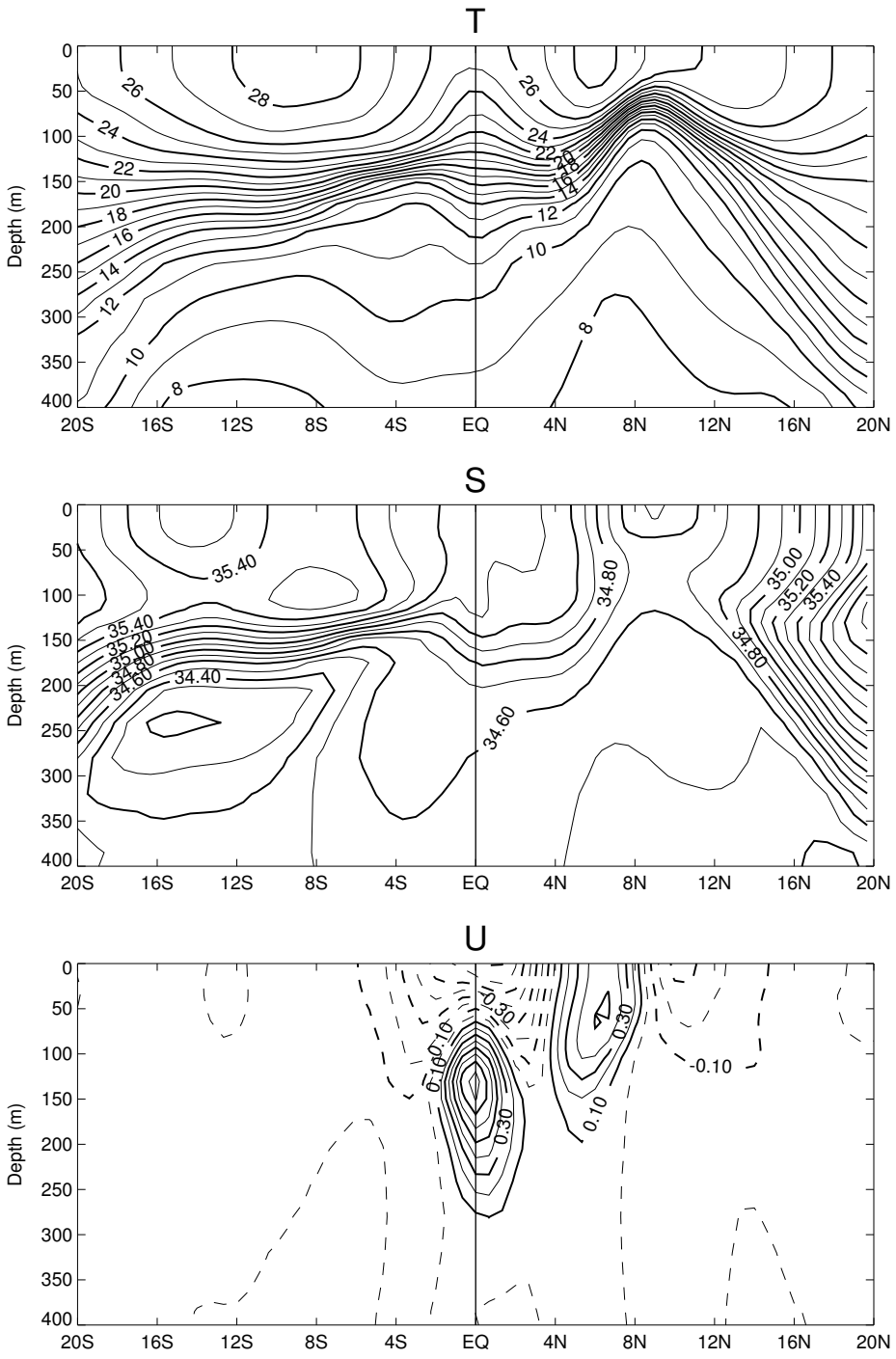

Figure 8a: Annual mean profile at 140°W in the tropics.Top: Temperature (°C), Middle: Salinity, Bottom: Zonal Current (m s^{-1}). Model cross-section from 20°S to 20°N. Contour intervals are 1°C for temperature, 0.1 for salinity, and 0.1 m s^{-1} for zonal current.

Annual Mean at 140°W from Observations

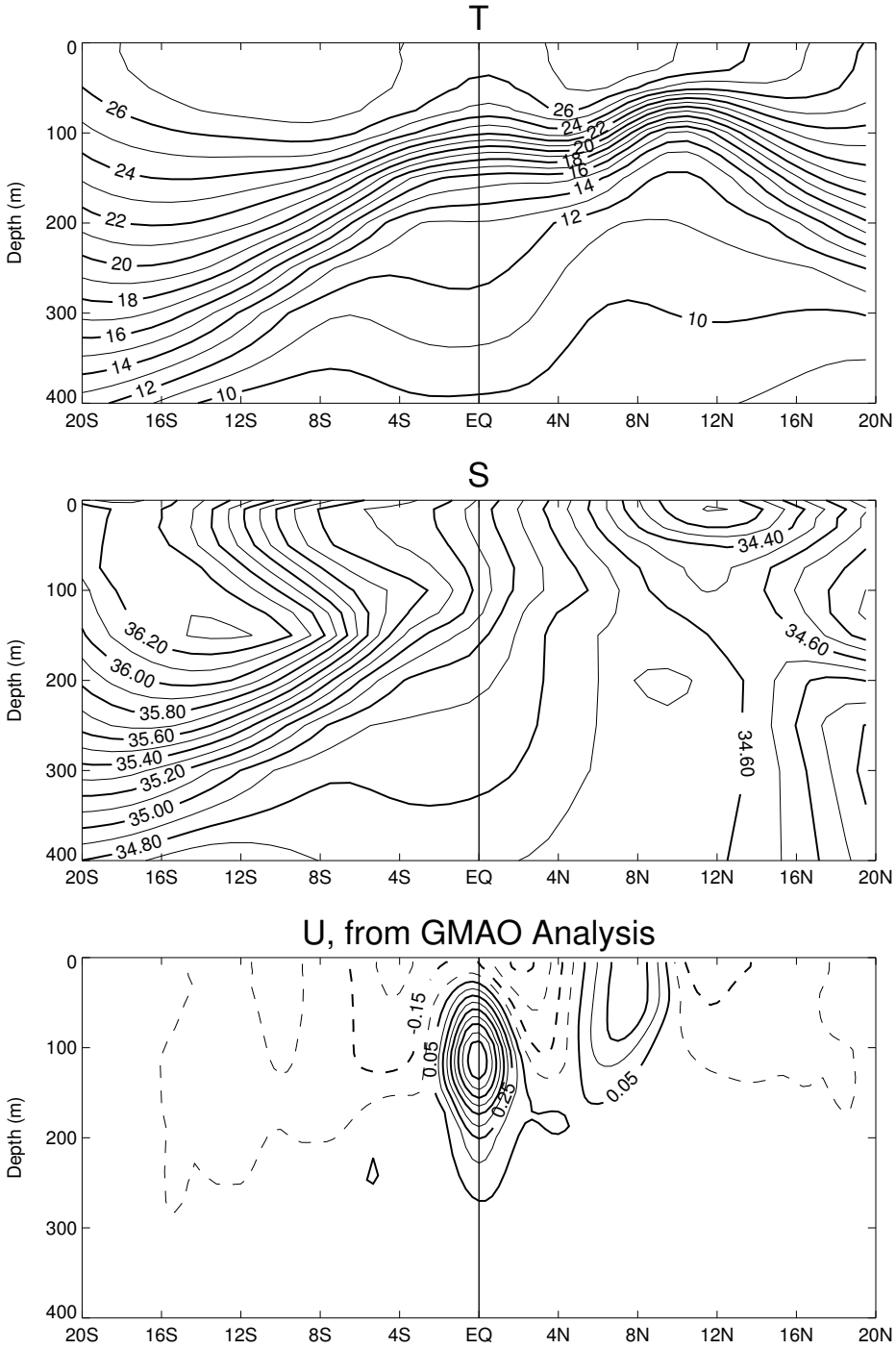

Figure 8b: Annual mean profile at 140°W in the tropics.Top: Temperature (°C), Middle: Salinity, Bottom: Zonal Current (m s^{-1}). Temperature and salinity data from World Ocean Atlas. Zonal current data from GMAO Analysis. Cross-section extends from 20°S to 20°N. Contour intervals are 1°C for temperature, 0.1 for salinity, and 0.1 m s^{-1} for zonal current.

Annual Mean at 110°W from Model

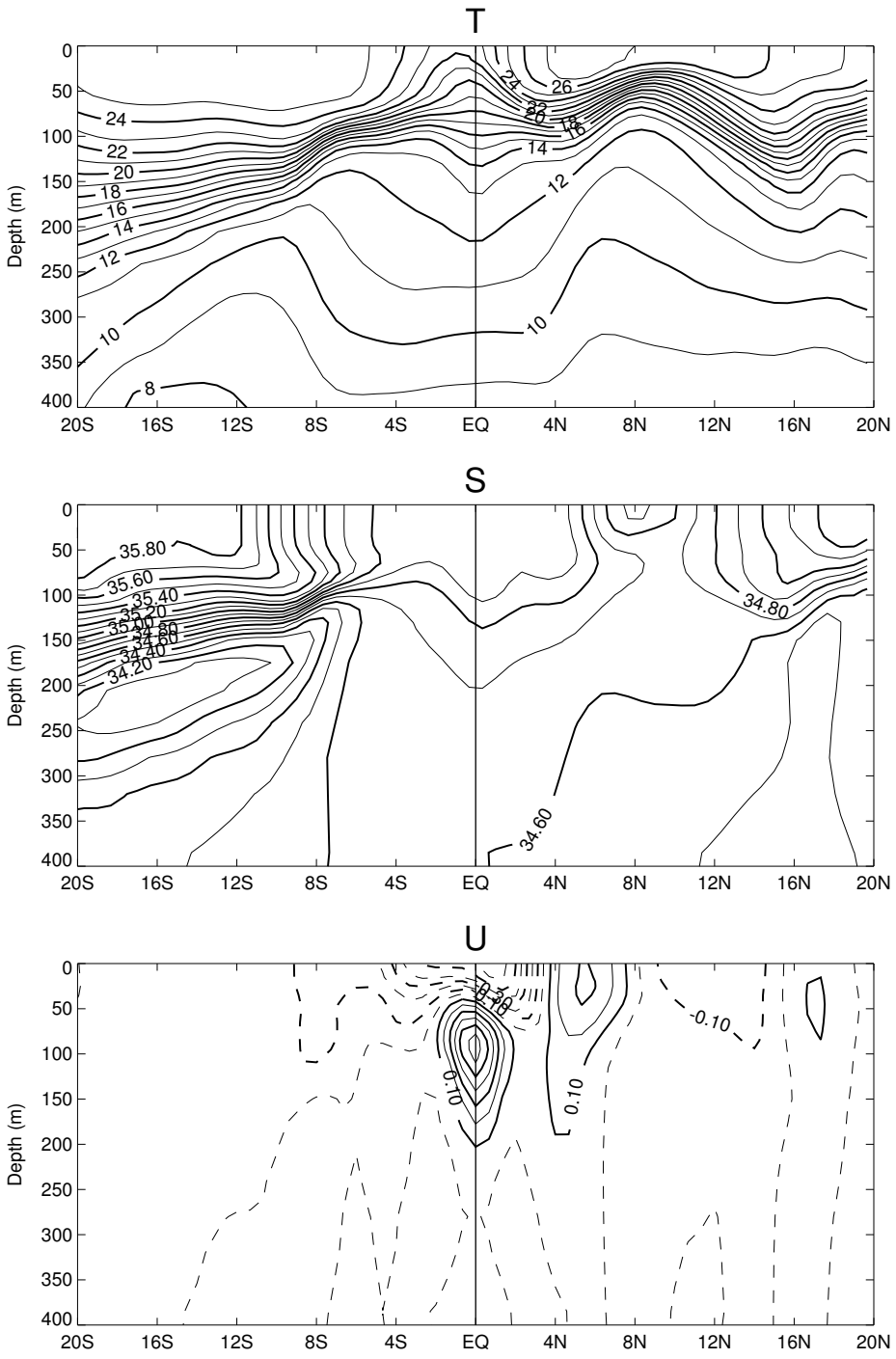

Figure 9a: Annual mean profile at 110°W in the tropics.Top: Temperature (°C), Middle: Salinity, Bottom: Zonal Current (m s^{-1}). Model cross-section from 20°S to 20°N. Contour intervals are 1°C for temperature, 0.1 for salinity, and 0.1 m s^{-1} for zonal current.

Annual Mean at 110°W from Observations

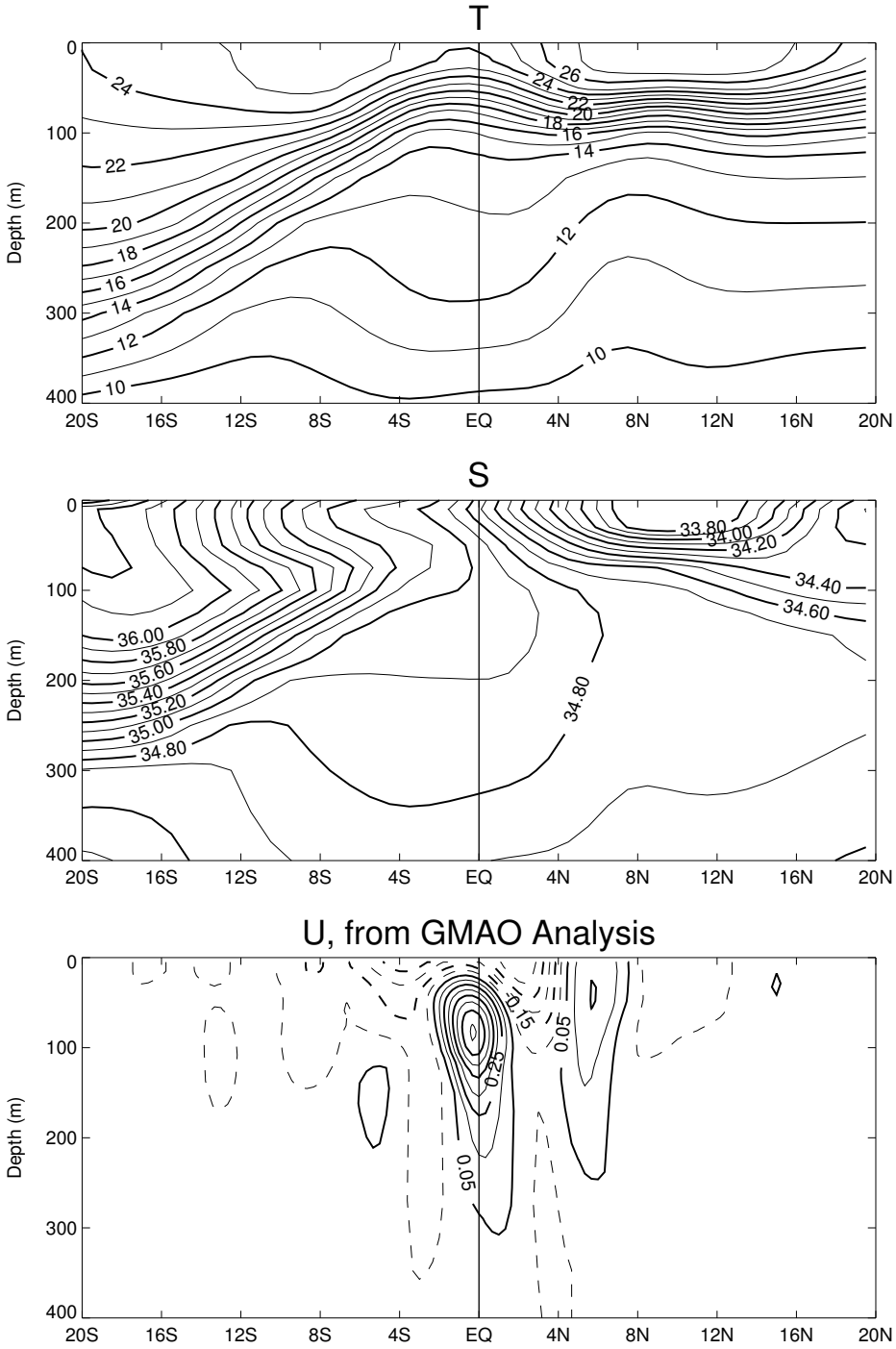

Figure 9b: Annual mean profile at 110°W in the tropics.Top: Temperature (°C), Middle: Salinity, Bottom: Zonal Current (m s^{-1}). Temperature and salinity data from World Ocean Atlas. Zonal current data from GMAO Analysis. Cross-section extends from 20°S to 20°N. Contour intervals are 1°C for temperature, 0.1 for salinity, and 0.1 m s^{-1} for zonal current.

Ice Fraction

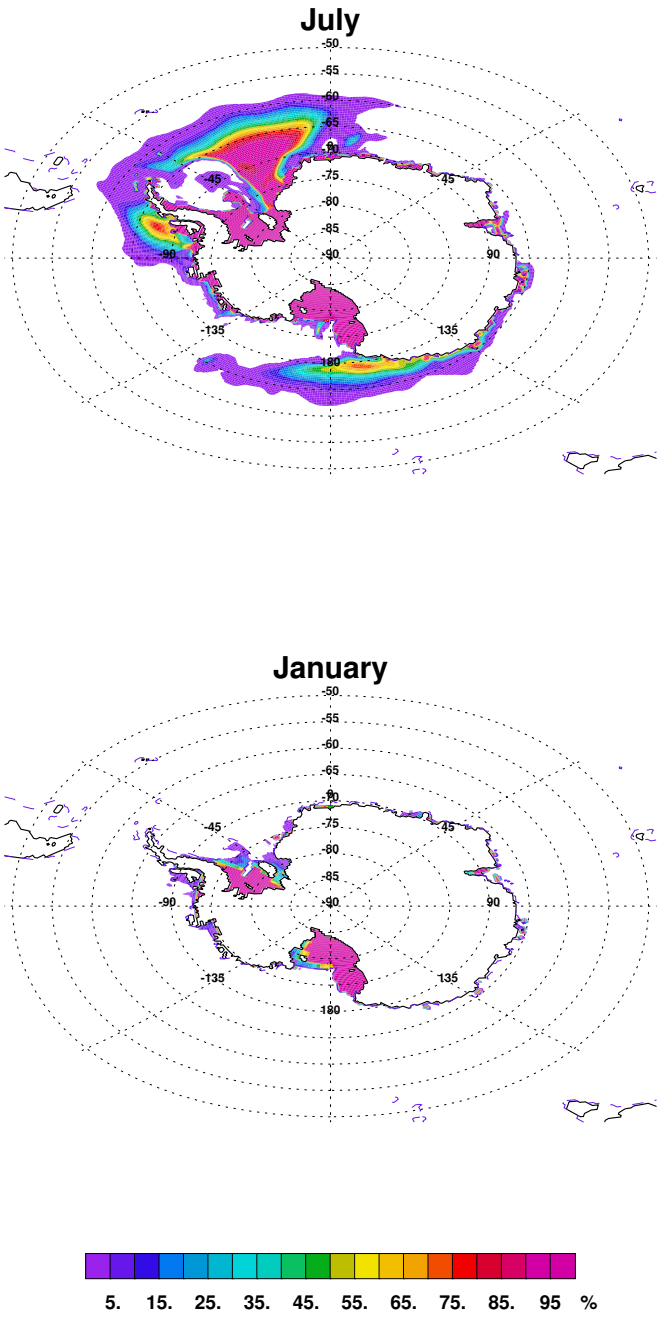

Figure 10a: Ice Fraction in the Antarctic Ocean.Top: July, Bottom: January. Contour interval is 5%

Observed Ice Fraction

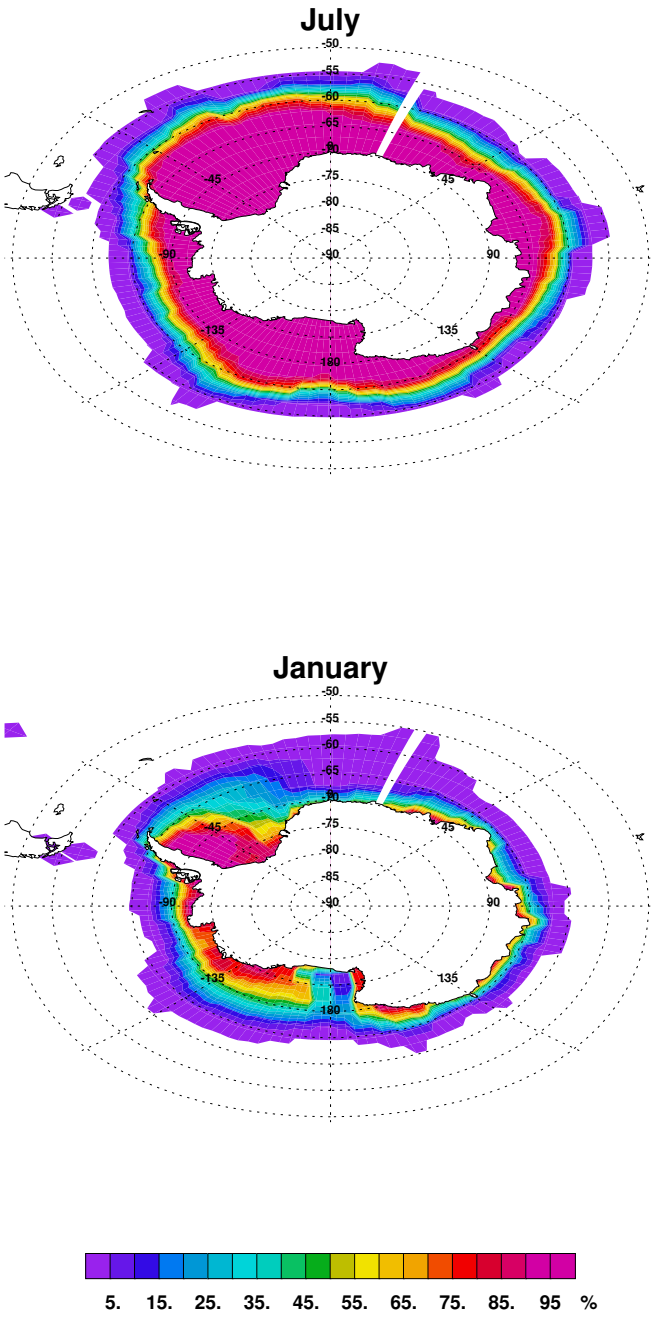

Figure 10b: Ice Fraction in the Antarctic Ocean.Observations from ISCCP ice cover climatology. Top: July, Bottom: January.

Ice Fraction

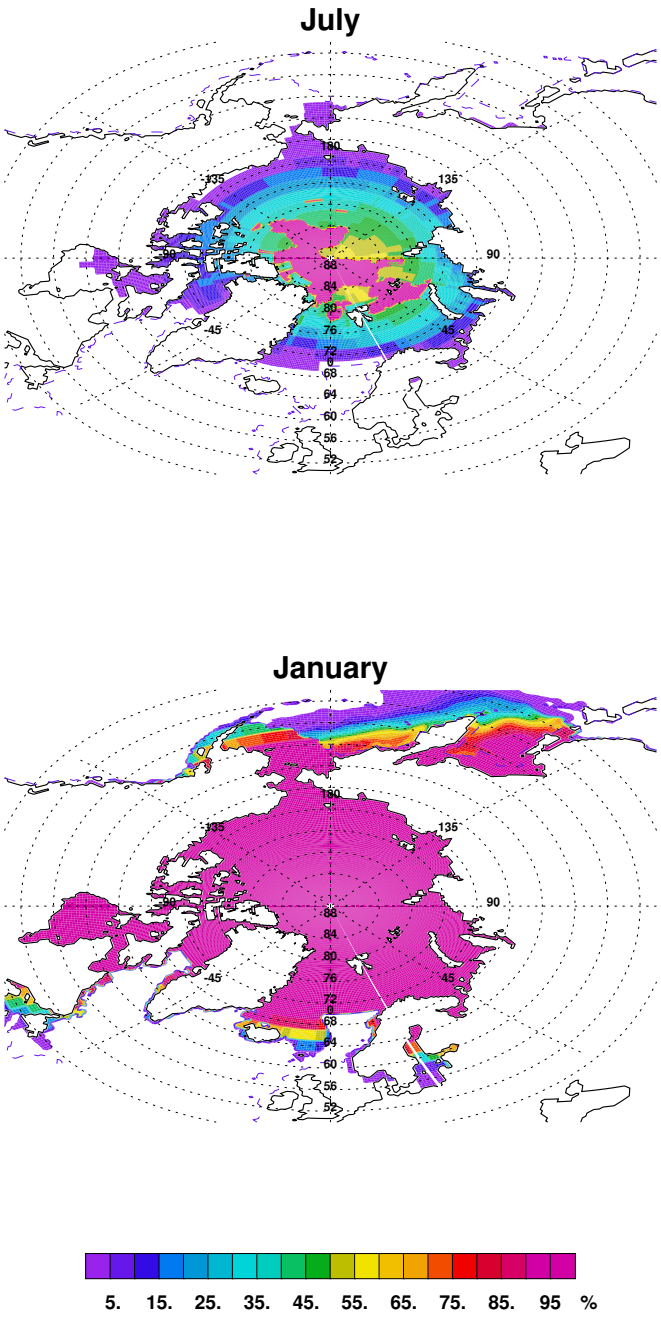

Figure 11a: Ice Fraction in the Arctic Ocean.Top: July, Bottom: January. Contour interval is 5%

Observed Ice Fraction

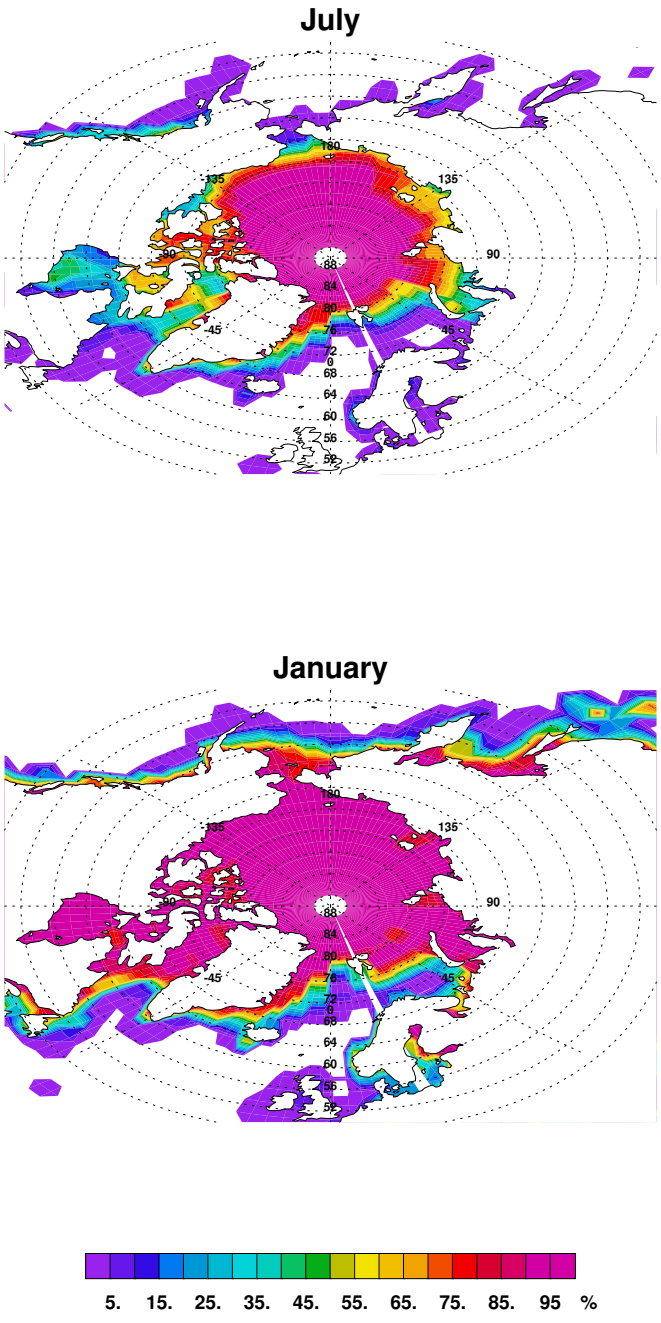

Figure 11b: Ice Fraction in the Arctic Ocean.Observations from ISCCP ice cover climatology. Top: July, Bottom: January. Contour interval is 5%

SEASONAL MEAN CLIMATOLOGY

(DJF, MAM, JJA, SON)

Zonal Wind at 200 mb

Eddy Geopotential Height at 200 mb

Sea Level Pressure

Precipitation

Net Surface Water Flux

Net Surface Heat Flux

Outgoing Longwave Radiation

Net Cloud Radiative Forcing

Net Shortwave Radiation at Surface

Zonal Surface Wind Stress

Meridional Surface Wind Stress

Sea Surface Temperature

Sea Surface Salinity

Sea Surface Height

Surface Current (Zonal)

Surface Current (Meridional)

Temperature at 300 m

Salinity at 300 m

Seasonal Anomaly in the Equatorial Pacific

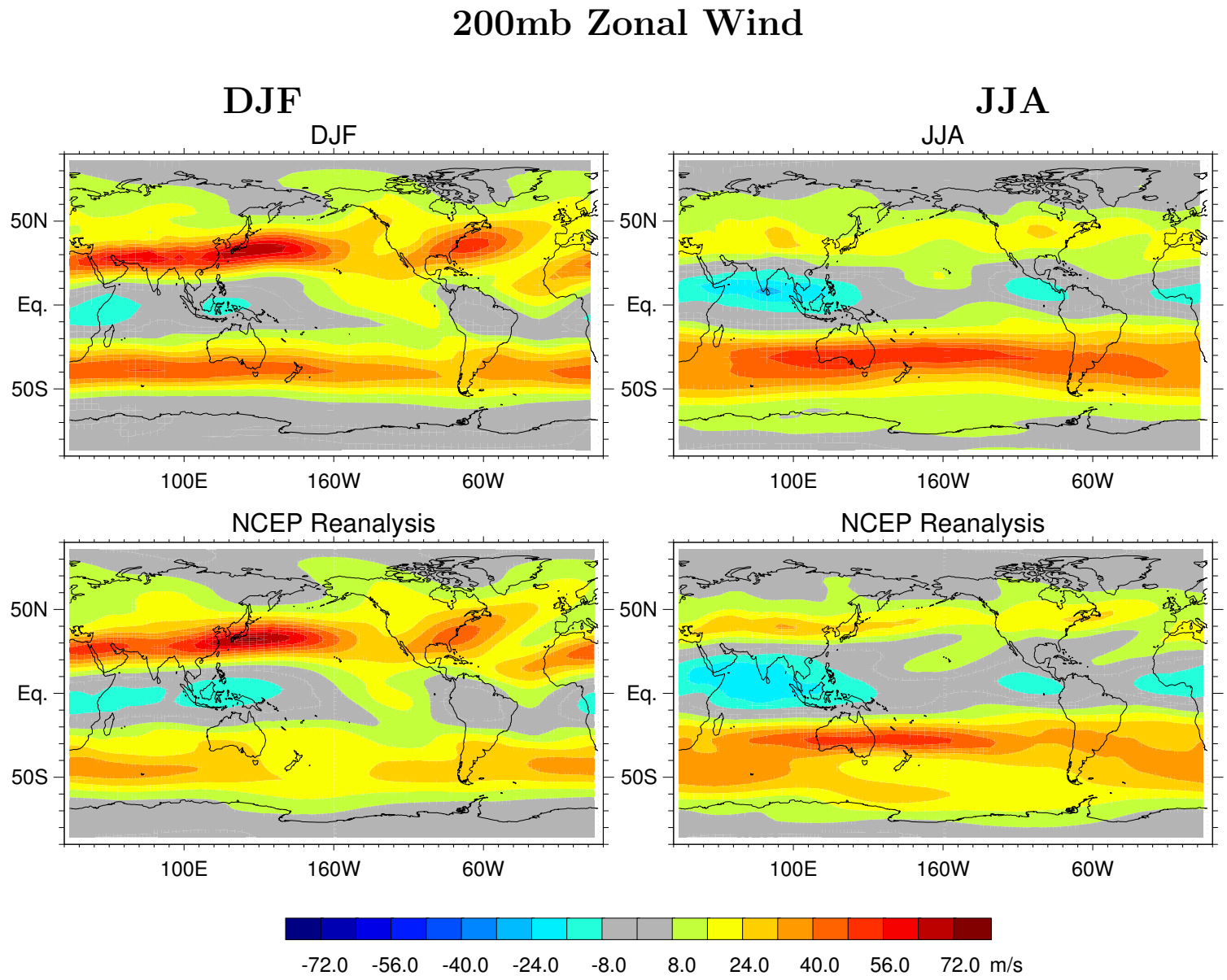

Figure 12a: Zonal wind at 200 mb (m s^{-1}). Upper panels: model; Lower panels: observations from NCEP Reanalysis; Left panels: December-January-February mean; Right panels: June-July-August mean. Contour interval is 8 m s^{-1}.

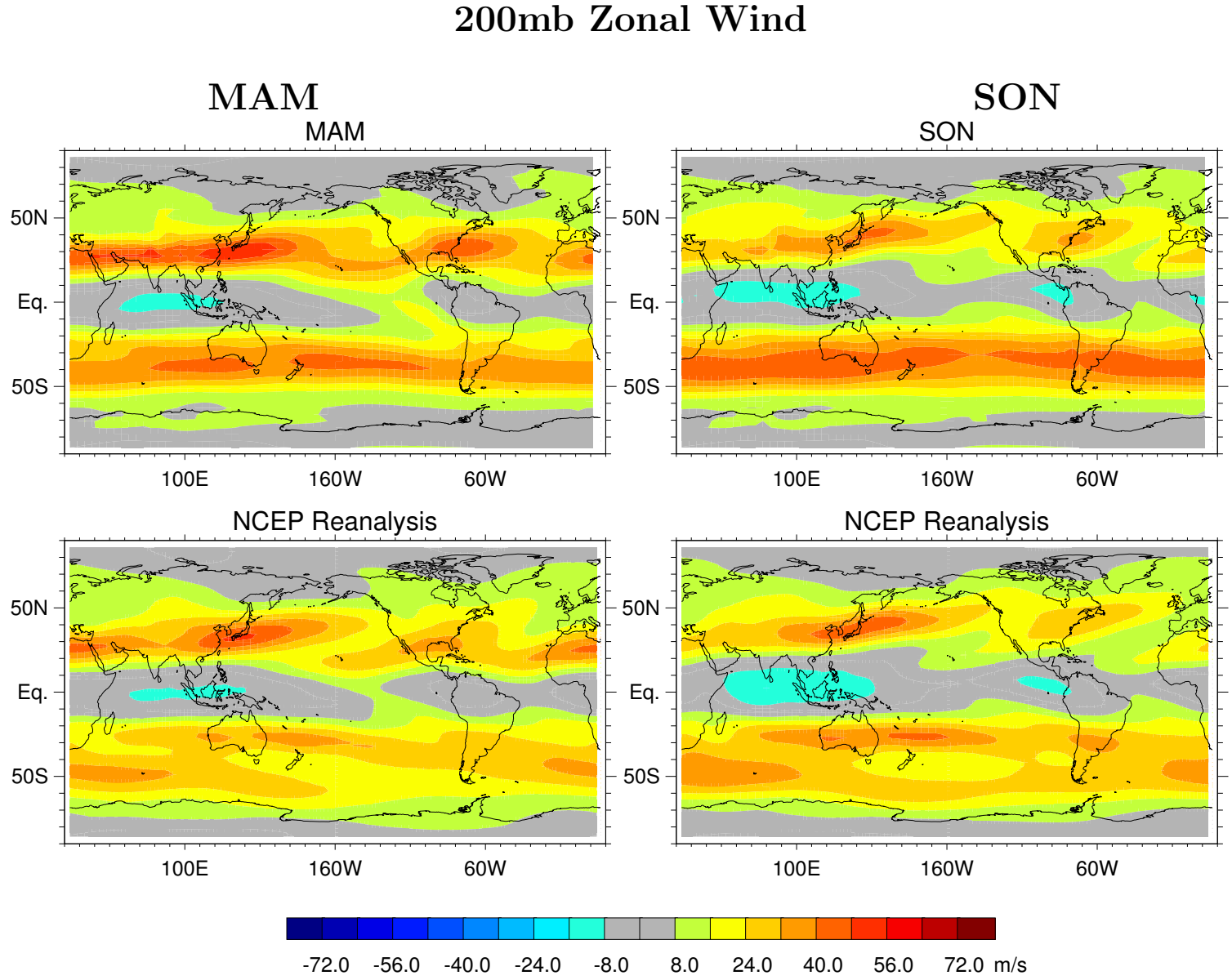

Figure 12b: Zonal wind at 200 mb (m s^{-1}). Upper panels: model; Lower panels: observations from NCEP Reanalysis; Left panels: March-April-May mean; Right panels: September-October-November mean. Contour interval is 8 m s^{-1}.

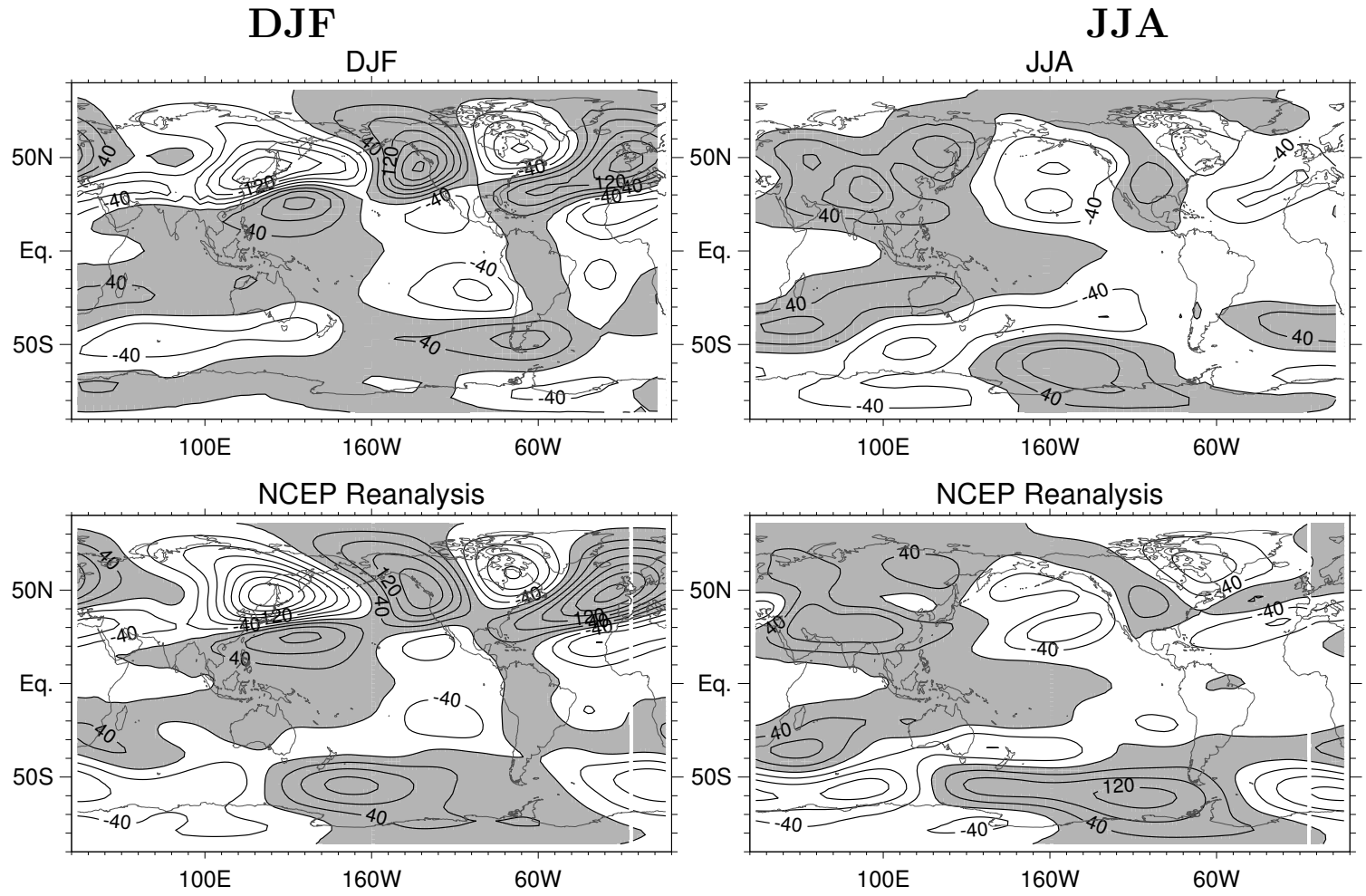

Figure 13a: Eddy geopotential height at 200 mb (m). Upper panels: model; Lower panels: observations from NCEP Reanalysis; Left panels: December-January-February mean; Right panels: June-July-August mean. Contour interval is 40 m.

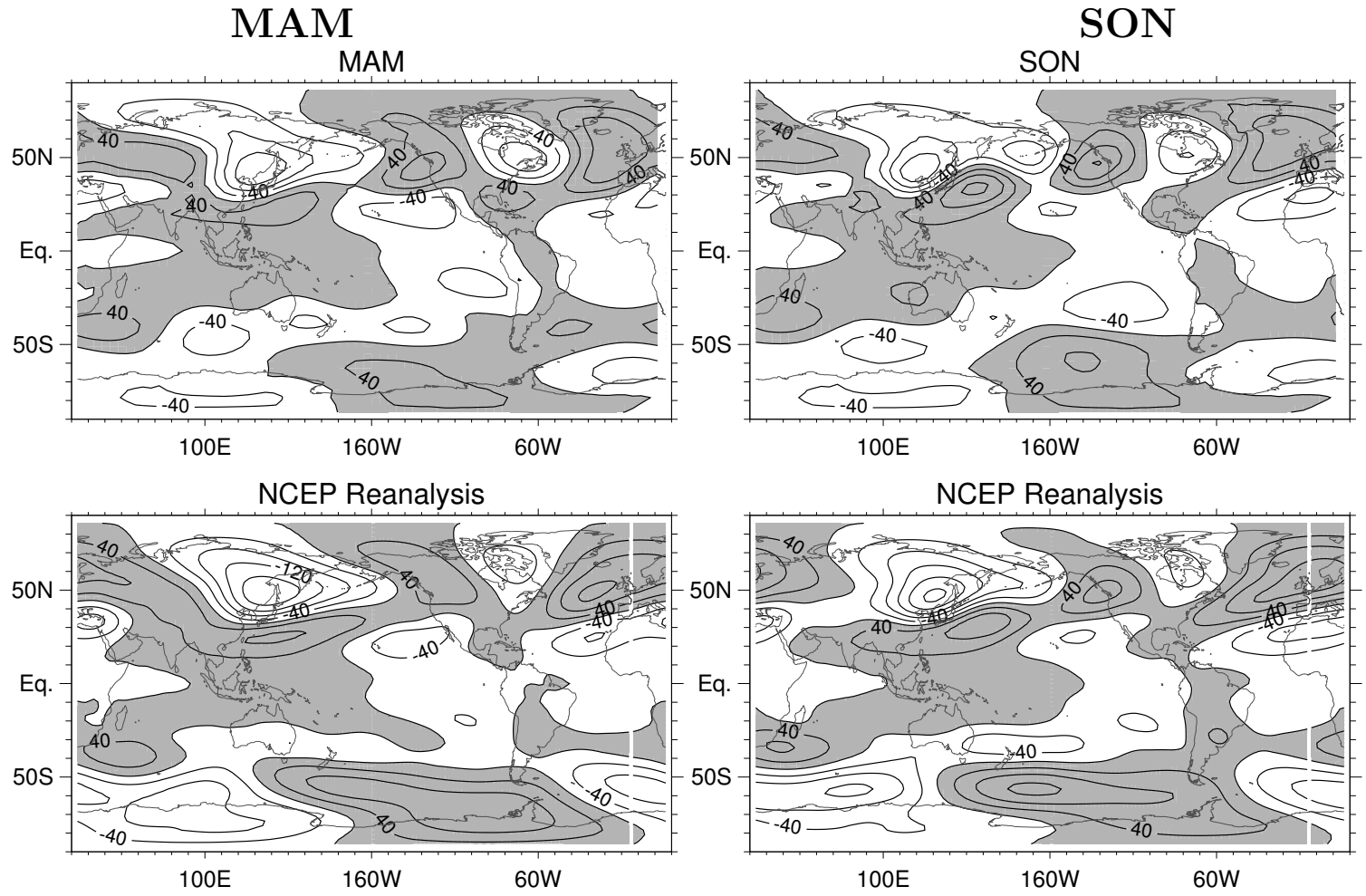

Figure 13b: Eddy geopotential height at 200 mb (m). Upper panels: model; Lower panels: observations from NCEP Reanalysis; Left panels: March-April-May mean; Right panels: September-October-November mean. Contour interval is 40 m.

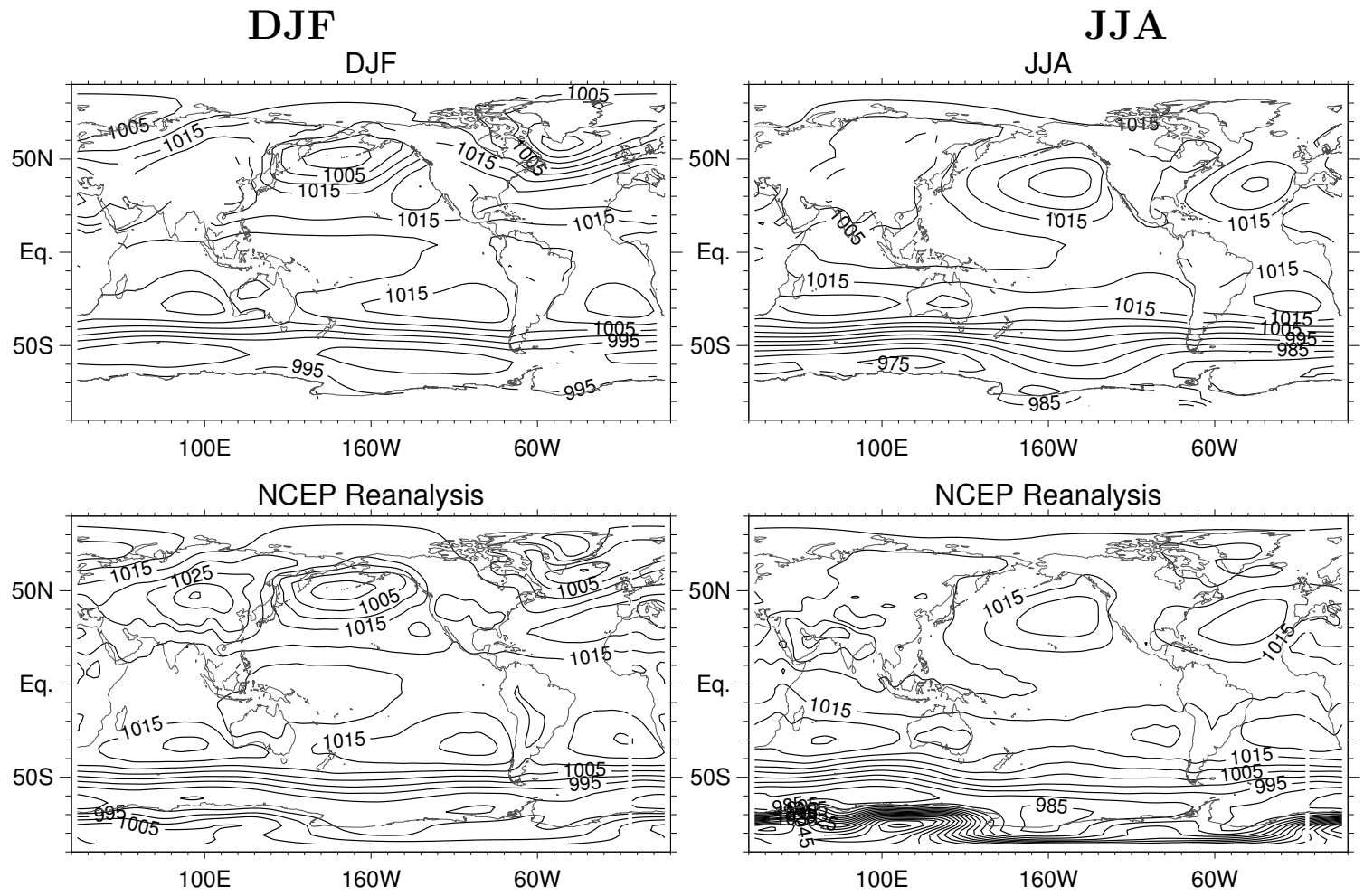

Figure 14a: Sea level pressure (mb). Upper panels: model; Lower panels: observations from NCEP Reanalysis; Left panels: December-January-February mean; Right panels: June-July-August mean. Contour interval is 5 mb.

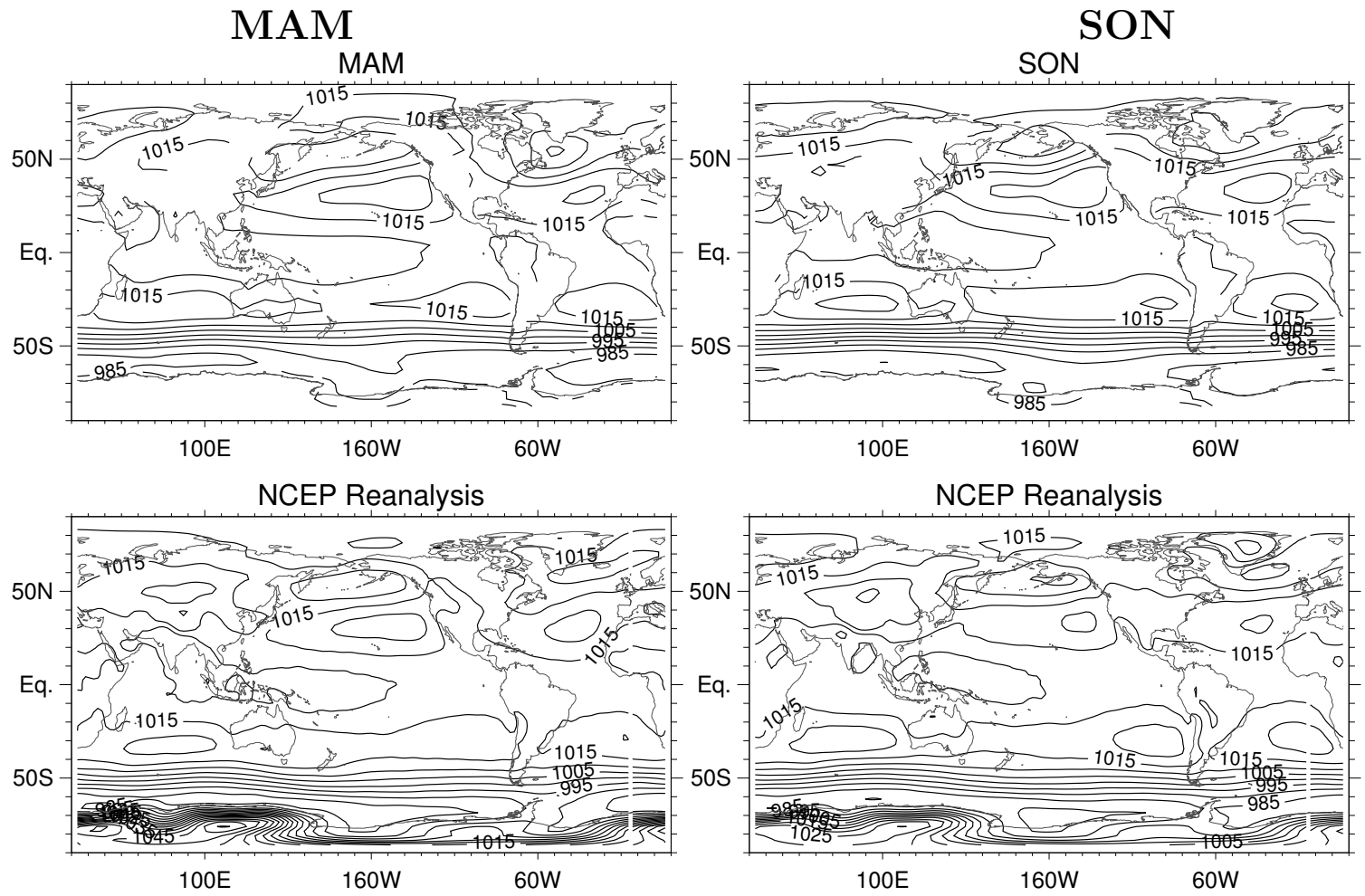

Figure 14b: Sea level pressure (mb). Upper panels: model; Lower panels: observations from NCEP Reanalysis; Left panels: March-April-May mean; Right panels: September-October-November mean. Contour interval is 5 mb.

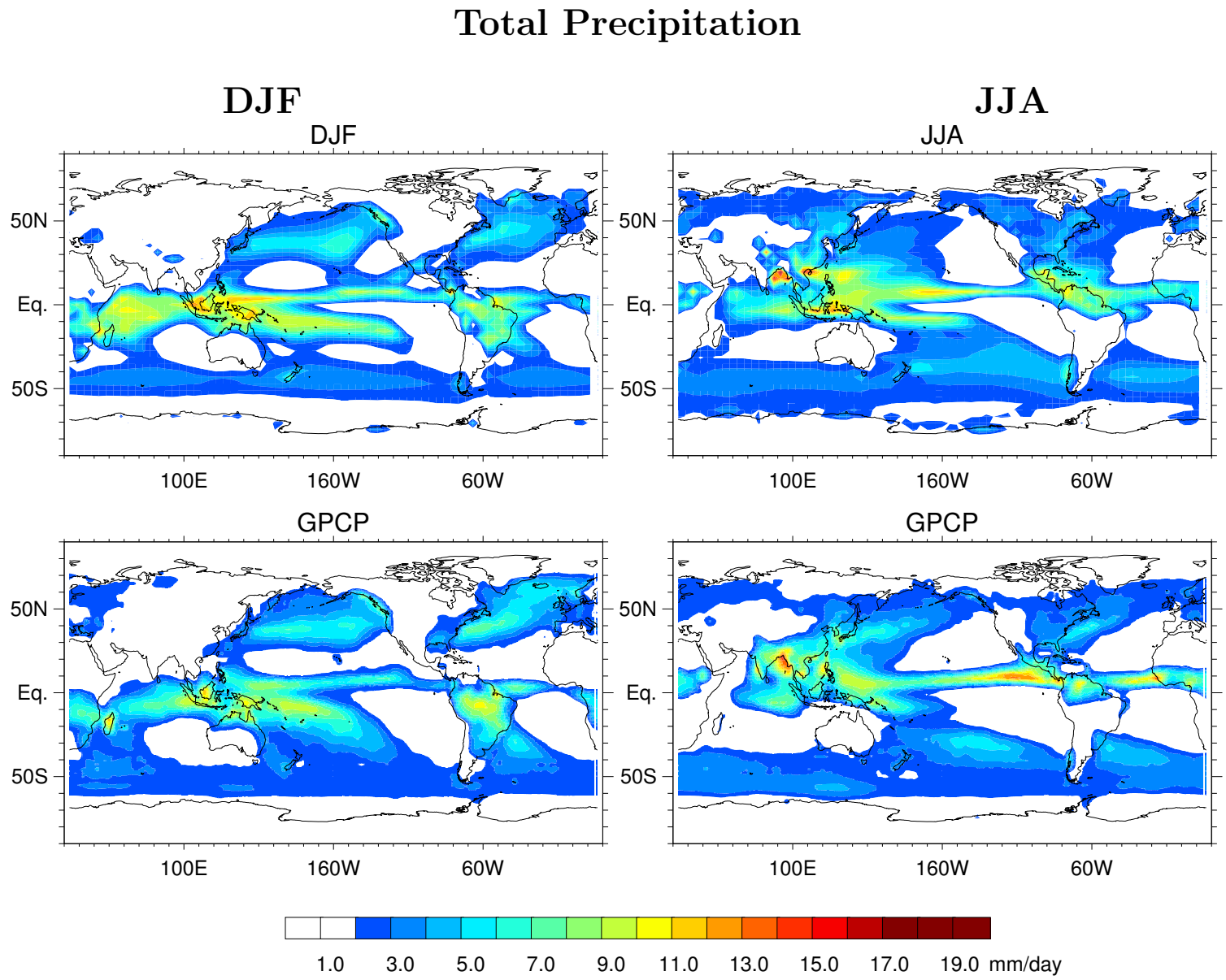

Figure 15a: Total precipitation (mm day^{-1}).Upper panels: model; Lower panels: observations from GPCP; Left panels: December-January-February mean; Right panels: June-July-August mean. Contour interval is 1 mm day^{-1}.

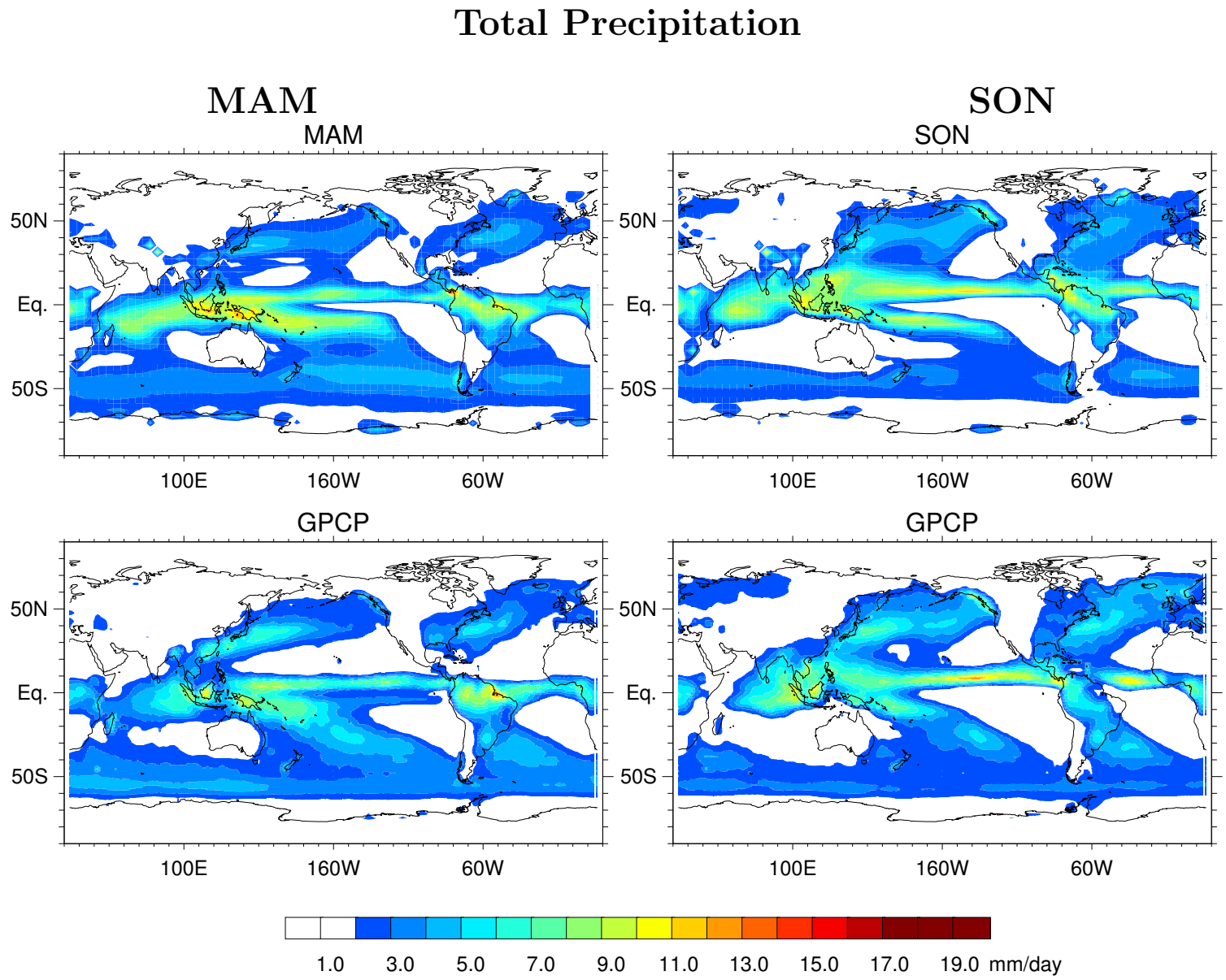

Figure 15b: Total precipitation (mm day^{-1}).Upper panels: model; Lower panels: observations from GPCP; Left panels: March-April-May mean; Right panels: September-October-November mean. Contour interval is 1 mm day^{-1}.

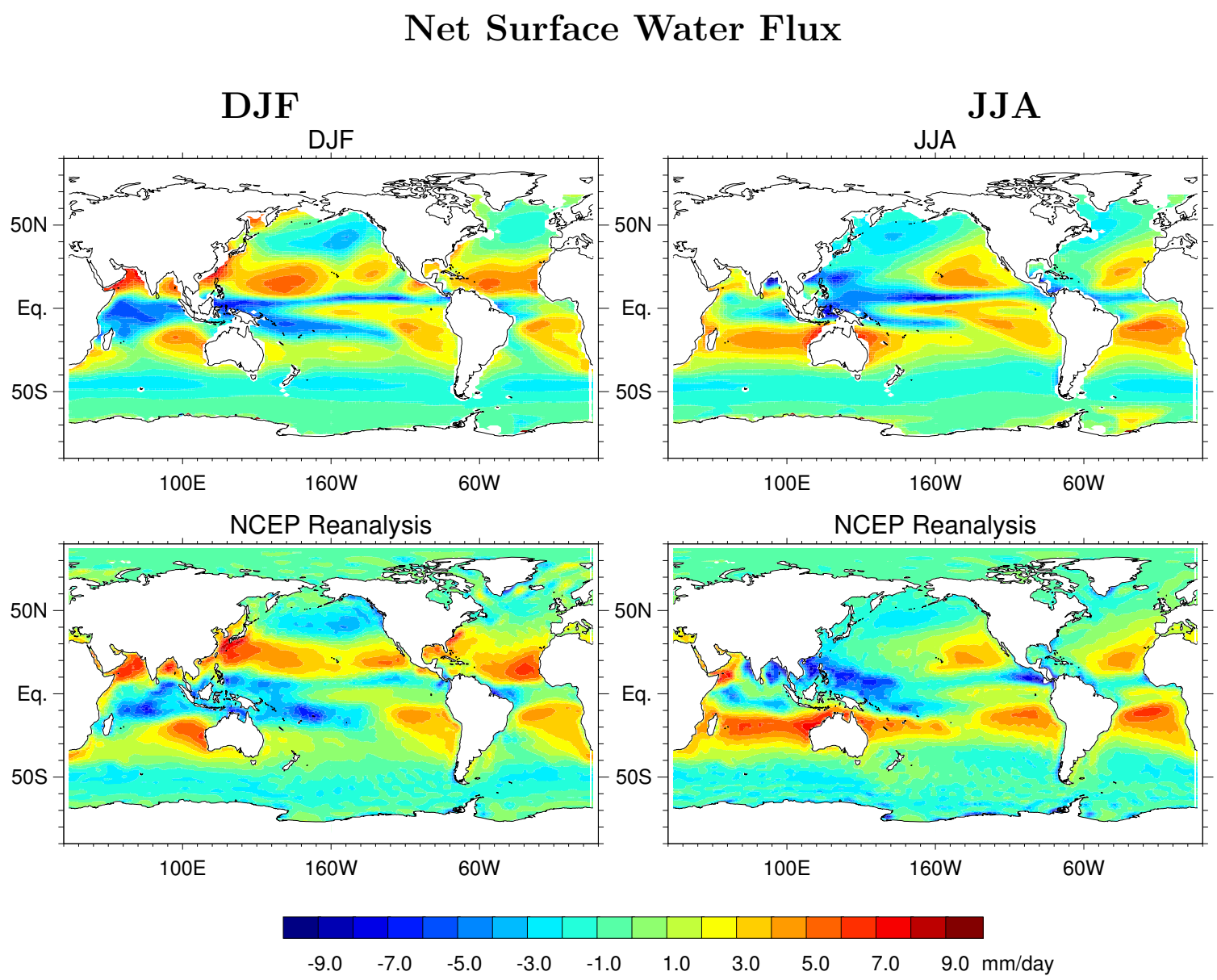

Figure 16a: Net surface water flux, expressed as evaporation minus precipitation (mm day^{-1}).Upper panels: model; Lower panels: observations from NCEP Reanalysis; Left panels: December-January-February mean; Right panels: June-July-August mean. Contour interval is 1 mm day^{-1}.

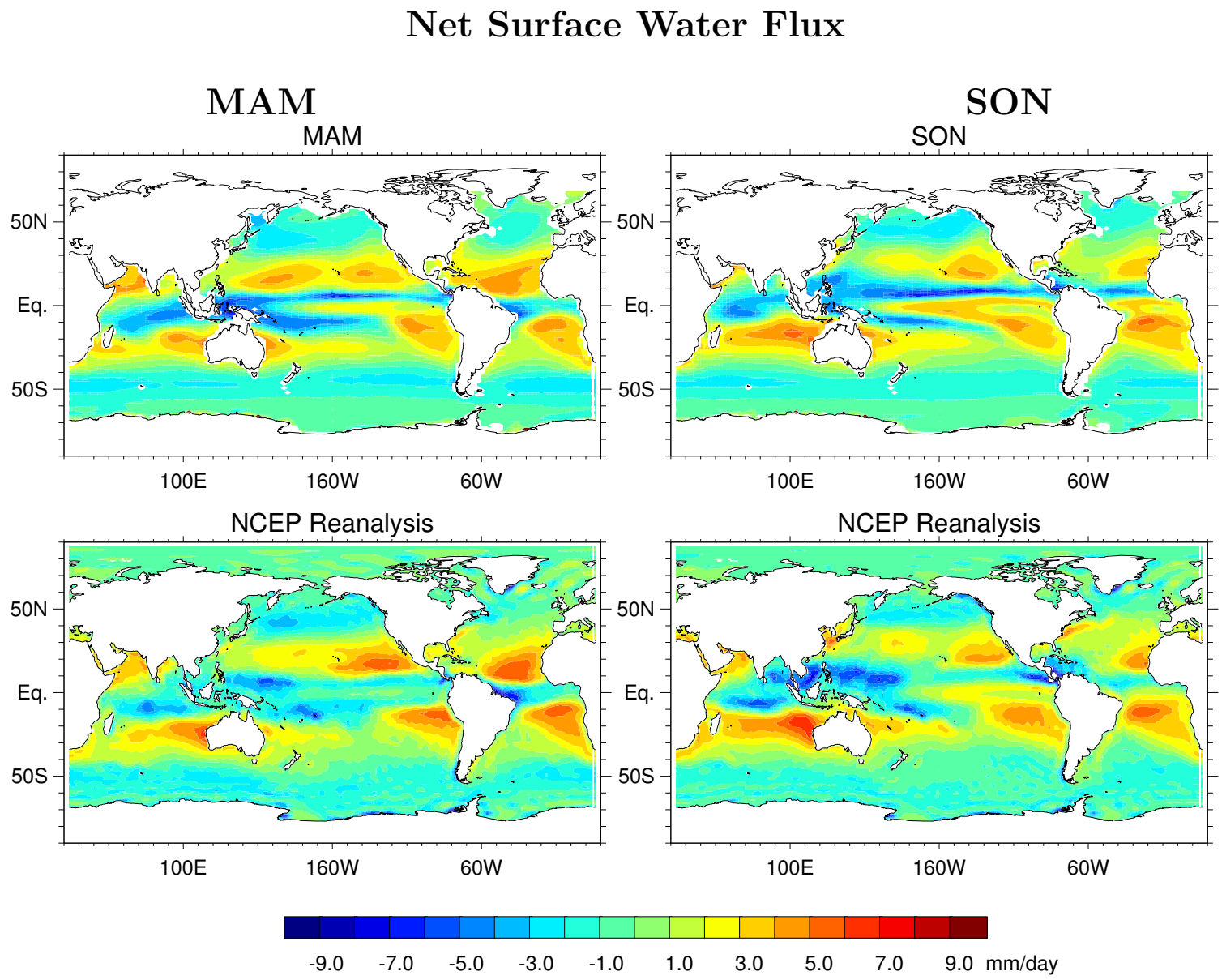

Figure 16b: Net surface water flux, expressed as evaporation minus precipitation (mm day^{-1}).Upper panels: model; Lower panels: observations from NCEP Reanalysis; Left panels: March-April-May mean; Right panels: September-October-November mean. Contour interval is 1 mm day^{-1}.

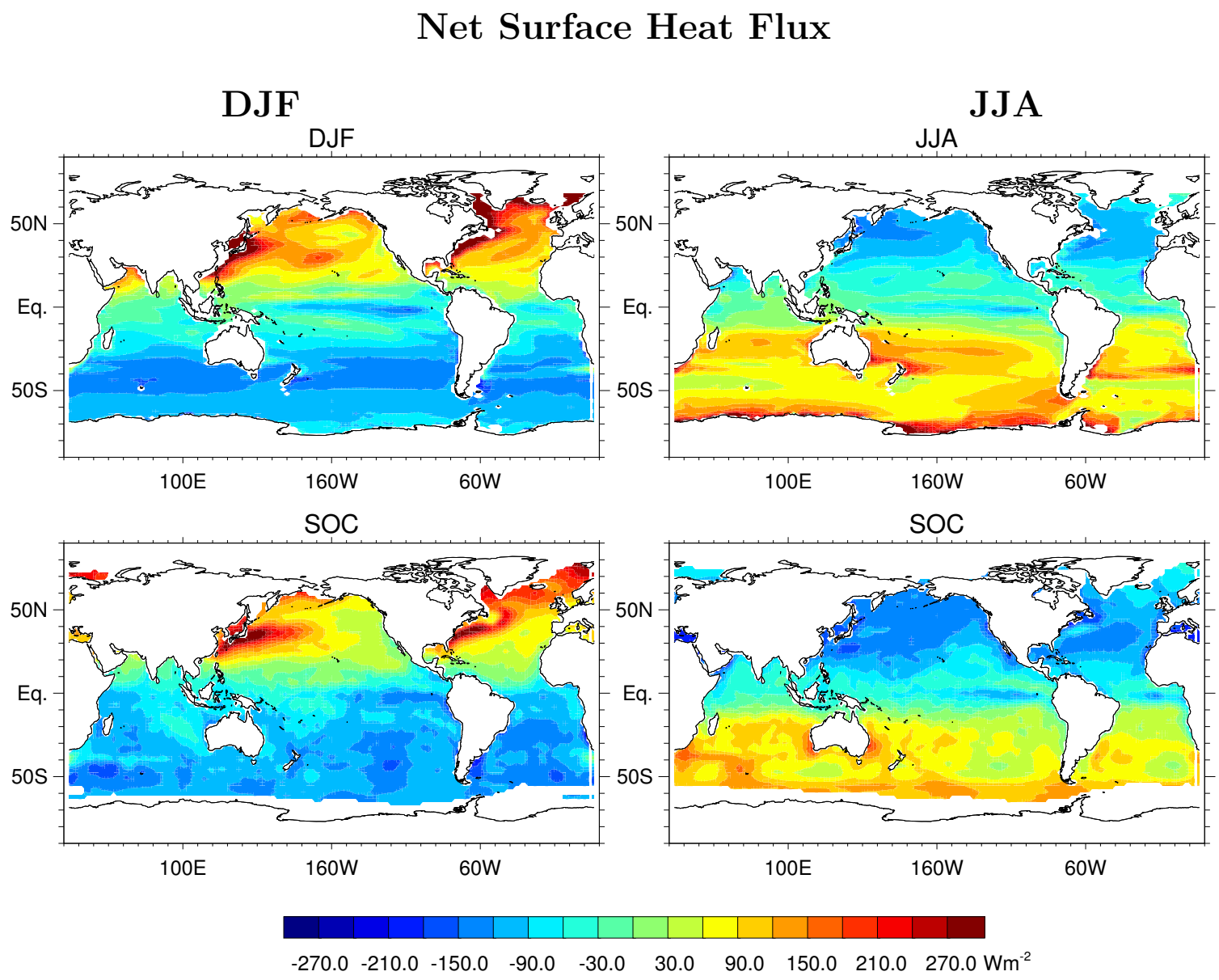

Figure 17a: Net surface heat flux (W m^{-2}). Positive values indicate a net upward flux. Upper panels: model; Lower panels: observations from Southampton Oceanography Centre; Left panels: December-January-February mean; Right panels: June-July-August mean. Contour interval is 30 W m^{-2}.

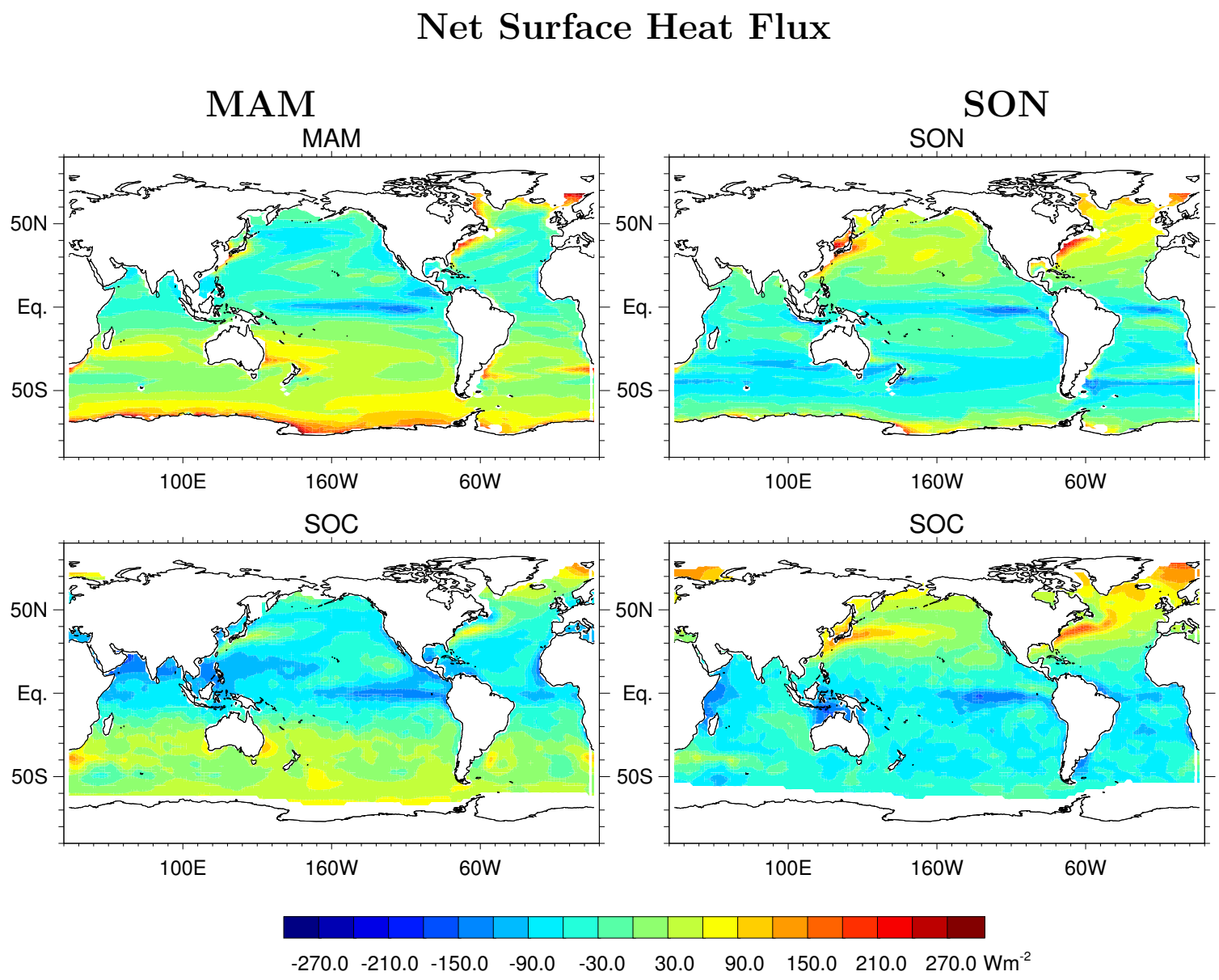

Figure 17b: Net surface heat flux (W m^{-2}). Positive values indicate a net upward flux. Upper panels: model; Lower panels: observations from Southampton Oceanography Centre; Left panels: March-April-May mean; Right panels: September-October-November mean. Contour interval is 30 W m^{-2}.

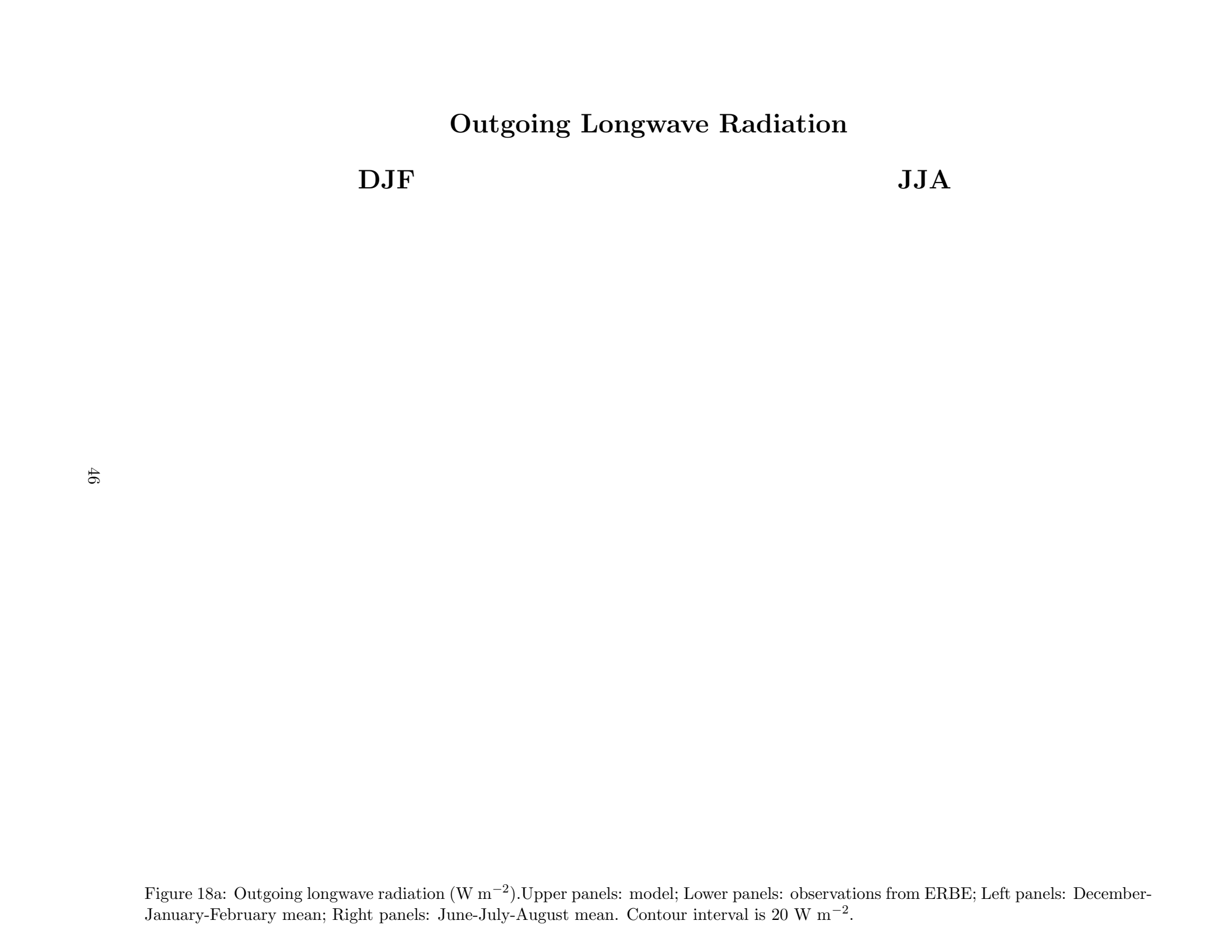

Figure 18a: Outgoing longwave radiation (W m^{-2}).Upper panels: model; Lower panels: observations from ERBE; Left panels: December-January-February mean; Right panels: June-July-August mean. Contour interval is 20 W m^{-2}.

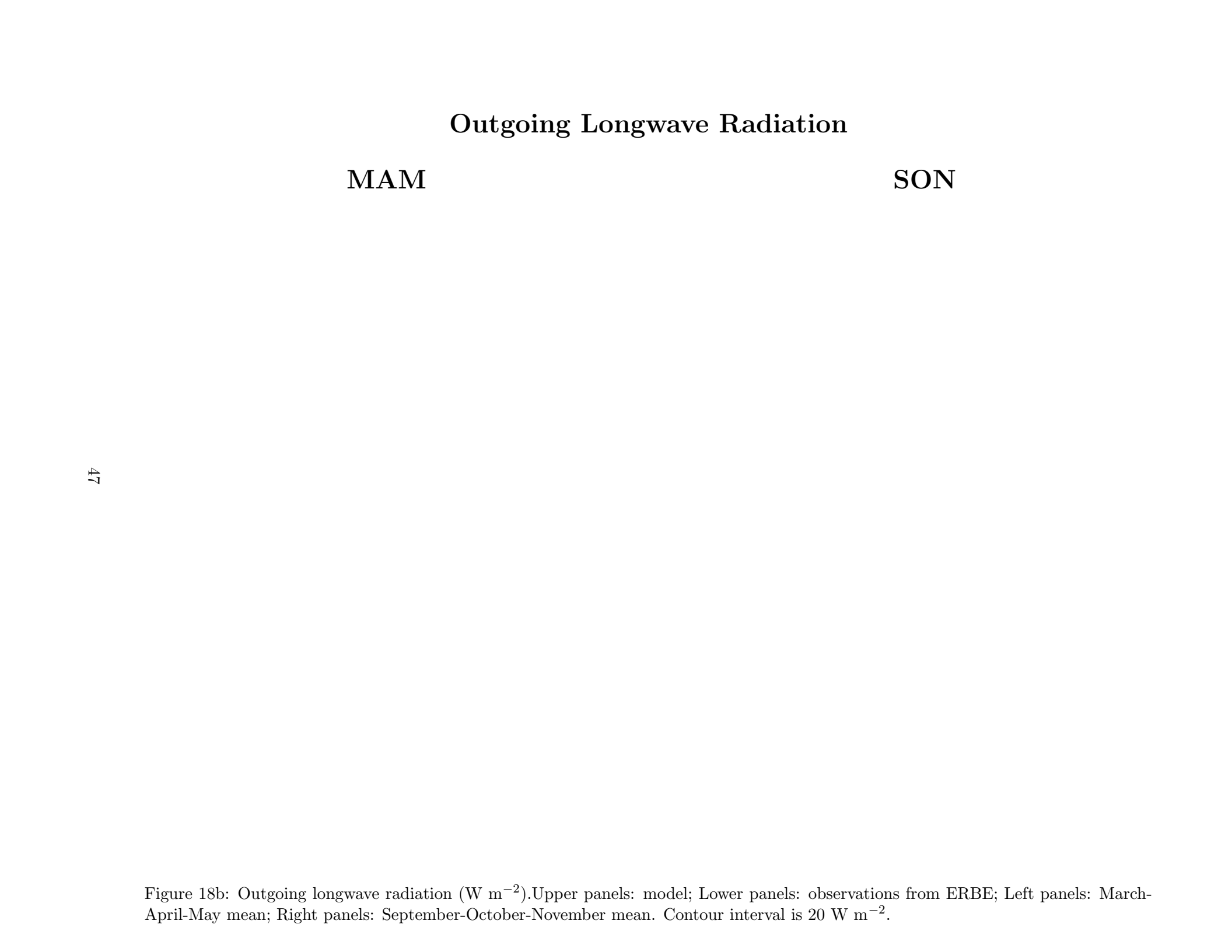

Figure 18b: Outgoing longwave radiation (W m^{-2}).Upper panels: model; Lower panels: observations from ERBE; Left panels: March-April-May mean; Right panels: September-October-November mean. Contour interval is 20 W m^{-2}.

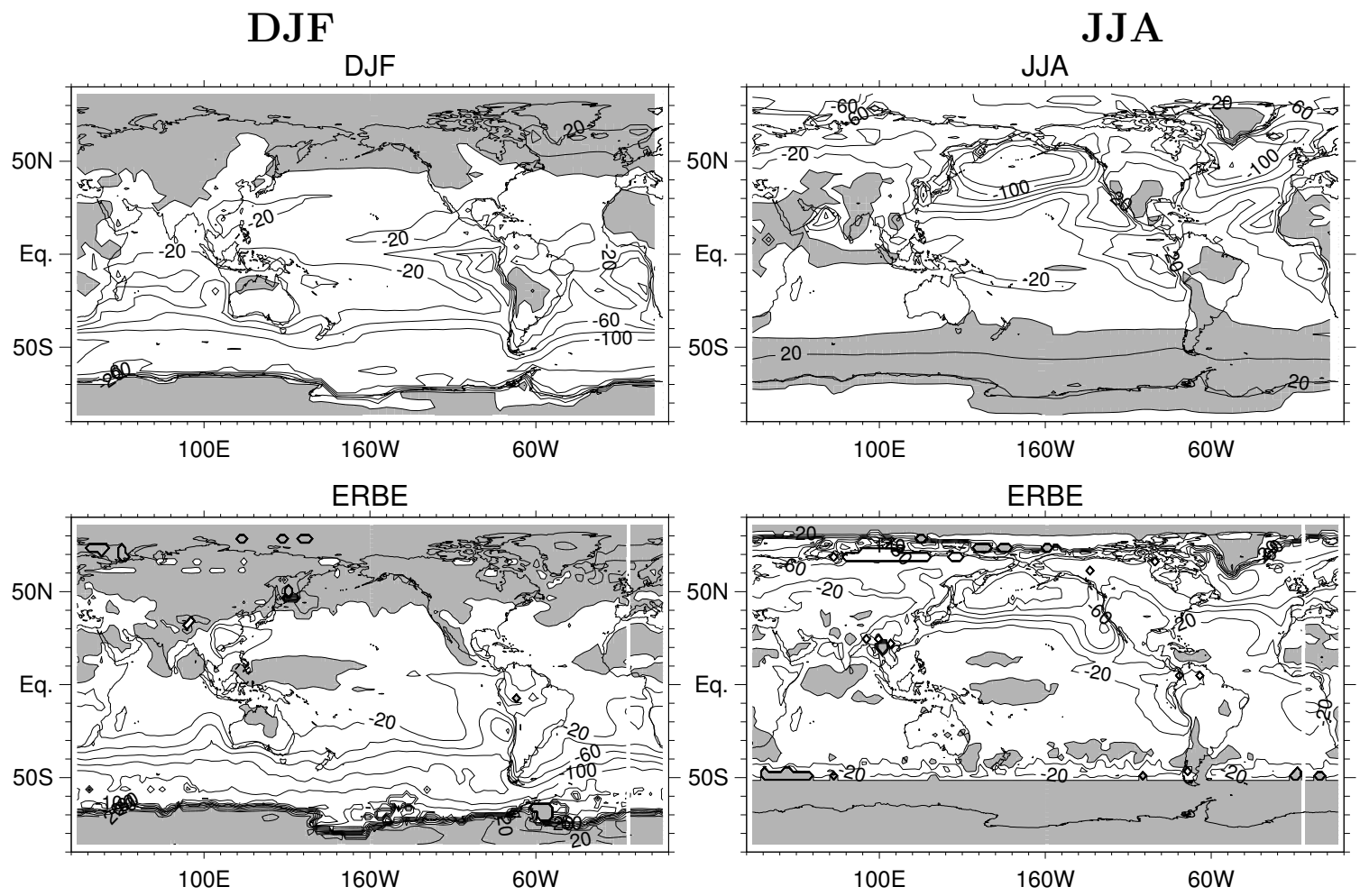

Figure 19a: Net cloud radiative forcing (W m^{-2}).Upper panels: model; Lower panels: observations from ERBE; Left panels: December-January-February mean; Right panels: June-July-August mean. Contour interval is 20 W m^{-2}.

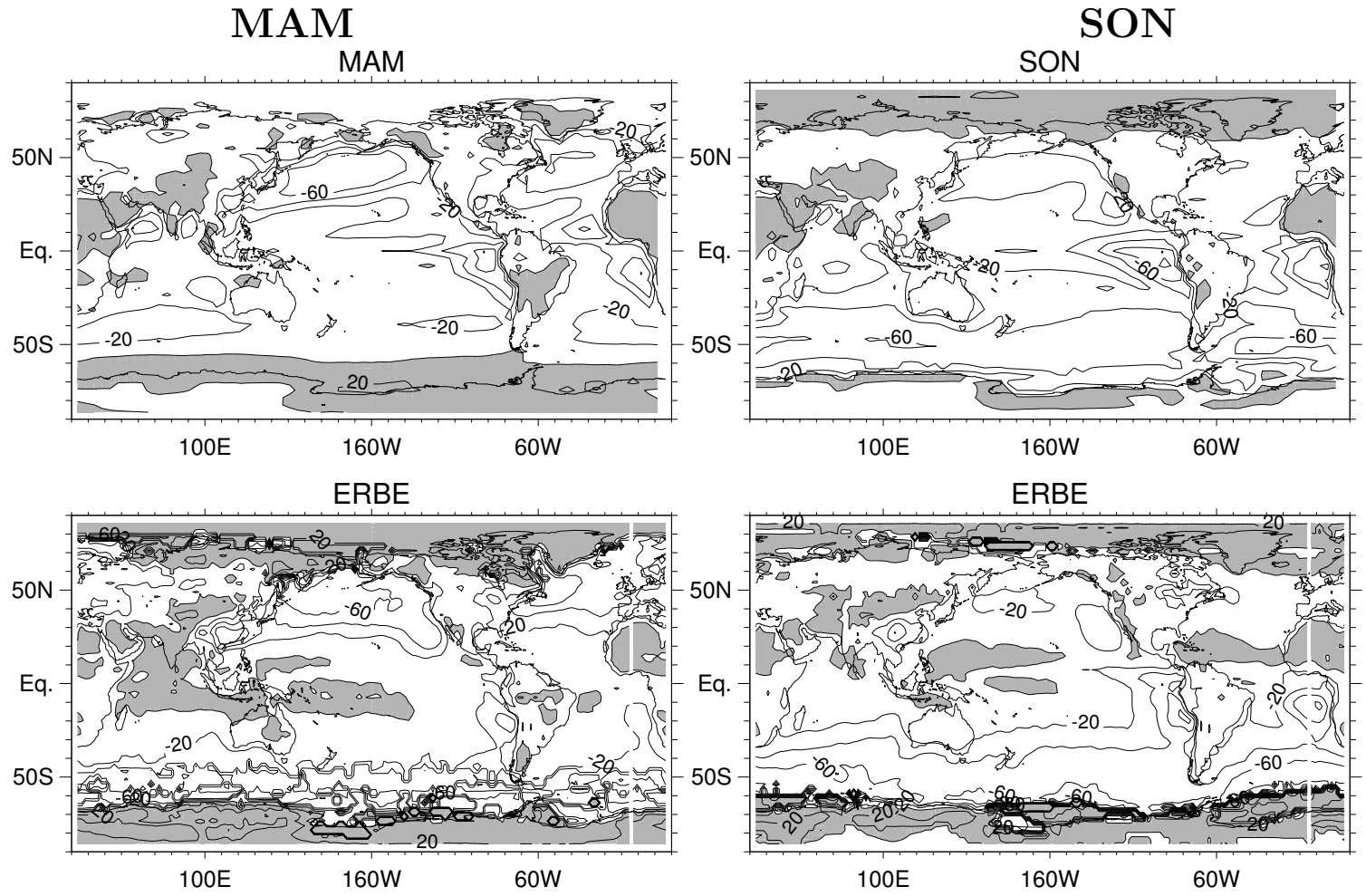

Figure 19b: Net cloud radiative forcing (W m^{-2}).Upper panels: model; Lower panels: observations from ERBE; Left panels: March-April-May mean; Right panels: September-October-November mean. Contour interval is 20 W m^{-2}.

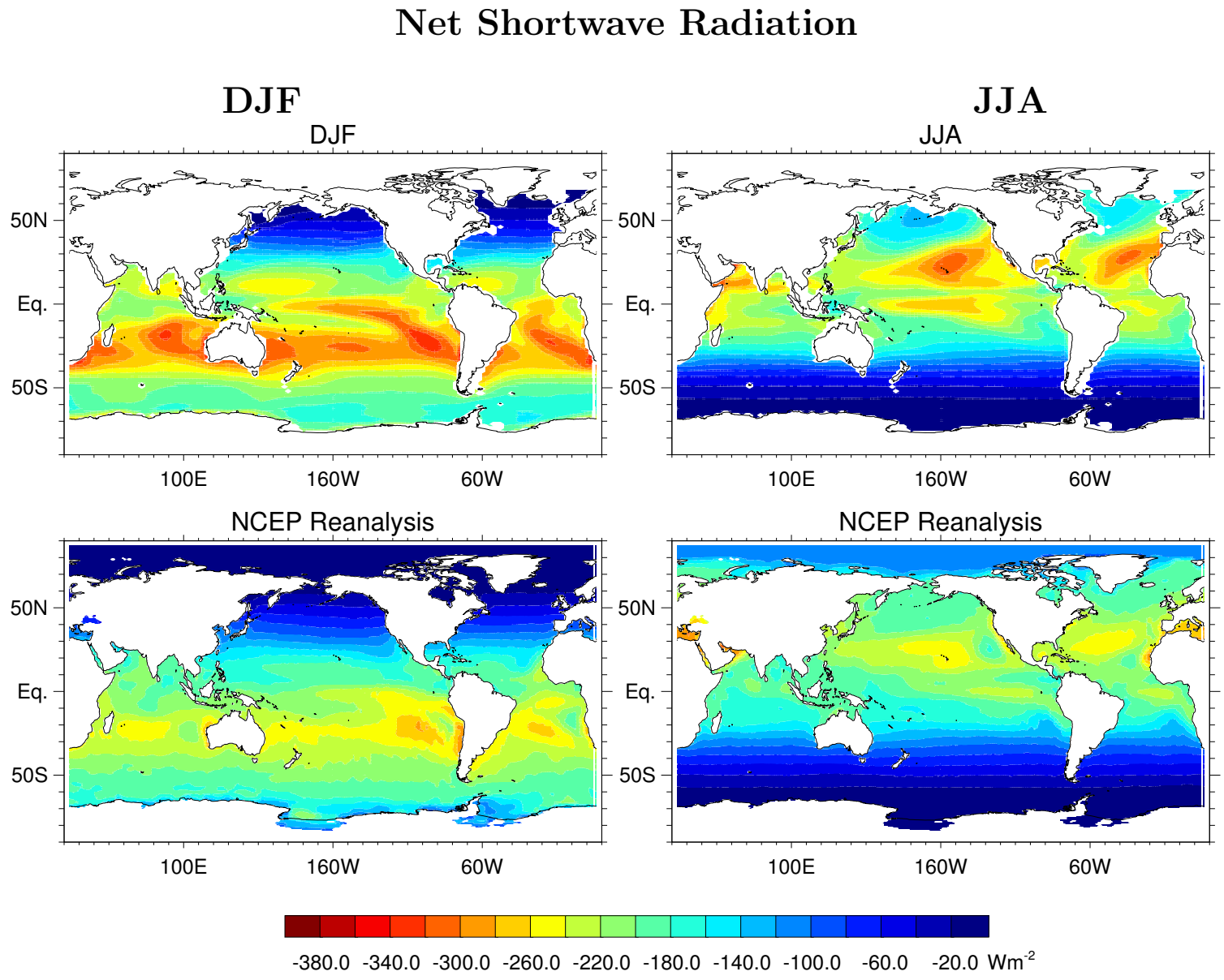

Figure 20a: Net shortwave radiation at surface (W m^{-2}). Positive values indicate upward flux. Upper panels: model; Lower panels: observations from ERBE; Left panels: December-January-February mean; Right panels: June-July-August mean. Contour interval is 20 W m^{-2}.

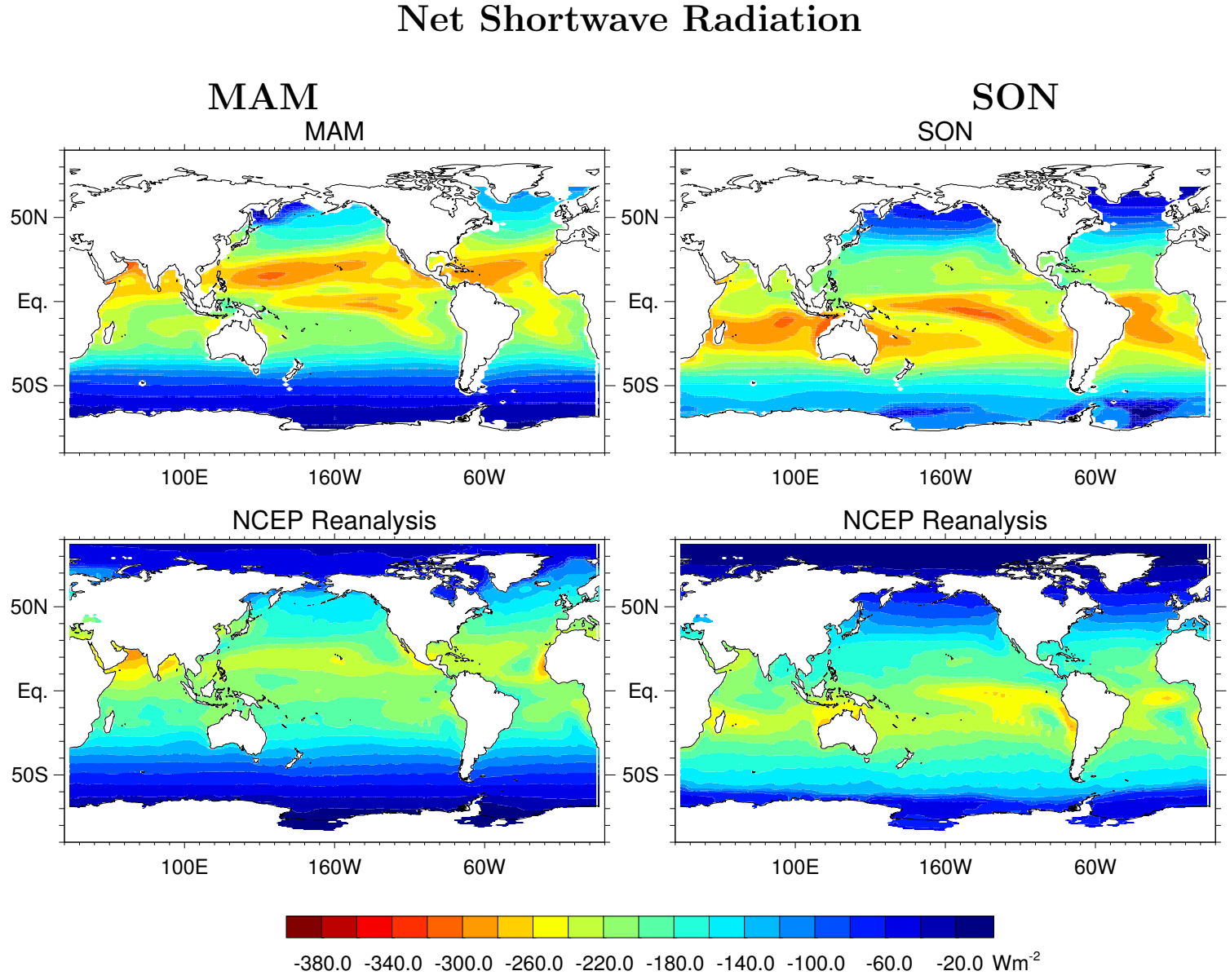

Figure 20b: Net shortwave radiation at surface (W m^{-2}). Positive values indicate upward flux. Upper panels: model; Lower panels: observations from ERBE; Left panels: March-April-May mean; Right panels: September-October-November mean. Contour interval is 20 W m^{-2}.

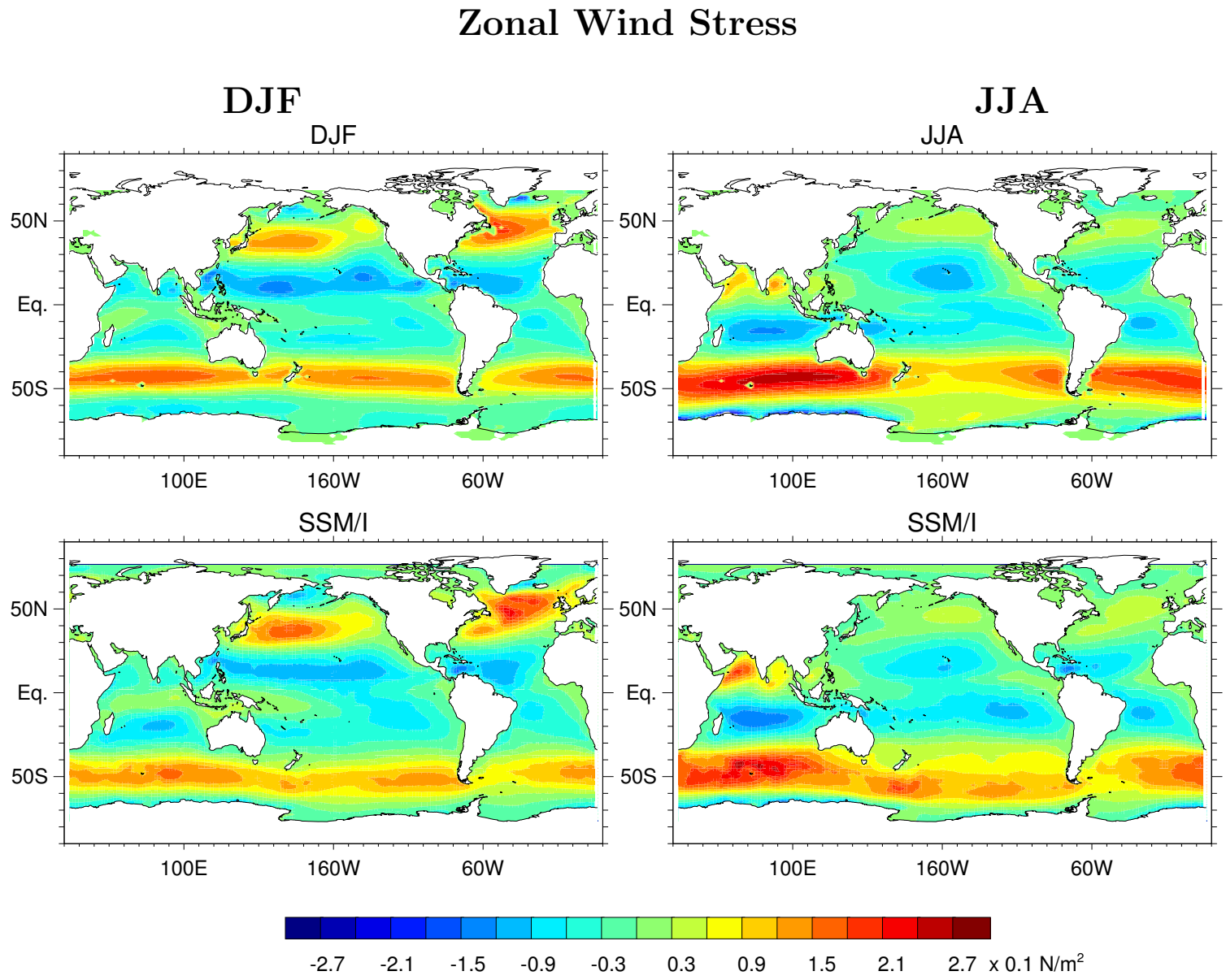

Figure 21a: Zonal wind stress (N m^{-2}). Upper panels: model; Lower panels: observations from SSM/I; Left panels: December-January-February mean; Right panels: June-July-August mean. Contour interval is 0.03 N m^{-2}.

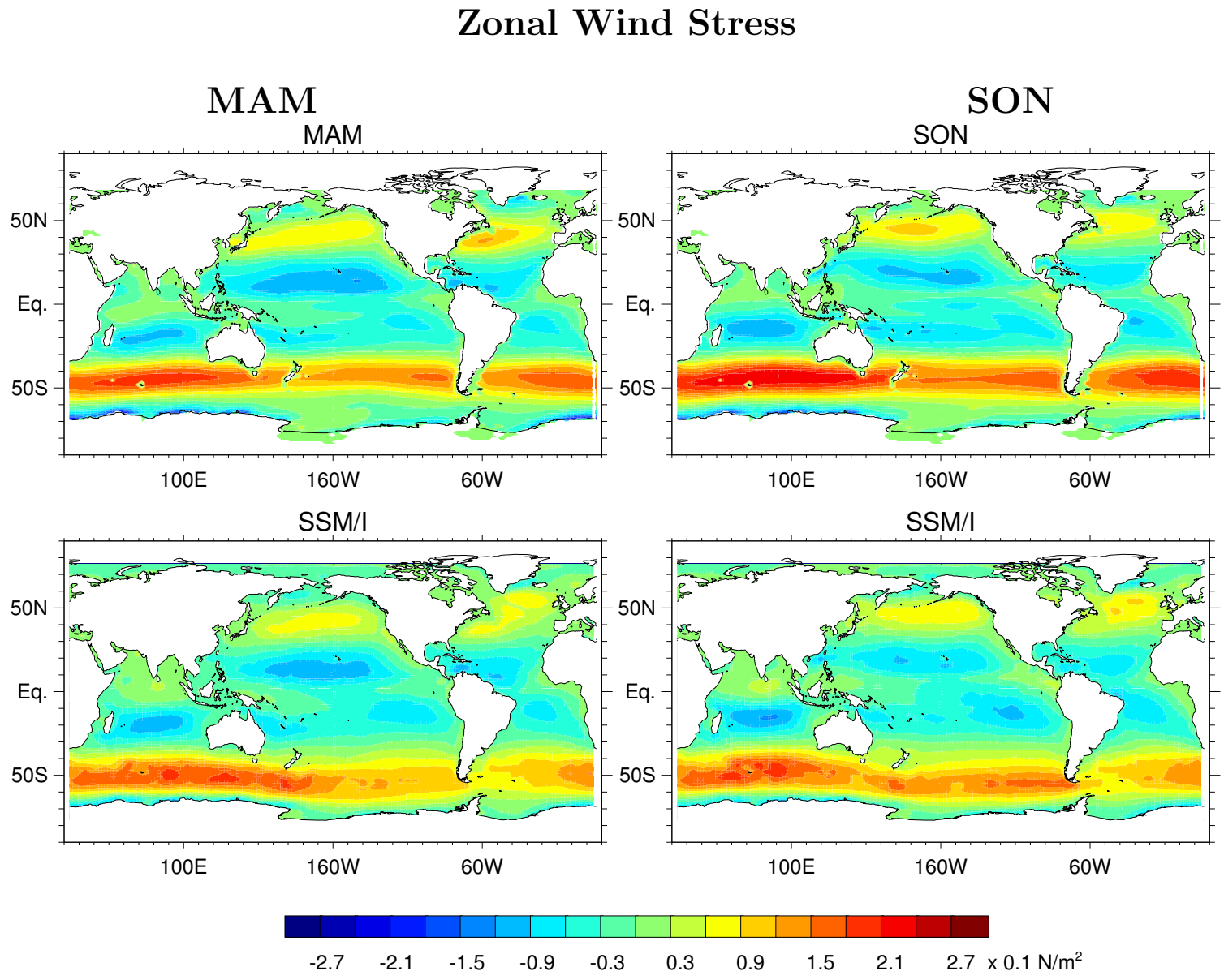

Figure 21b: Zonal wind stress (N m^{-2}). Upper panels: model; Lower panels: observations from SSM/I; Left panels: March-April-May mean; Right panels: September-October-November mean. Contour interval is 0.03 N m^{-2}.

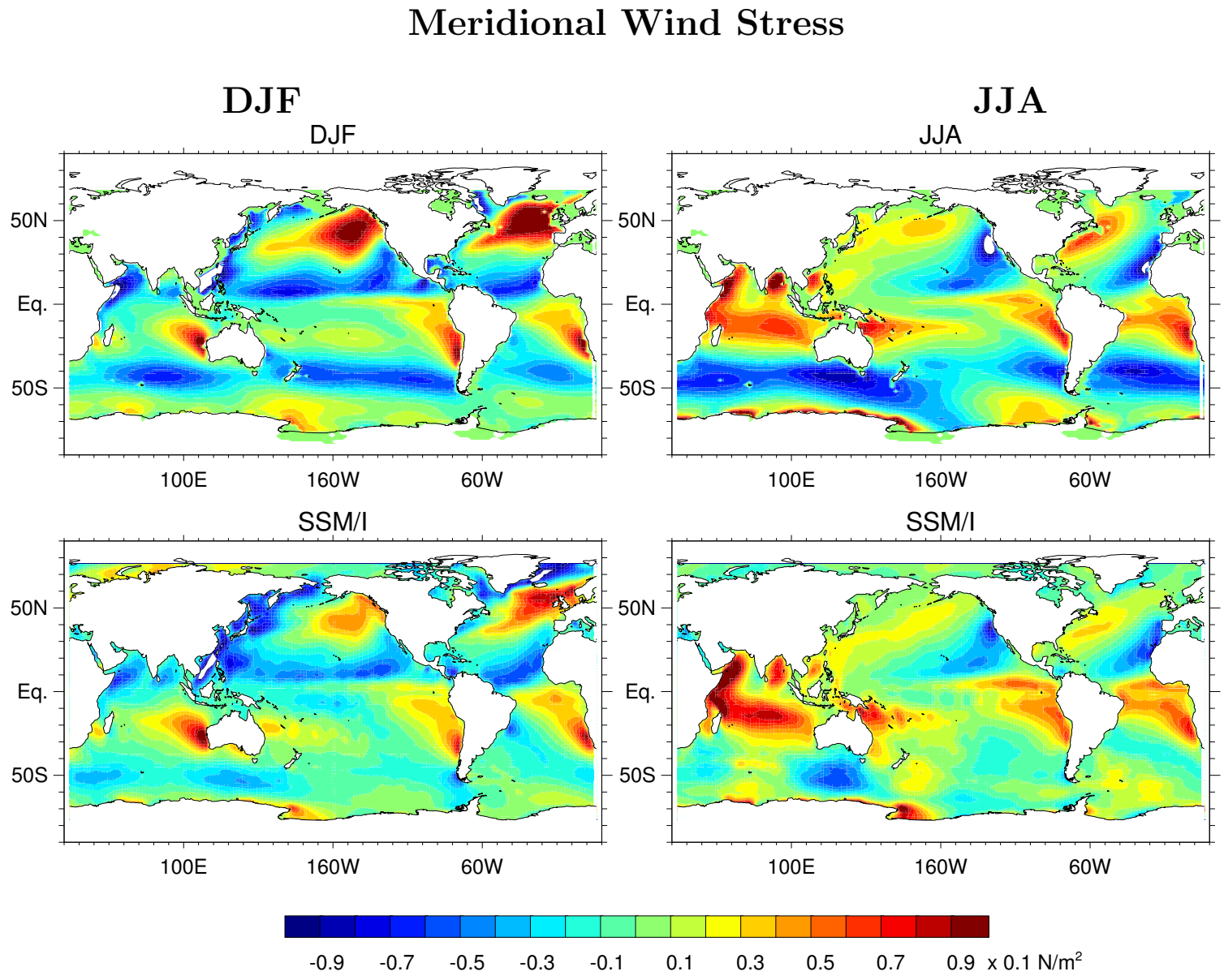

Figure 22a: Meridional wind stress (N m^{-2}). Upper panels: model; Lower panels: observations from SSM/I; Left panels: December-January-February mean; Right panels: June-July-August mean. Contour interval is 0.02 N m^{-2}.

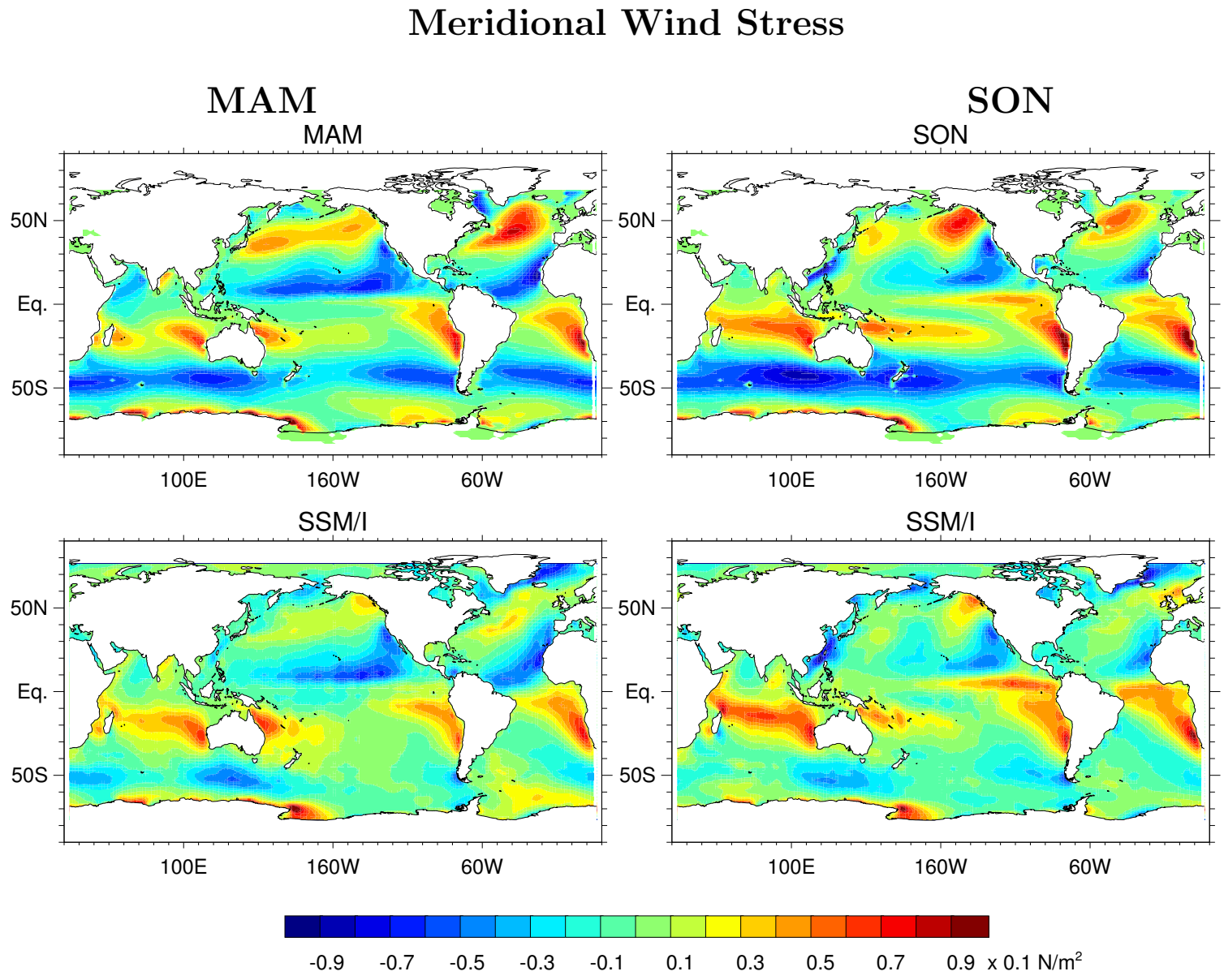

Figure 22b: Meridional wind stress (N m^{-2}). Upper panels: model; Lower panels: observations from SSM/I; Left panels: March-April-May mean; Right panels: September-October-November mean. Contour interval is 0.02 N m^{-2}.

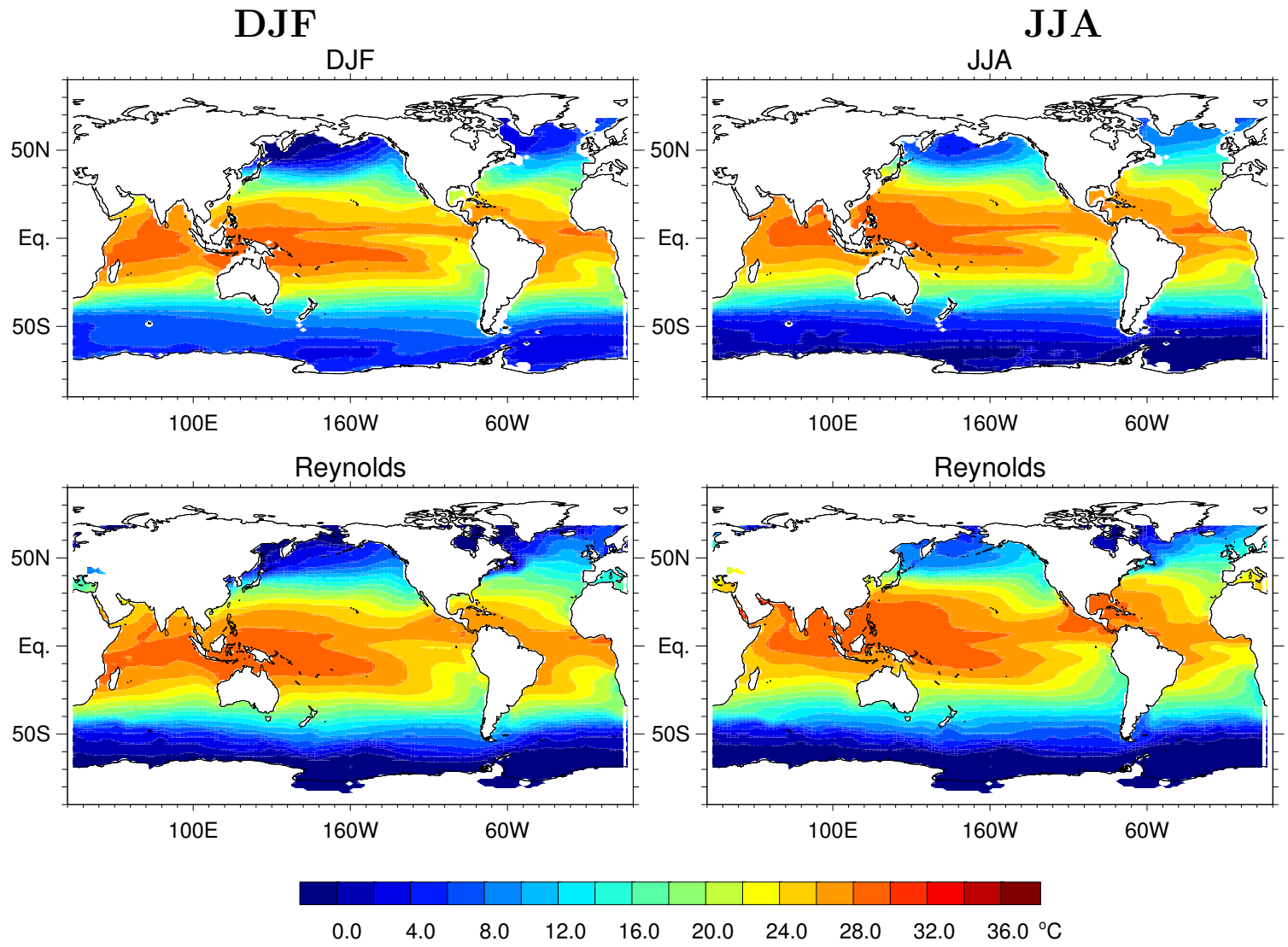

Figure 23a: Sea surface temperature (°C). Upper panels: model; Lower panels: observations from Reynolds and Smith (1994) OI SST; Left panels: December-January-February mean; Right panels: June-July-August mean. Contour interval is 2°C.

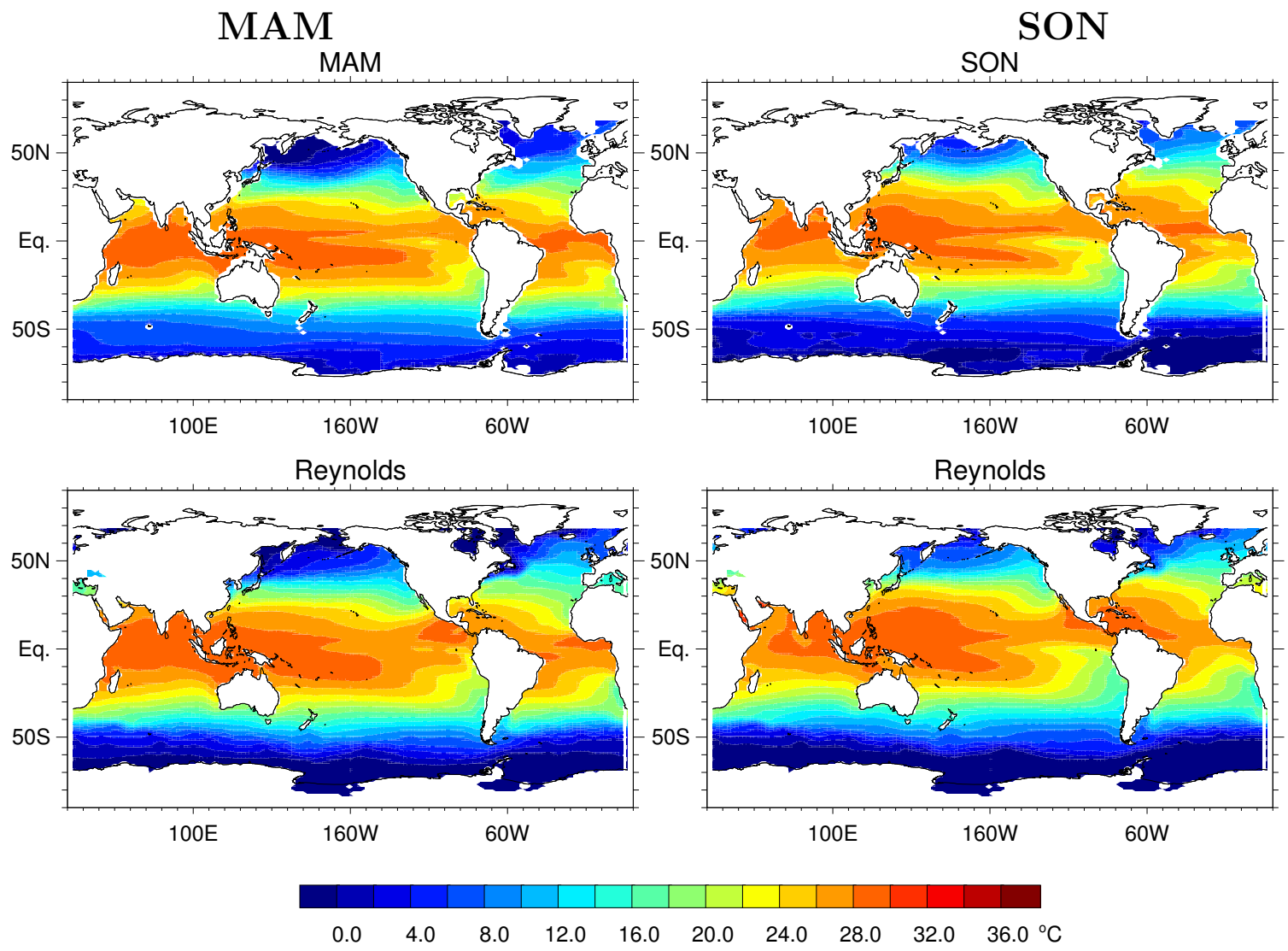

Figure 23b: Sea surface temperature (°C). Upper panels: model; Lower panels: observations from Reynolds and Smith (1994) OI SST; Left panels: March-April-May mean; Right panels: September-October-November mean. Contour interval is 2°C.

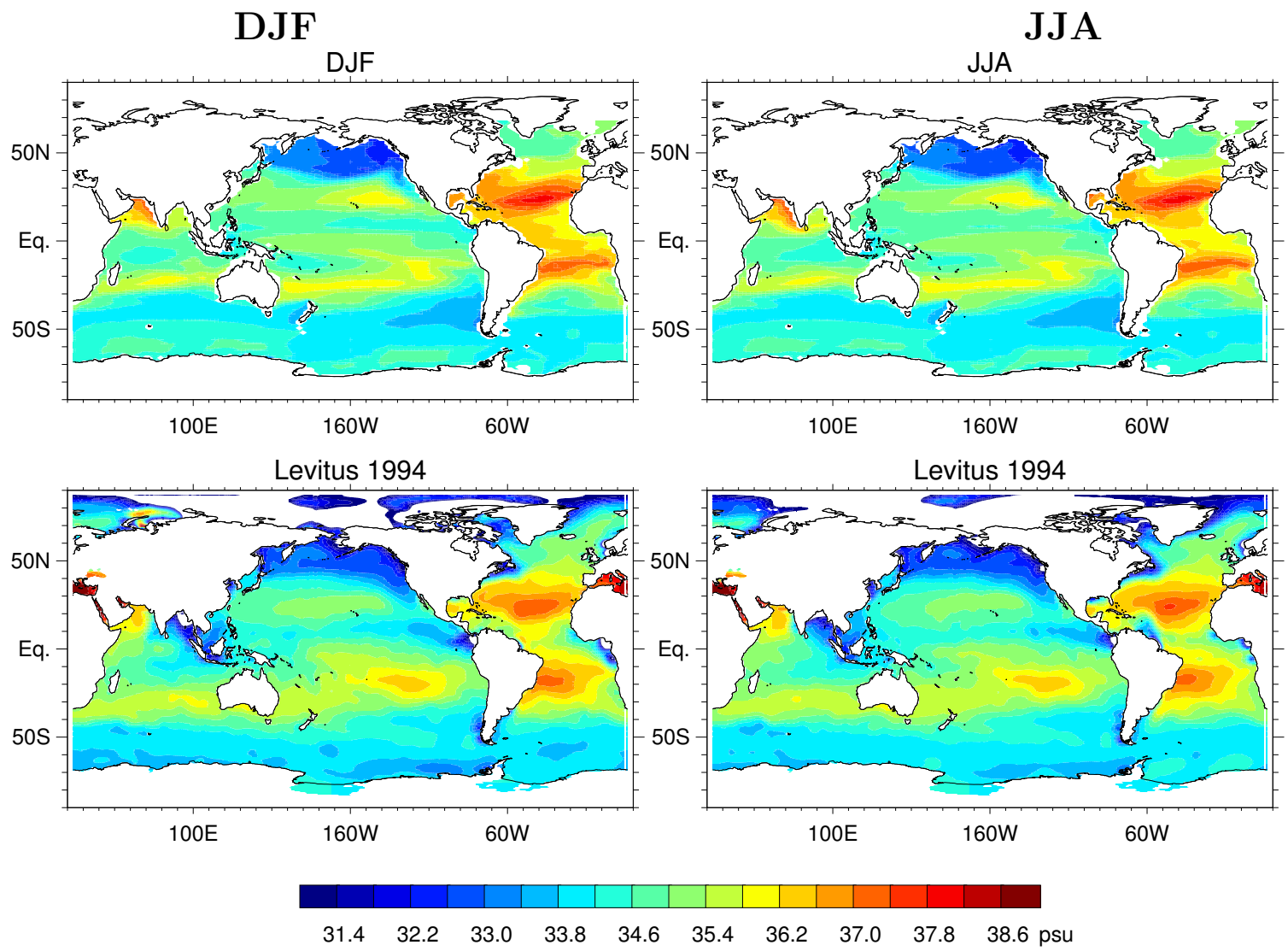

Figure 24a: Sea surface salinity.Upper panels: model; Lower panels: observations from World Ocean Atlas; Left panels: December-January-February mean; Right panels: June-July-August mean. Contour interval is 0.4.

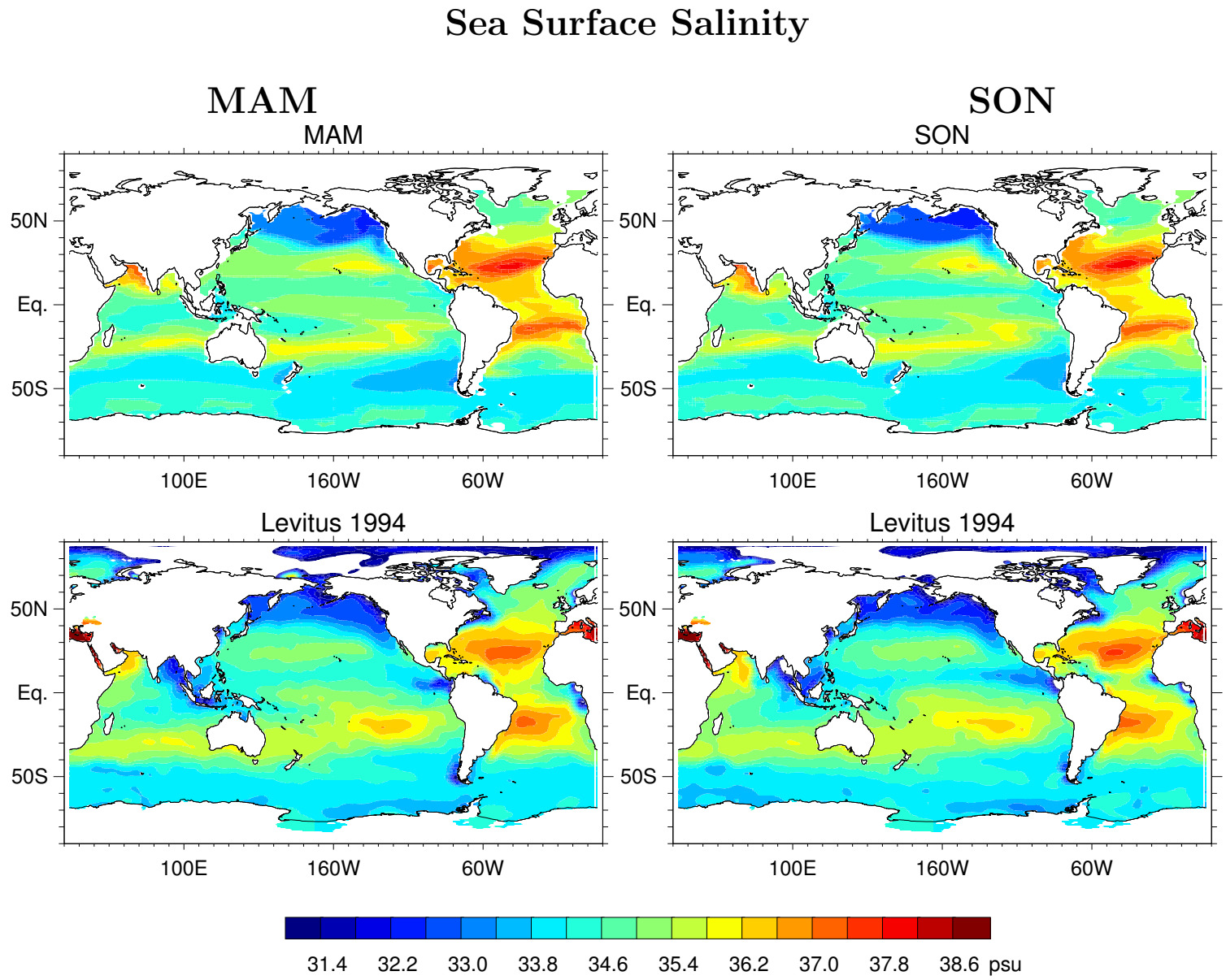

Figure 24b: Sea surface salinity.Upper panels: model; Lower panels: observations from World Ocean Atlas; Left panels: March-April-May mean; Right panels: September-October-November mean. Contour interval is 0.4.

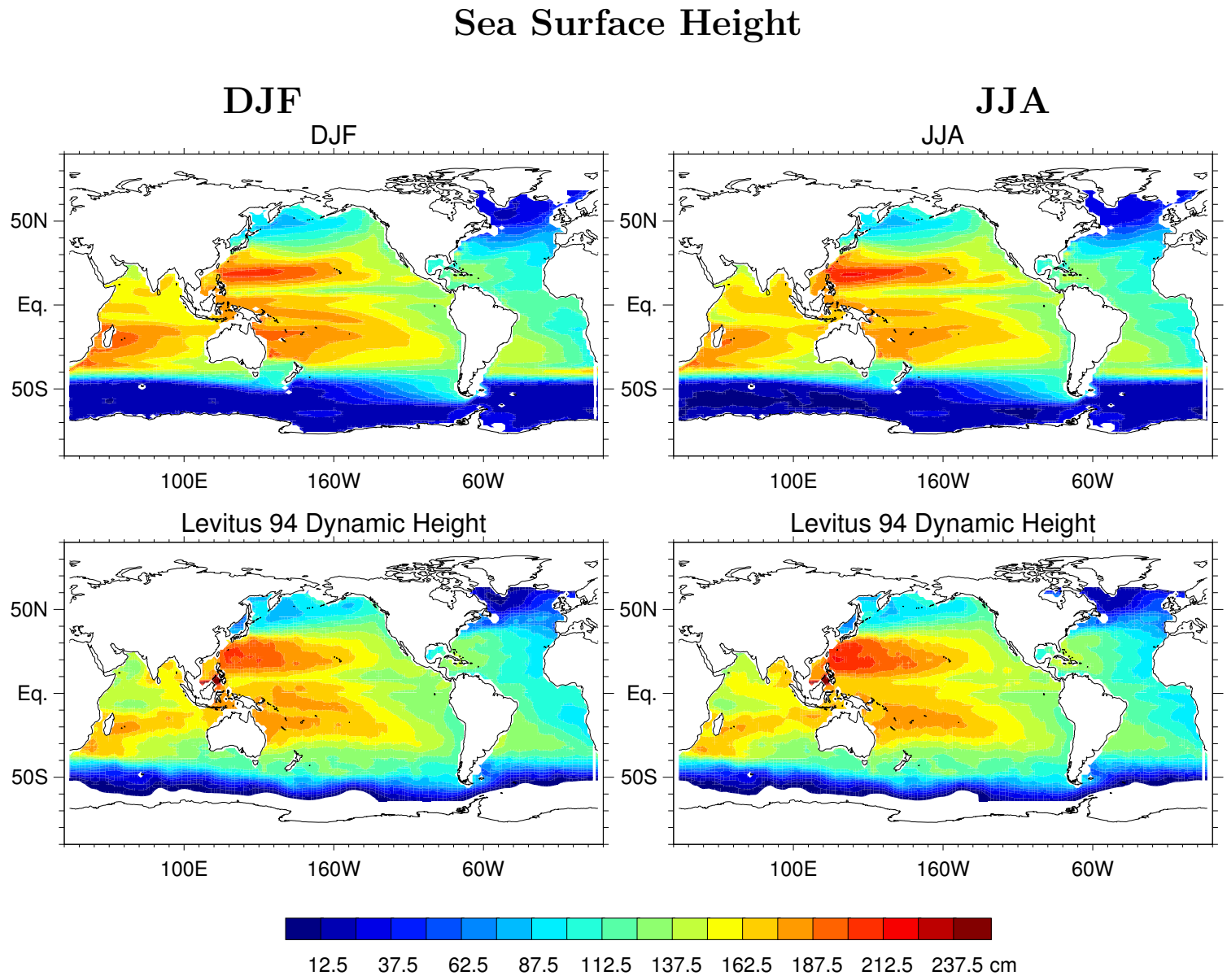

Figure 25a: Sea surface height (m).Upper panels: model; Lower panels: observations from World Ocean Atlas; Left panels: December-January-February mean; Right panels: June-July-August mean. Contour interval is 12.5 m.

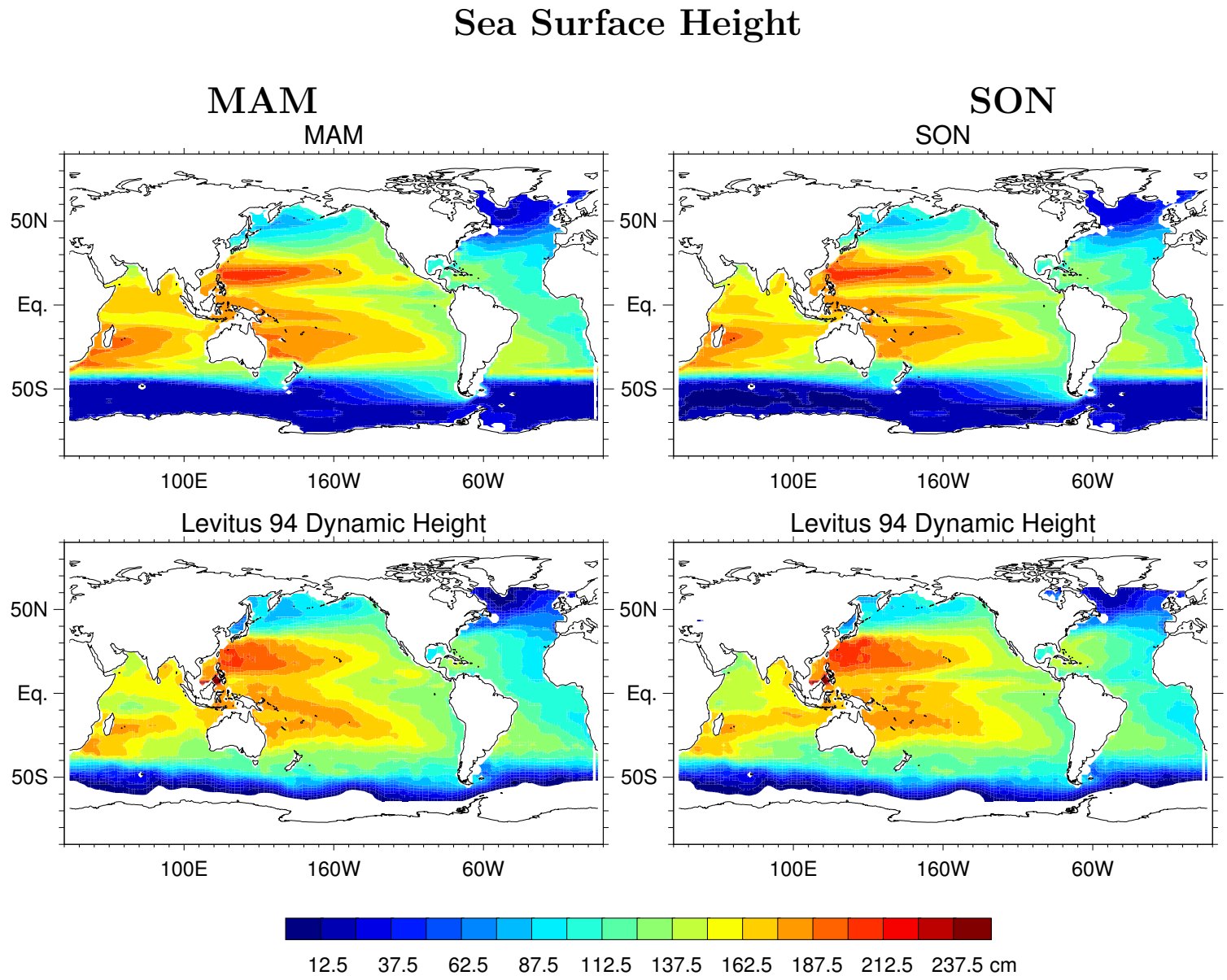

Figure 25b: Sea surface height (m).Upper panels: model; Lower panels: observations from World Ocean Atlas; Left panels: March-April-May mean; Right panels: September-October-November mean. Contour interval is 12.5 m.

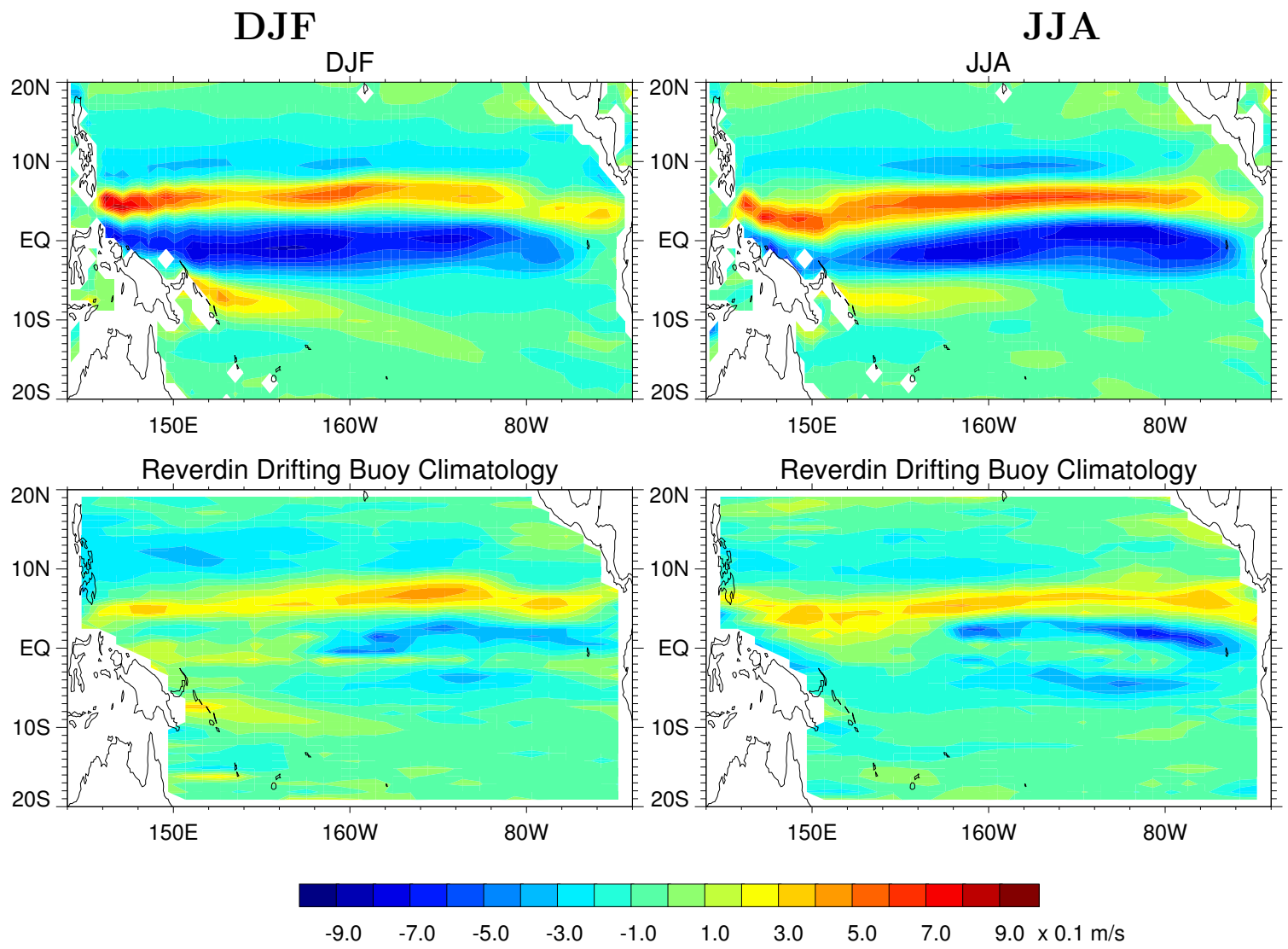

Figure 26a: Zonal surface current (m s^{-1}). Upper panels: model; Lower panels: observations from Reverdin; Left panels: December-January-February mean; Right panels: June-July-August mean. Contour interval is 0.1 m s^{-1}.

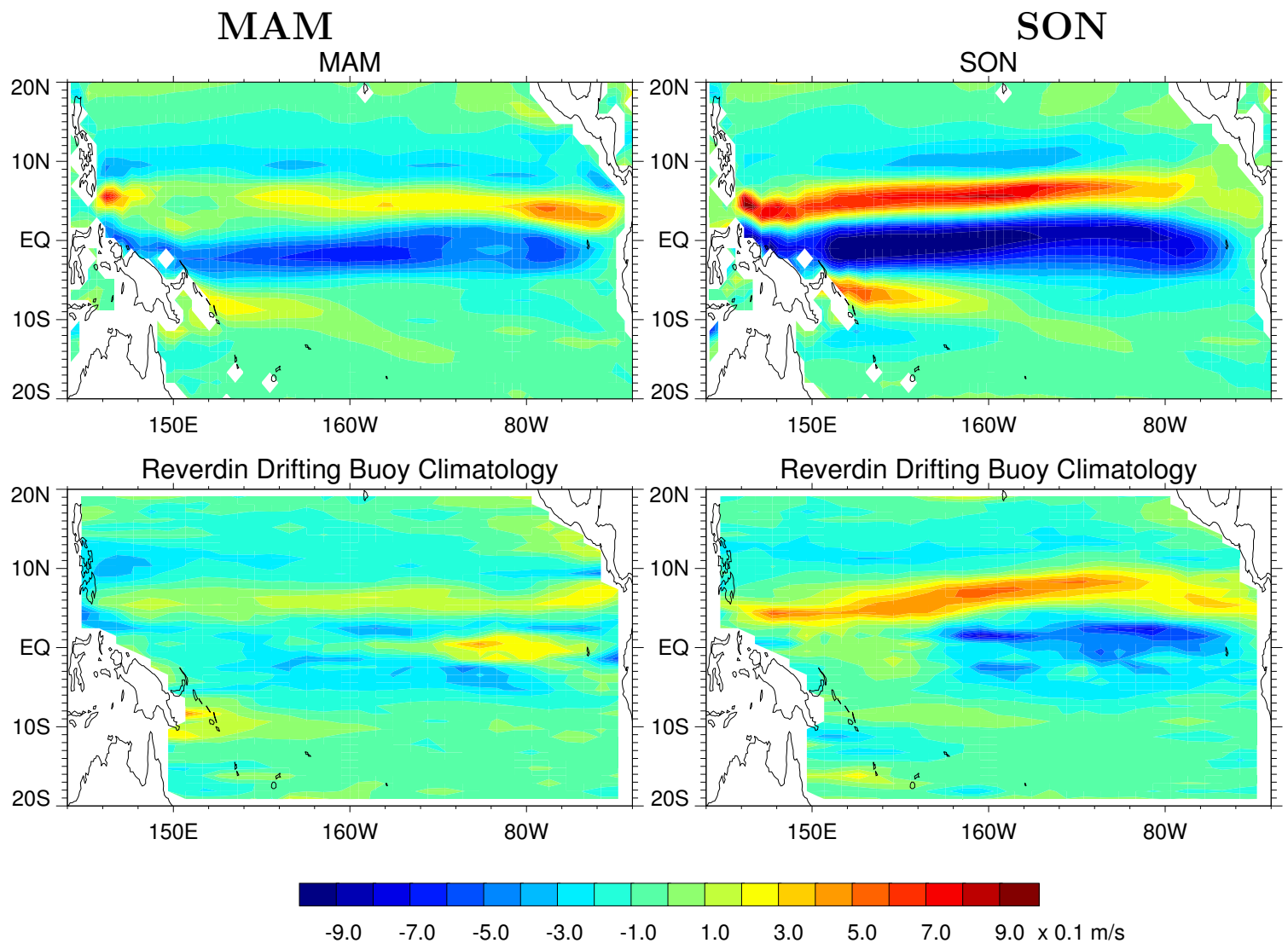

Figure 26b: Zonal surface current (m s^{-1}). Upper panels: model; Lower panels: observations from Reverdin; Left panels: March-April-May mean; Right panels: September-October-November mean. Contour interval is 0.1 m s^{-1}.

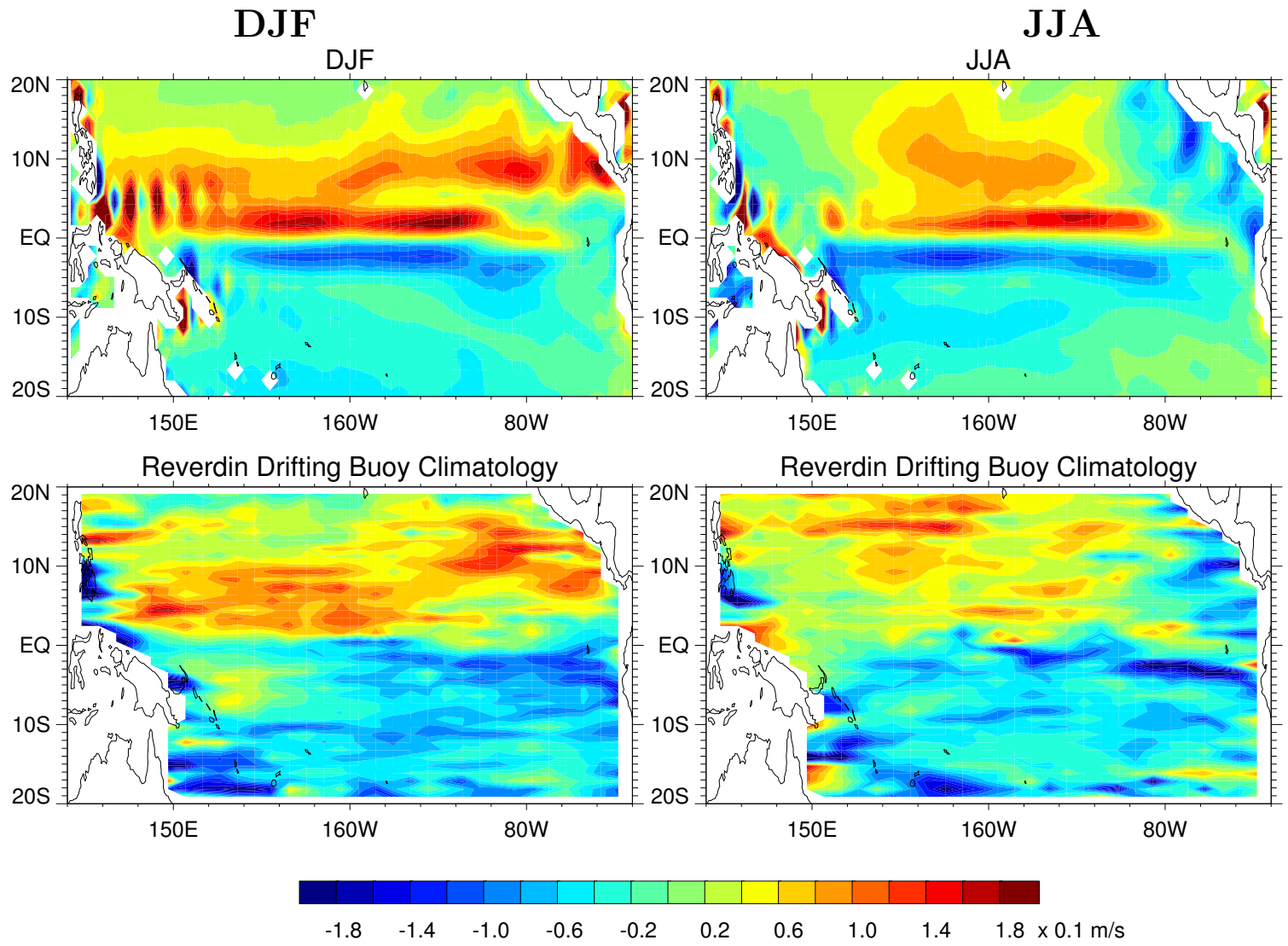

Figure 27a: Meridional surface current (m s^{-1}). Upper panels: model; Lower panels: observations from Reverdin; Left panels: December-January-February mean; Right panels: June-July-August mean. Contour interval is 0.02 m s^{-1}.

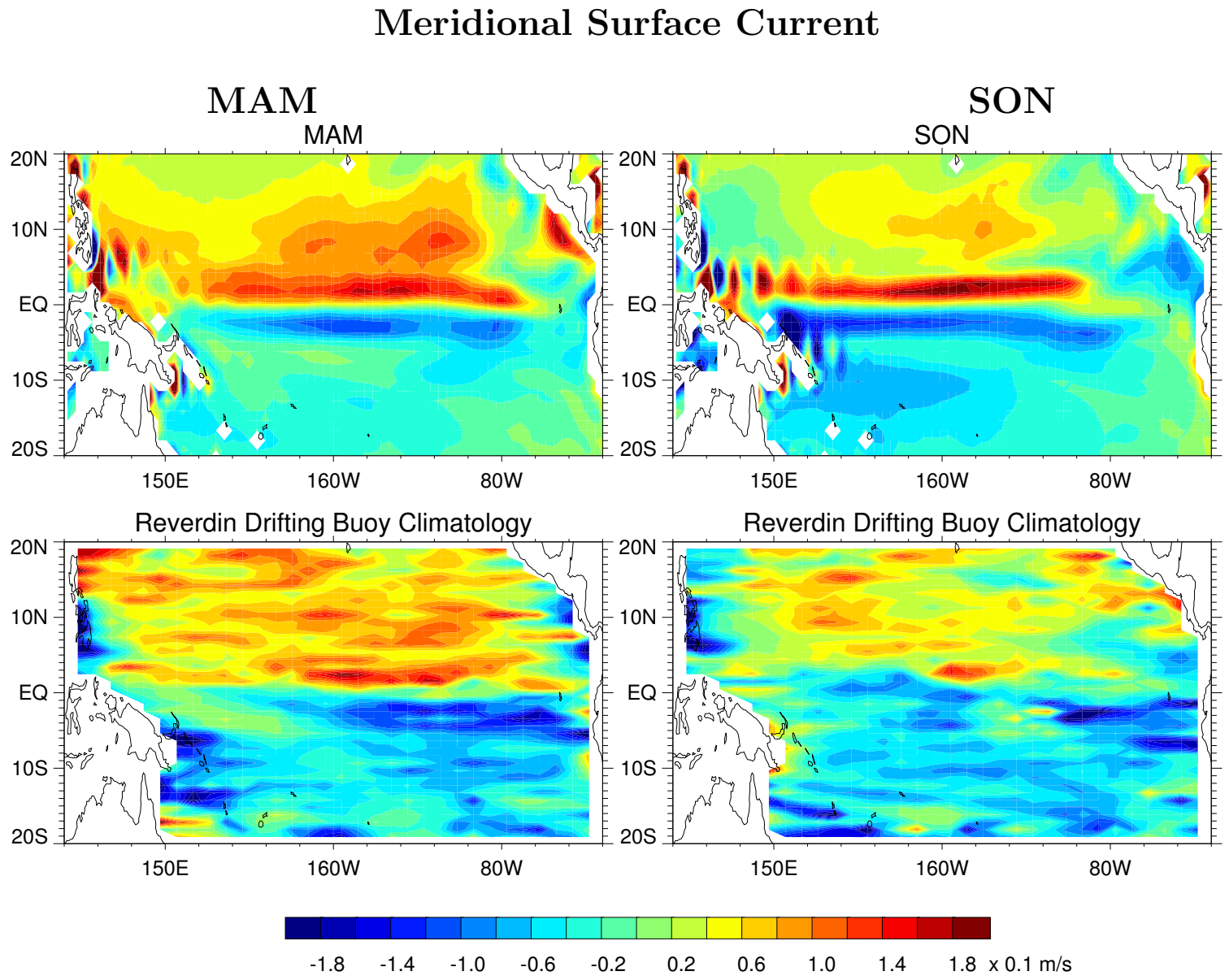

Figure 27b: Meridional surface current (m s^{-1}). Upper panels: model; Lower panels: observations from Reverdin; Left panels: March-April-May mean; Right panels: September-October-November mean. Contour interval is 0.02 m s^{-1}.

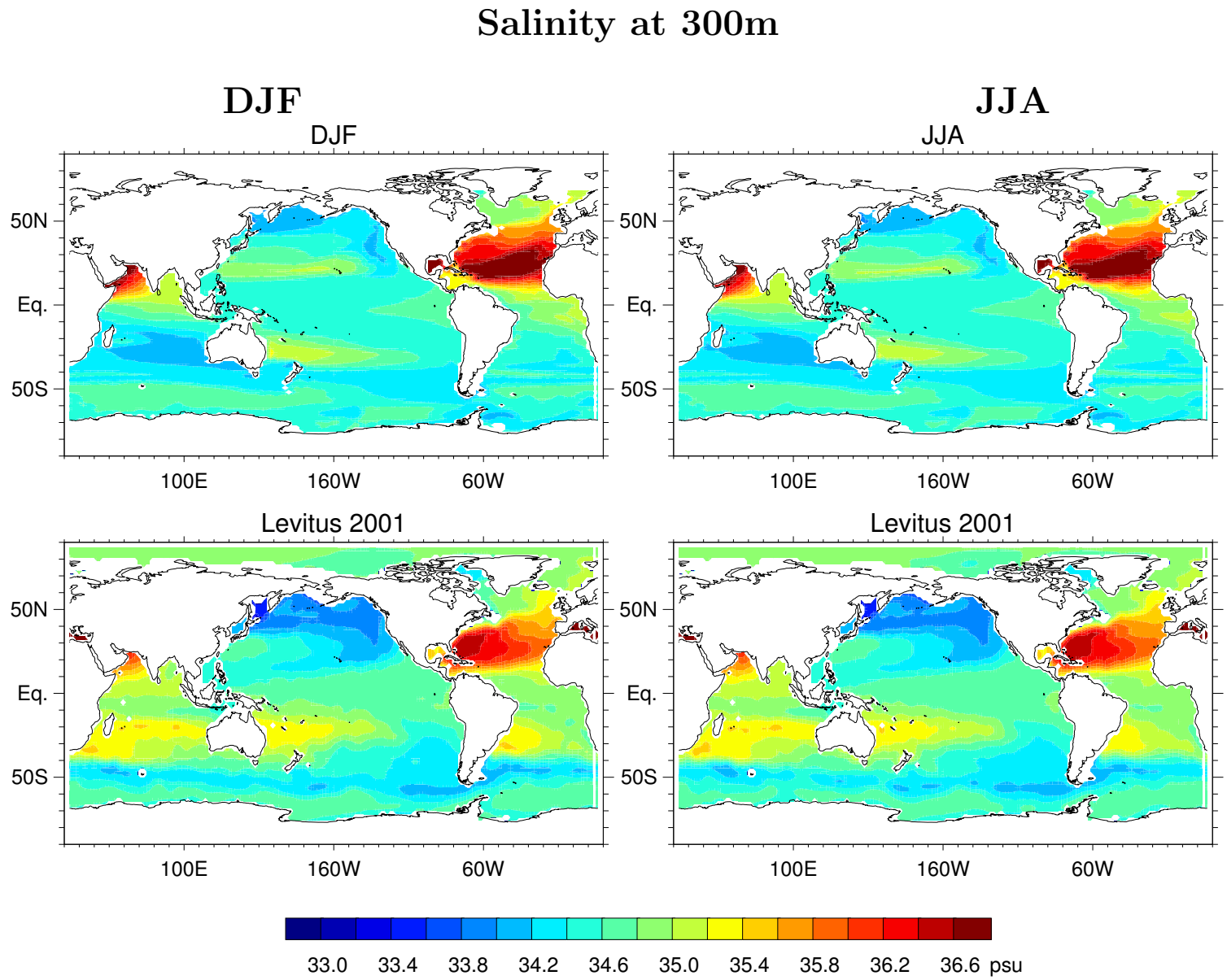

Figure 28a: Salinity at 300m depth. Upper panels: model; Lower panels: observations from World Ocean Atlas; Left panels: December-January-February mean; Right panels: June-July-August mean. Contour interval is 0.2

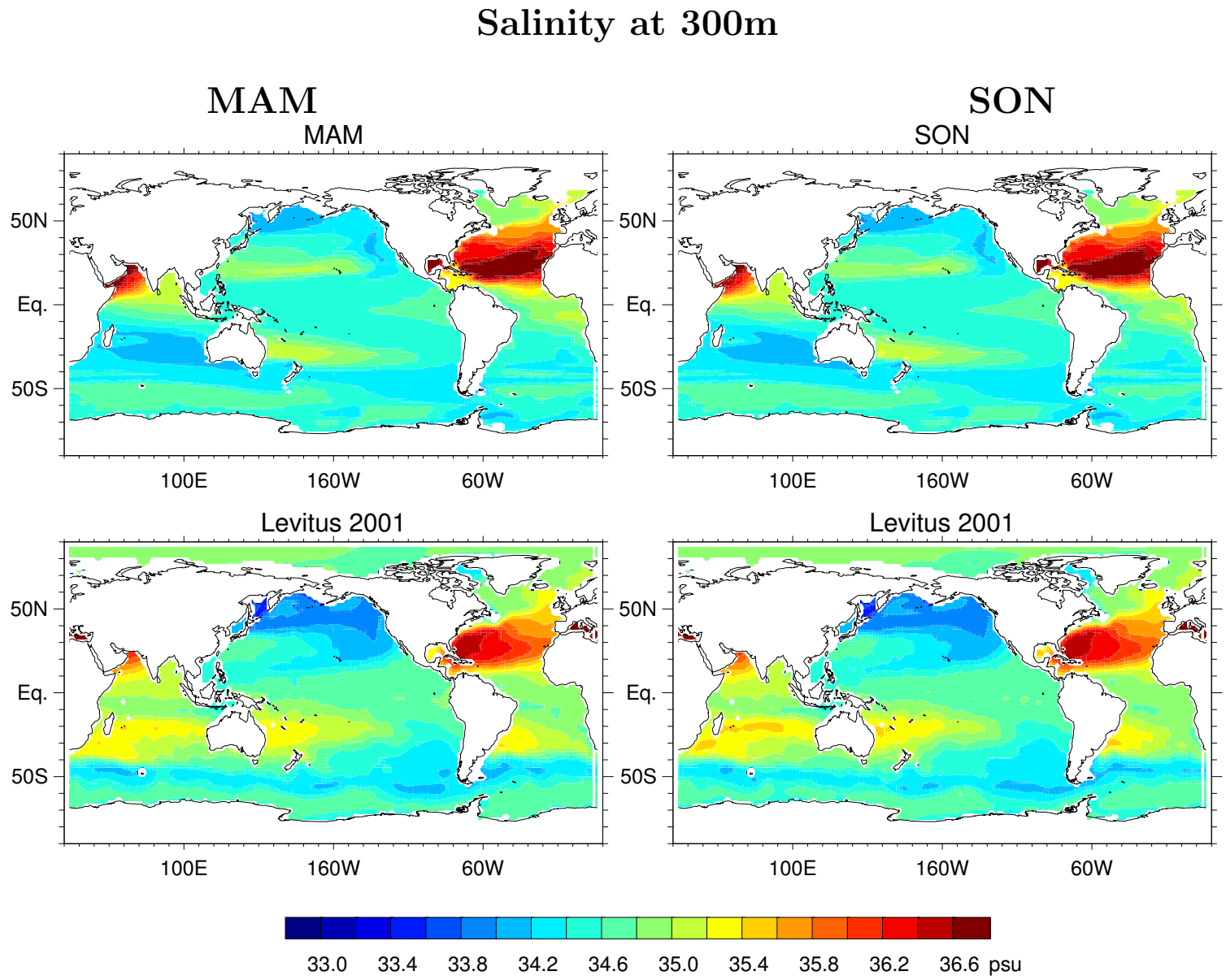

Figure 28b: Salinity at 300m depth. Upper panels: model; Lower panels: observations from World Ocean Atlas; Left panels: March-April-May mean; Right panels: September-October-November mean. Contour interval is 0.2

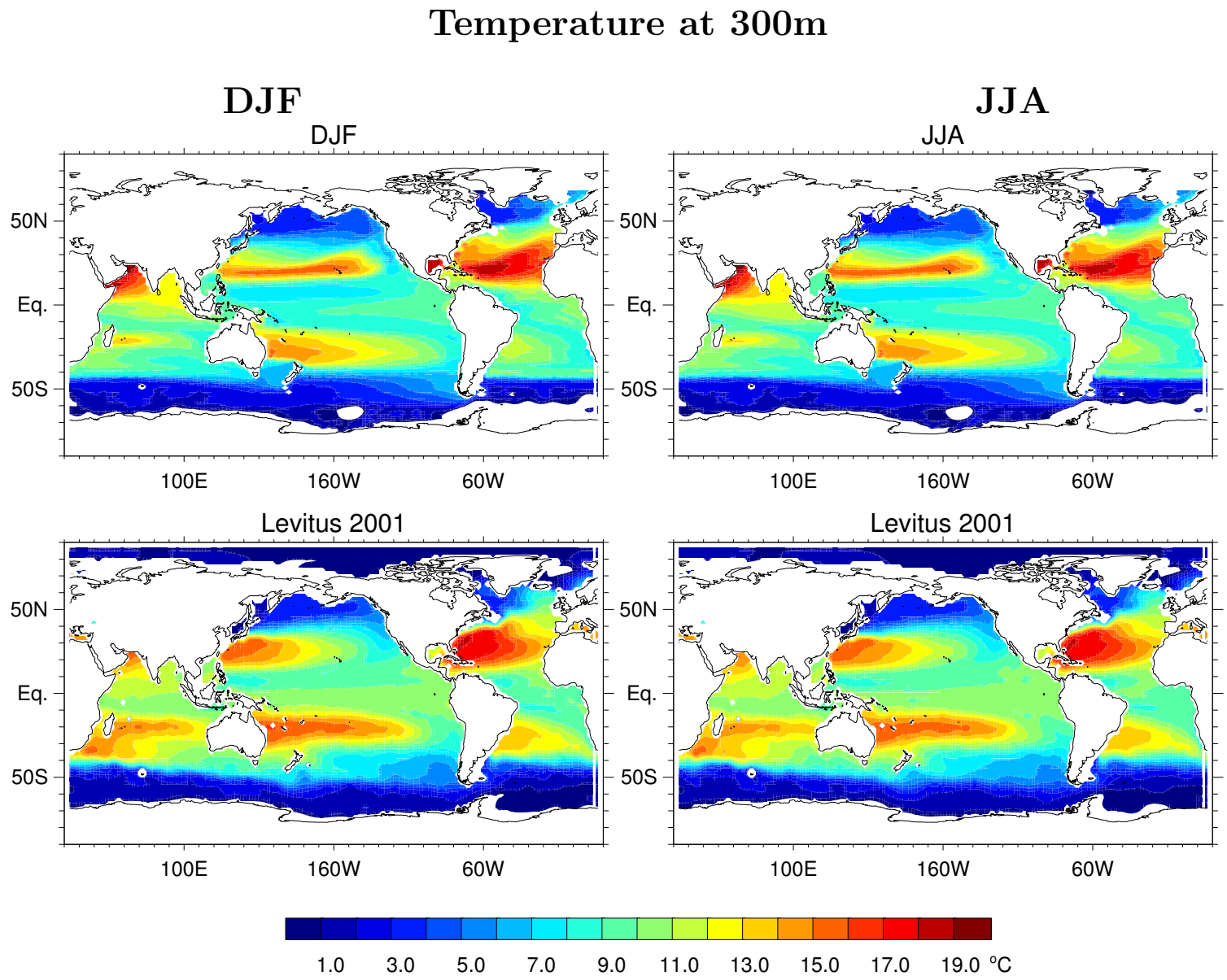

Figure 29a: Temperature at 300m depth (°C). Upper panels: model; Lower panels: observations from World Ocean Atlas; Left panels: December-January-February mean; Right panels: June-July-August mean. Contour interval is 1°C.

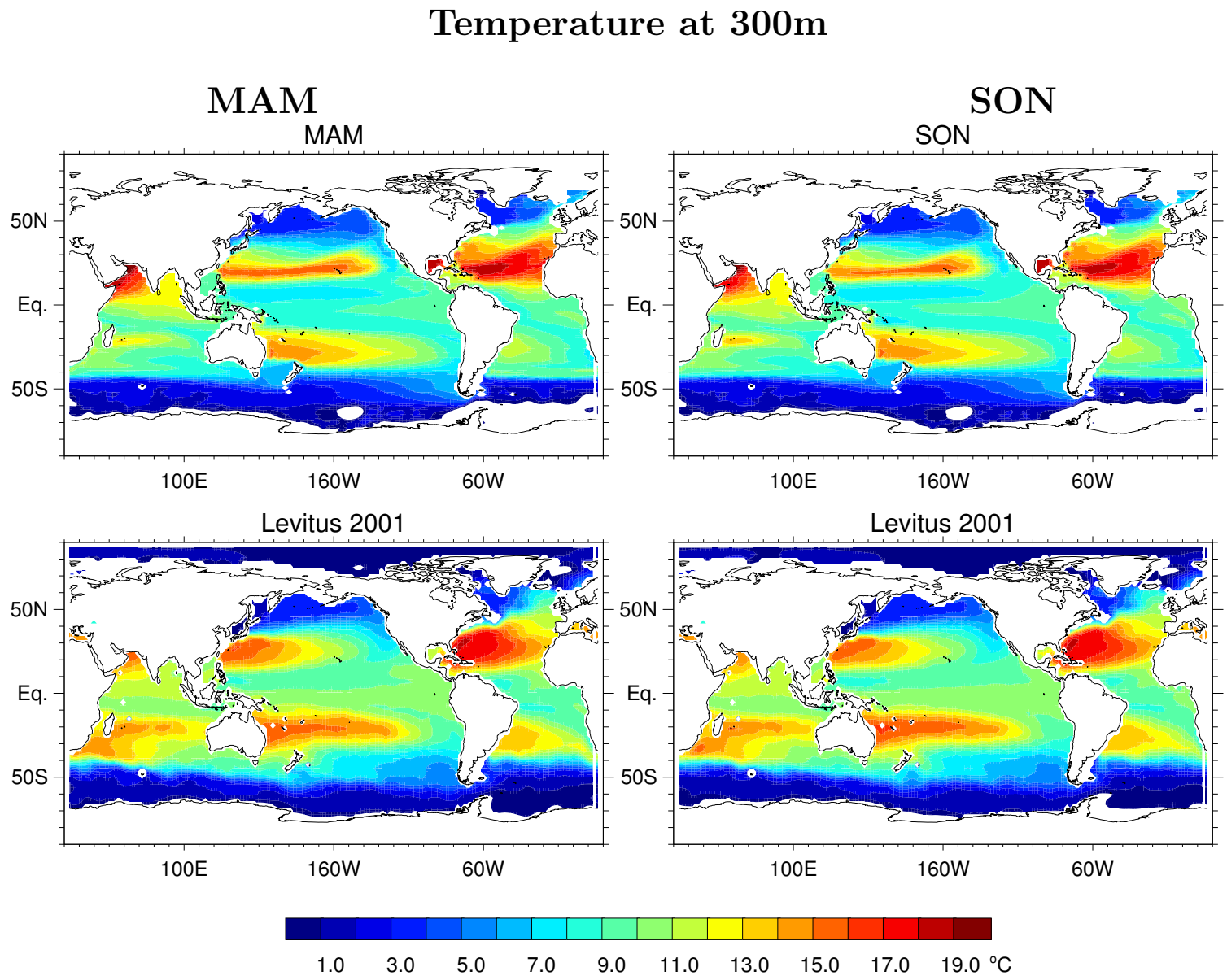

Figure 29b: Temperature at 300m depth (°C). Upper panels: model; Lower panels: observations from World Ocean Atlas; Left panels: March-April-May mean; Right panels: September-October-November mean. Contour interval is 1°C.

Seasonal Anomaly at Equator

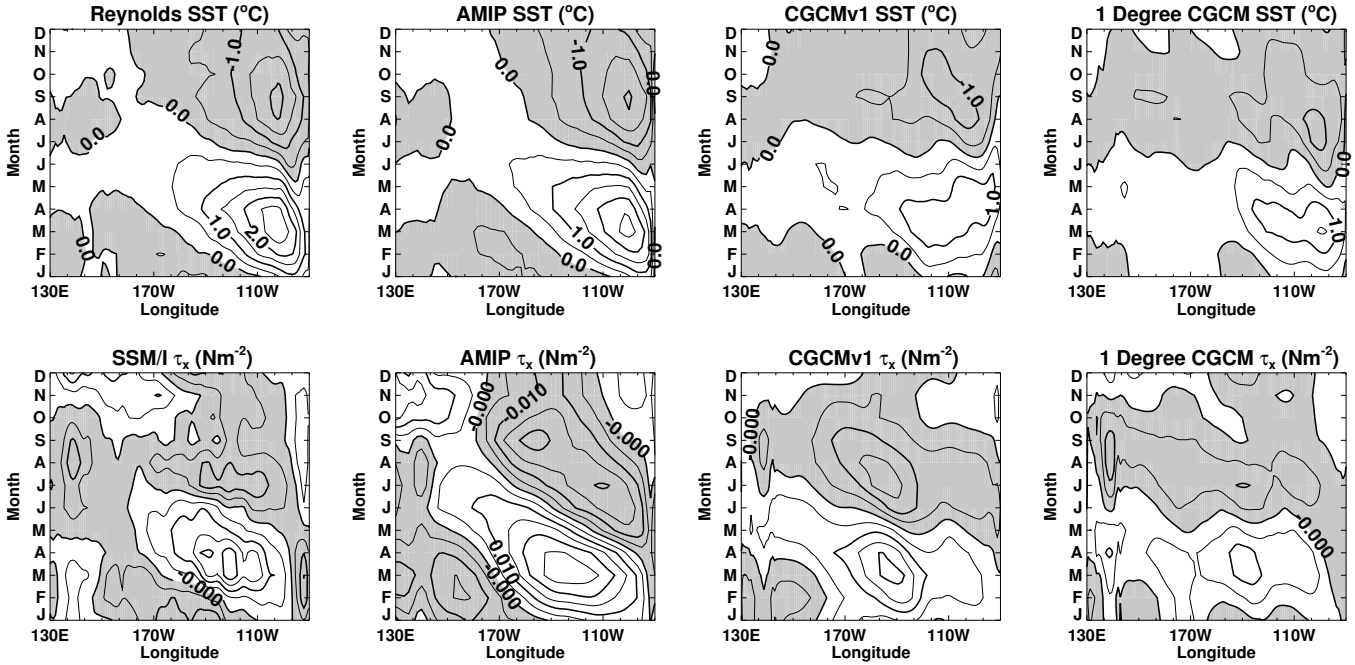

Figure 30: Seasonal anomaly in the Equatorial Pacific (averaged 2°S to 2°N).Upper panels: sea surface temperature; Lower panels: zonal wind stress; Left panels: Observations; Middle left panels: results from NSIPP-1 AMIP experiment; Middle right: model; Right panels: model with 1° atmosphere. Contour interval for SST is 0.5 °C. Contour interval for zonal wind stress is 0.005 N m^{-2}.

INTERANNUAL VARIABILITY

Standard Deviation of Sea Surface Temperature

Equatorial Pacific Sea Surface Temperature

Equatorial Pacific Zonal Wind Stress

Equatorial Pacific Depth of the 20°C Isotherm

NINO3 Index

Global Patterns and Teleconnections Correlated with NINO3

Empirical Orthogonal Functions of Sea Surface Temperature

North Pacific Index

Indian Ocean Dipole

Tropical Atlantic Dipole

North Atlantic Oscilliation (NAO)

Sea Surface Temperature Standard Deviation

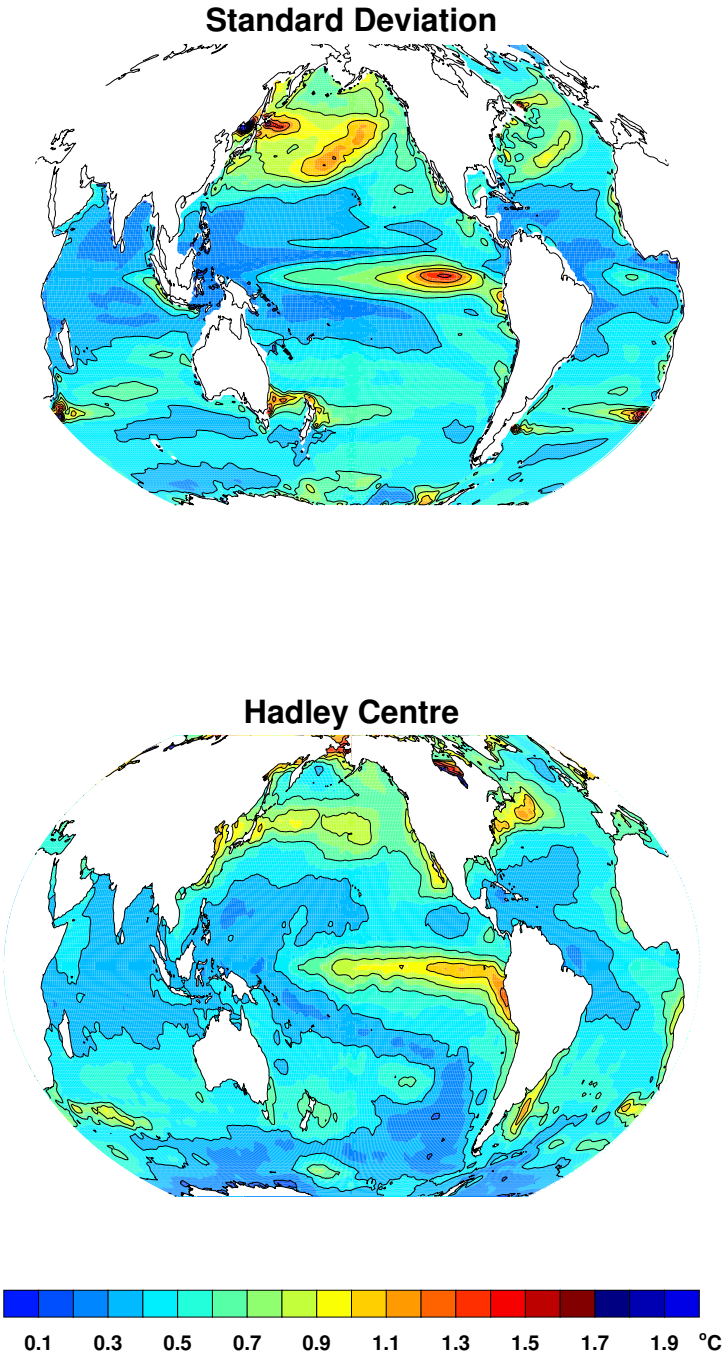

Figure 31: Standard deviation of sea surface temperature (°C).Top: Model, Bottom: Observations from Hadley Centre. Contour interval is 0.1°C.

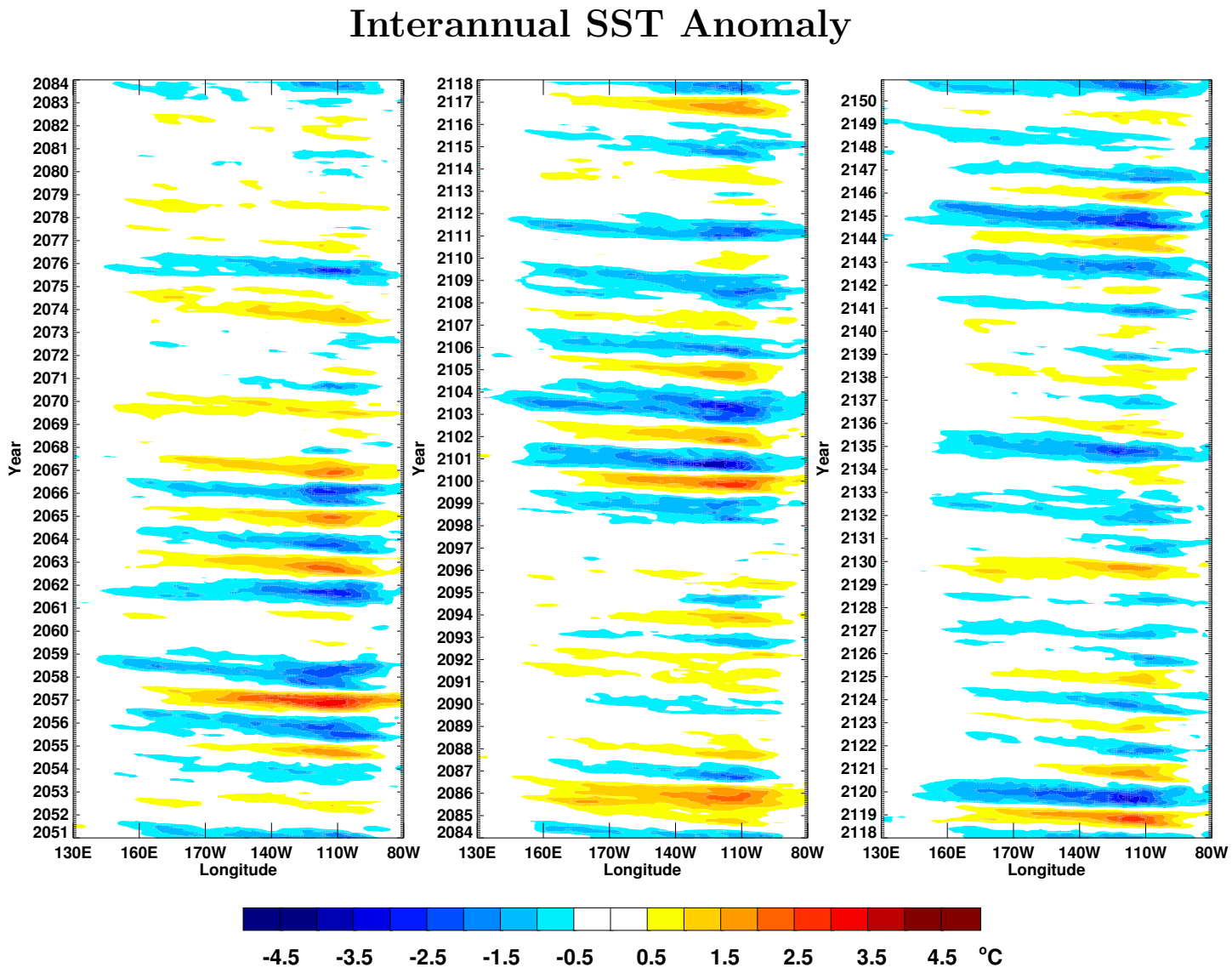

Figure 32: Interannual anomaly of sea surface temperature (SST) across the Equatorial Pacific.Hovmuller diagram of SST anomaly for 100 years of the experiment. Years progress from bottom to top and left to right. Contour interval is 0.5°C.

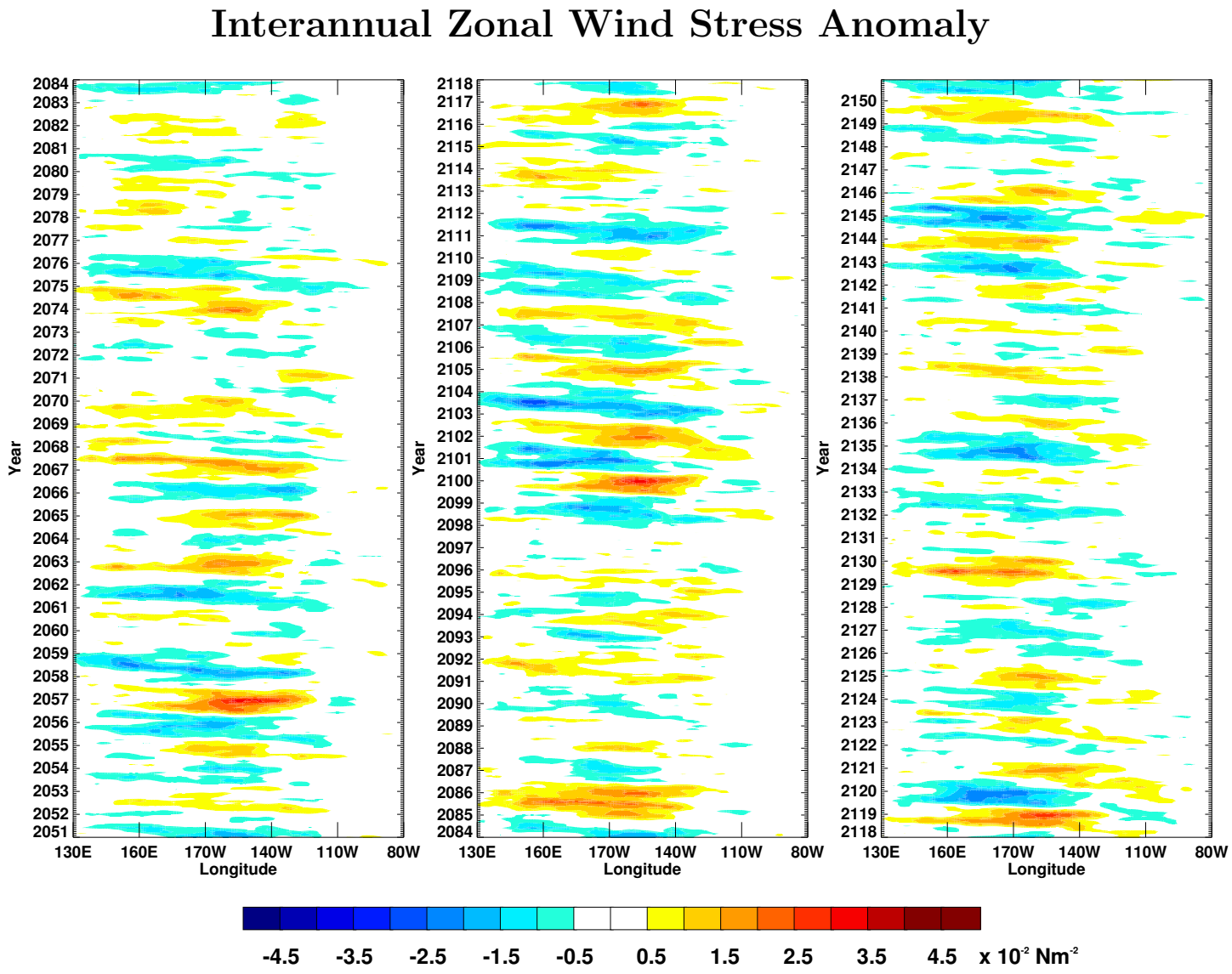

Figure 33: Interannual anomaly of zonal wind stress across the Equatorial Pacific.Hovmuller diagram of zonal wind stress anomaly for 100 years of the model experiment. Years progress from bottom to top and left to right. Contour interval is 0.005 N m^{-2}.

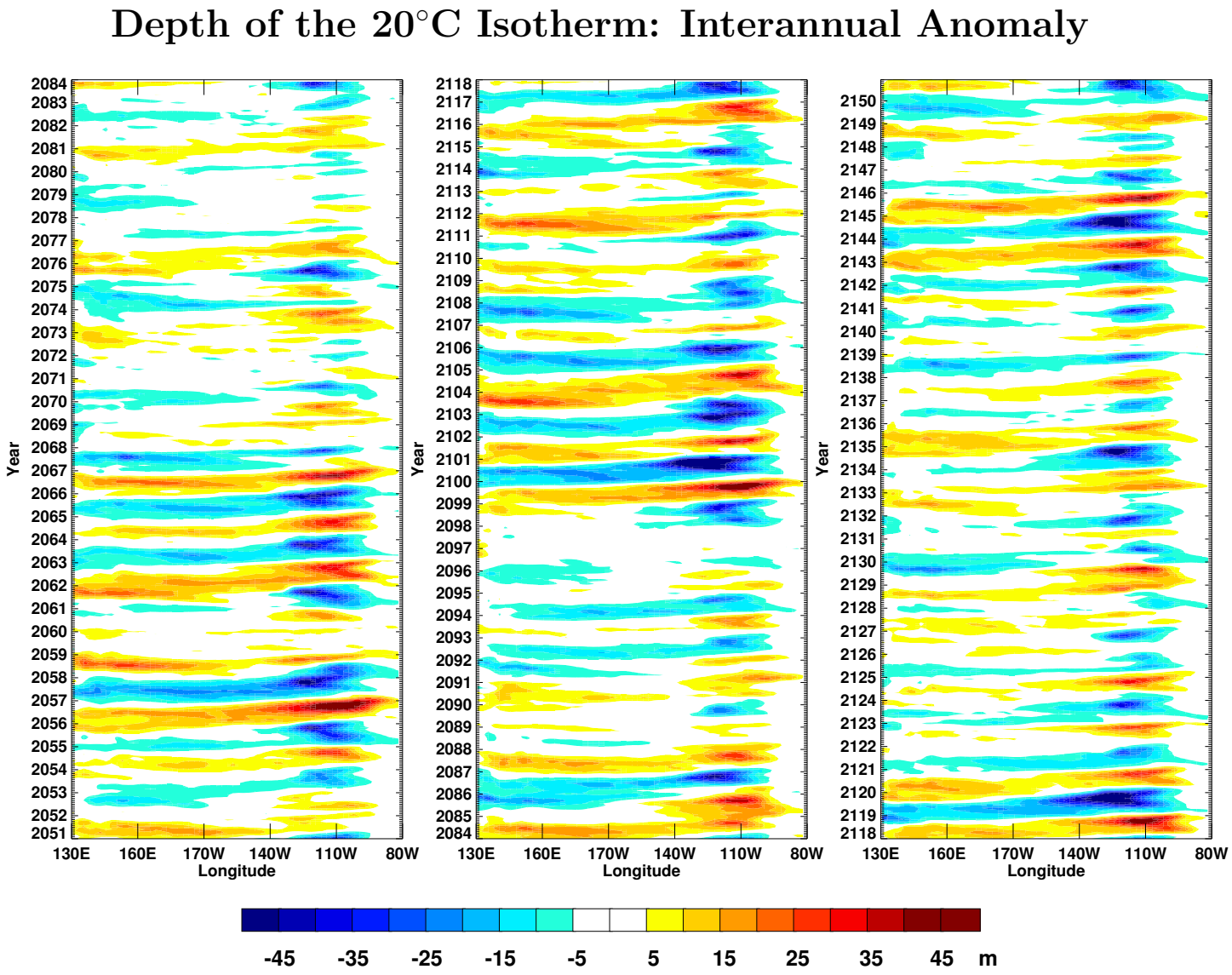

Figure 34: Interannual anomaly of depth of the 20°C isotherm across the Equatorial Pacific.Hovmuller diagram of the interannual anomaly of an estimate of thermocline depth for 100 years of the model experiment. Years progress from bottom to top and left to right. Contour interval is 5 m.

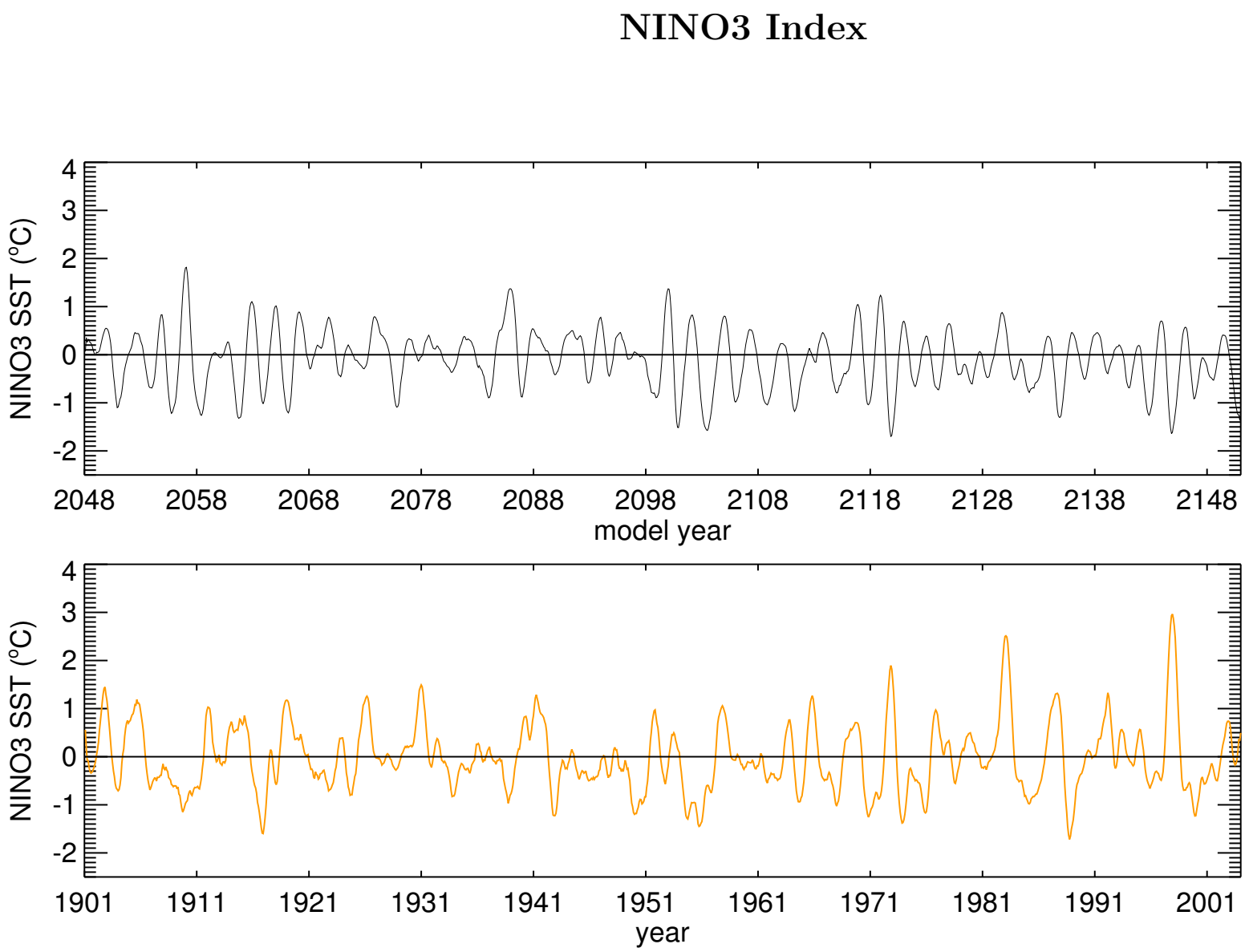

Figure 35: NINO3 Sea Surface Temperature Index.Black line: model; Orange line: SST data from the Hadley Centre. The NINO3 index box extends from 5°S to 5°N and from 90°W to 150°W.

Correlation of NINO3 and SST

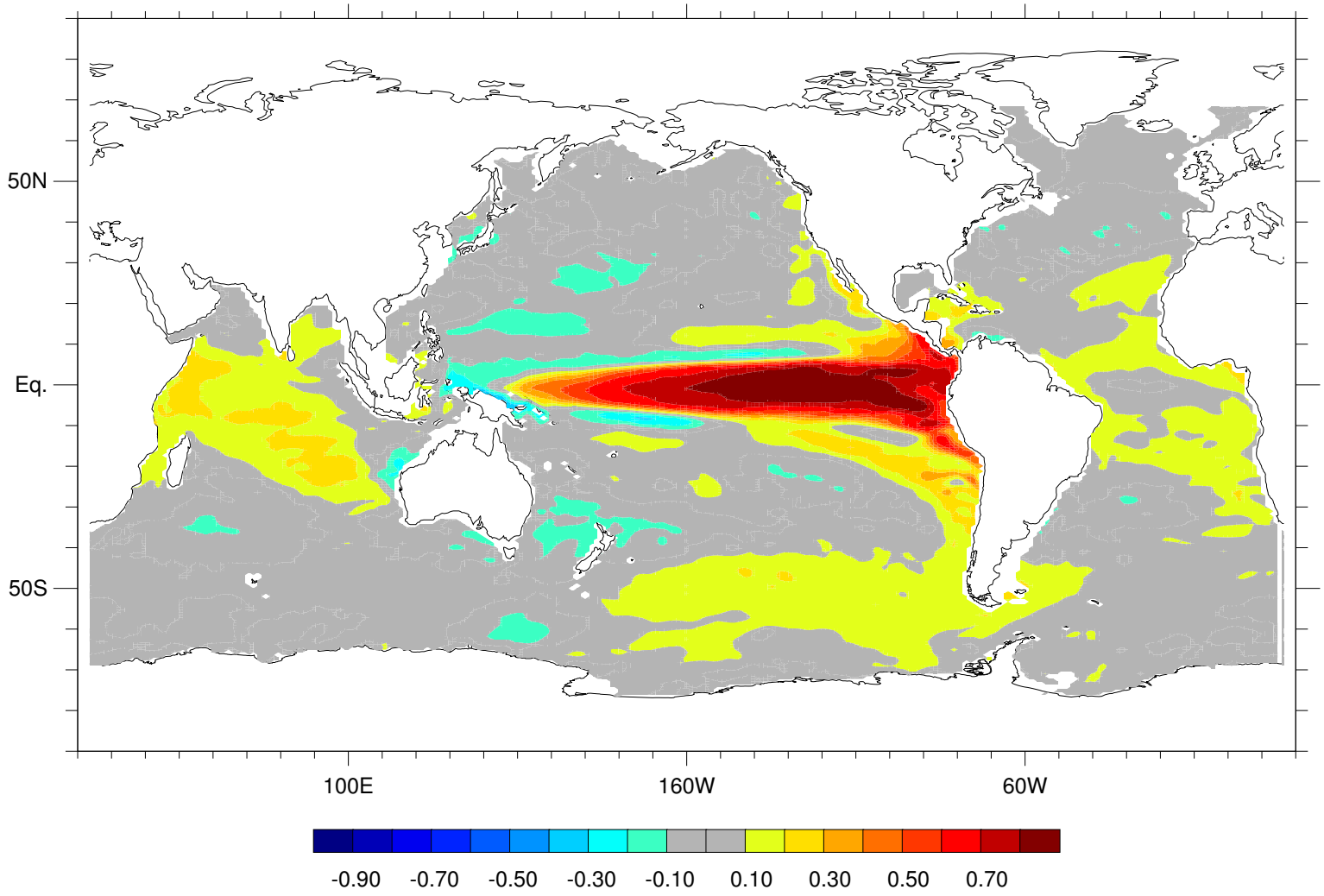

Figure 36a: Pointwise correlation of NINO3 index and sea surface temperature.Contour interval is 0.1.

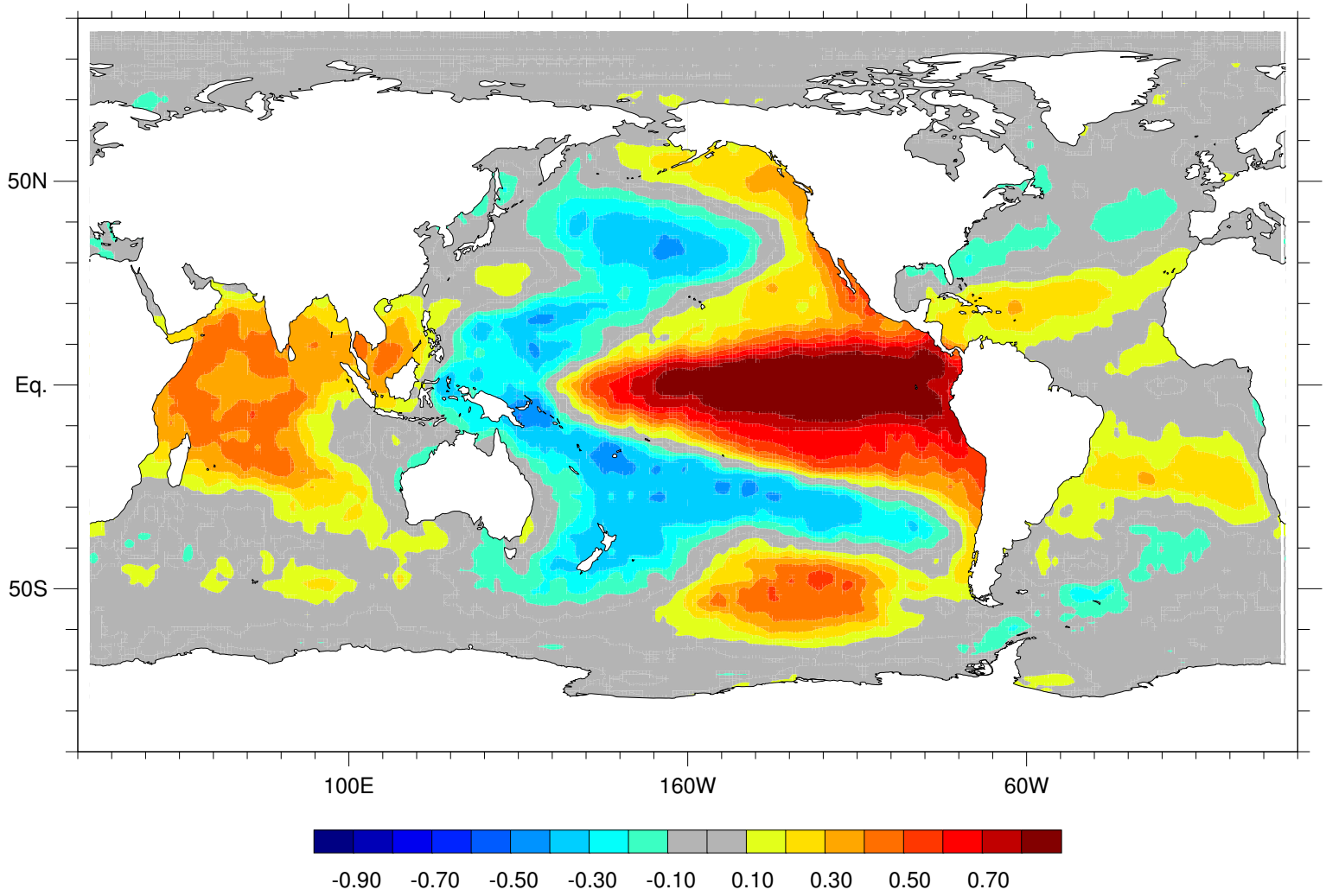

Figure 36b: Pointwise correlation of NINO3 index and sea surface temperature.. SST data and NINO3 index from Hadley Centre. Contour interval is 0.1.

Correlation of NINO3 and 200mb Height

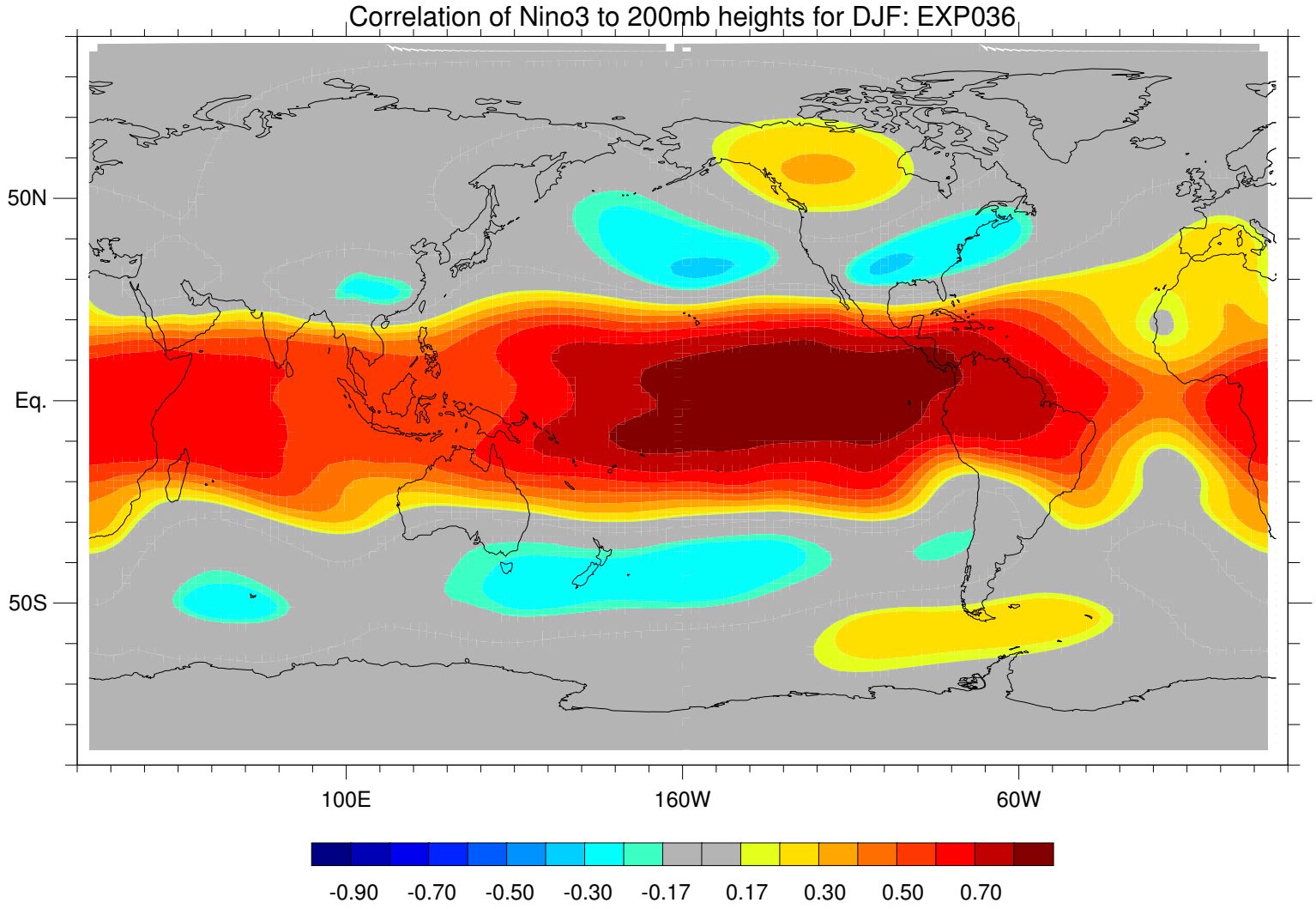

Figure 37a: Pointwise correlation of NINO3 index and 200mb geopotential height.Contour interval is 0.1.

Correlation of Hadley Centre NINO3 and NCEP Reanalysis 200mb Height

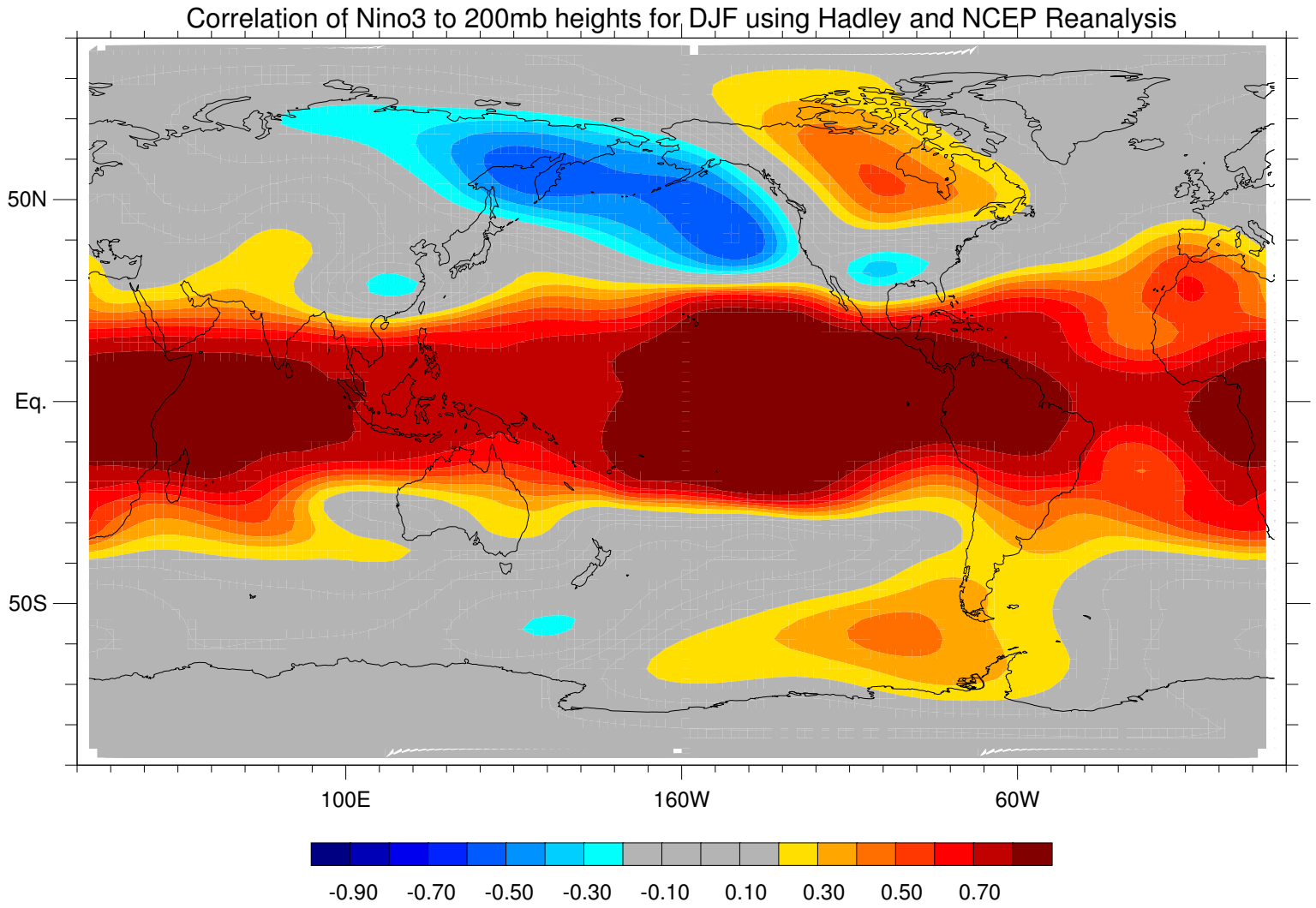

Figure 37b: Pointwise correlation of NINO3 index and 200mb geopotential height.Sea surface temperature data from Hadley Centre. Data for 200mb geopotential height from NCEP reanalysis. Contour interval is 0.1.

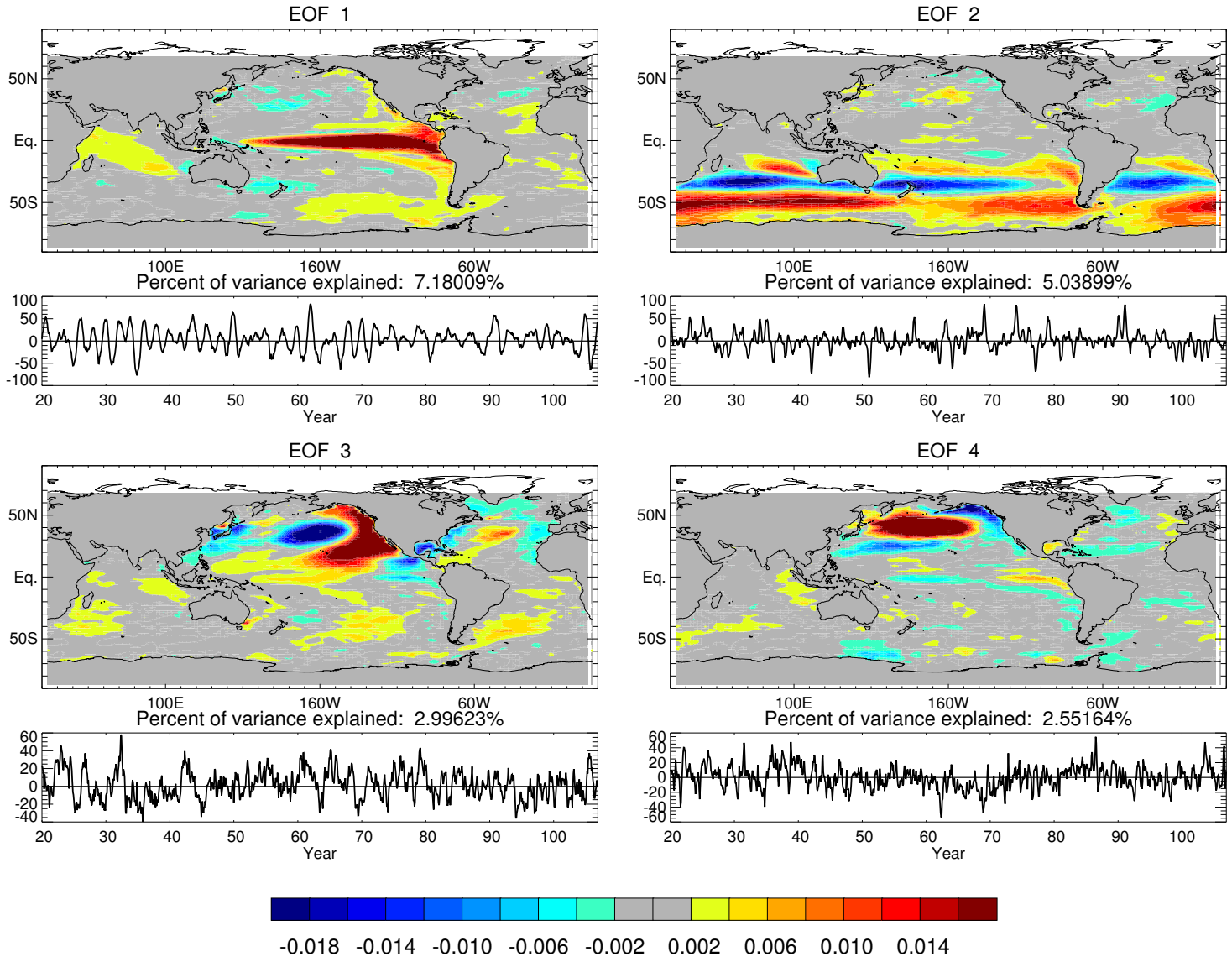

Figure 38: Empirical orthogonal function (EOF) of model sea surface temperature.Only the first four rotated EOFs are shown. The associated principal component timeseries is plotted below each EOF.

North Pacific Index

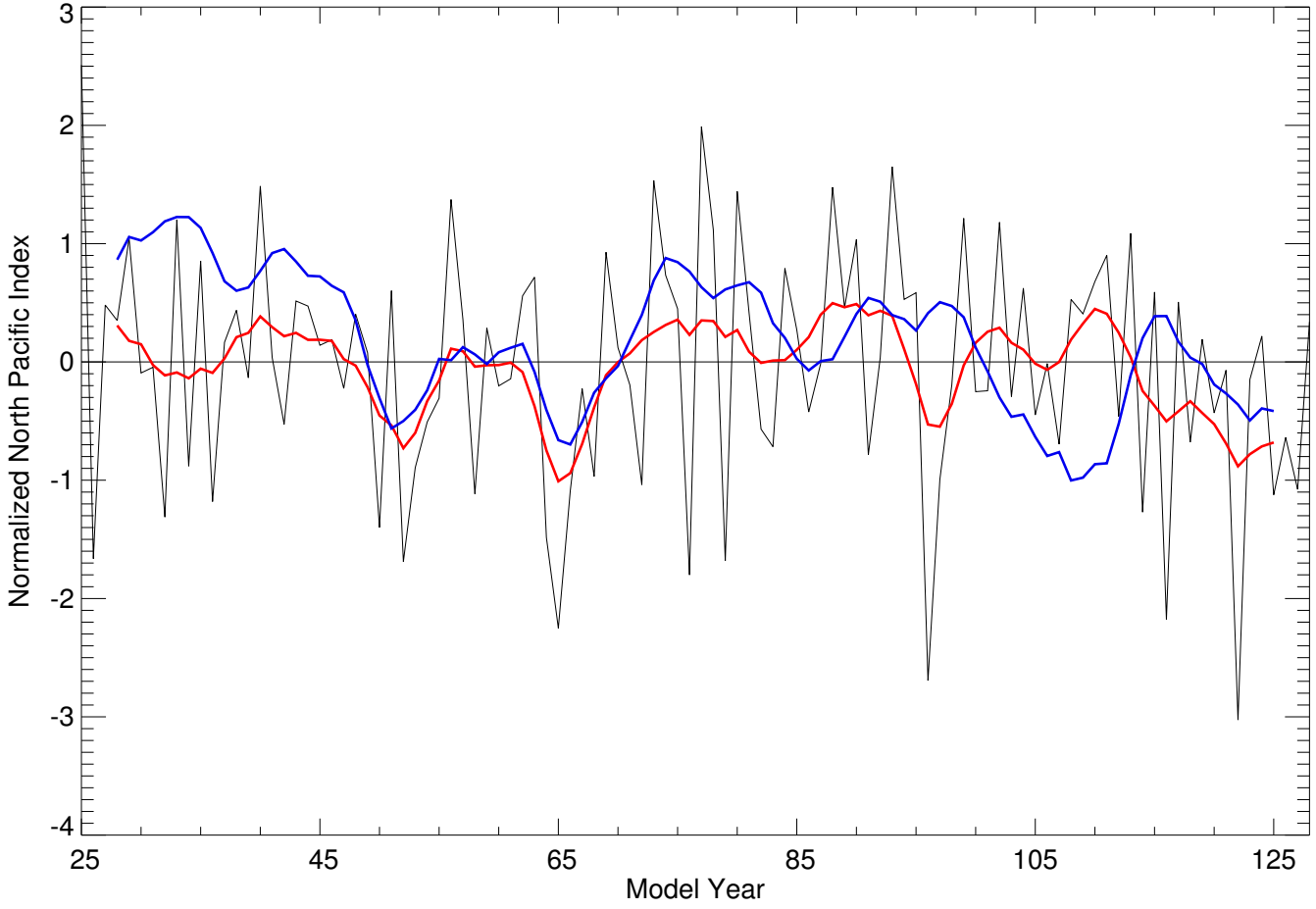

Figure 39: North Pacific Index of normalized sea level pressure anomaly.Black line: Raw North Pacific Index (NPI) from model; Red: NPI filtered by a weighted seven point moving average; Blue: Filtered NPI from observations from 1901-2003, adapted from Trenberth and Hurrell (1994). NPI normalized by standard deviations of 1.9 mb (model) and 2.2 mb (data). NPI consists of a weighted average of northern winter sea level pressure anomaly in the area of 30°N to 65°N and 160°E to 140°W.

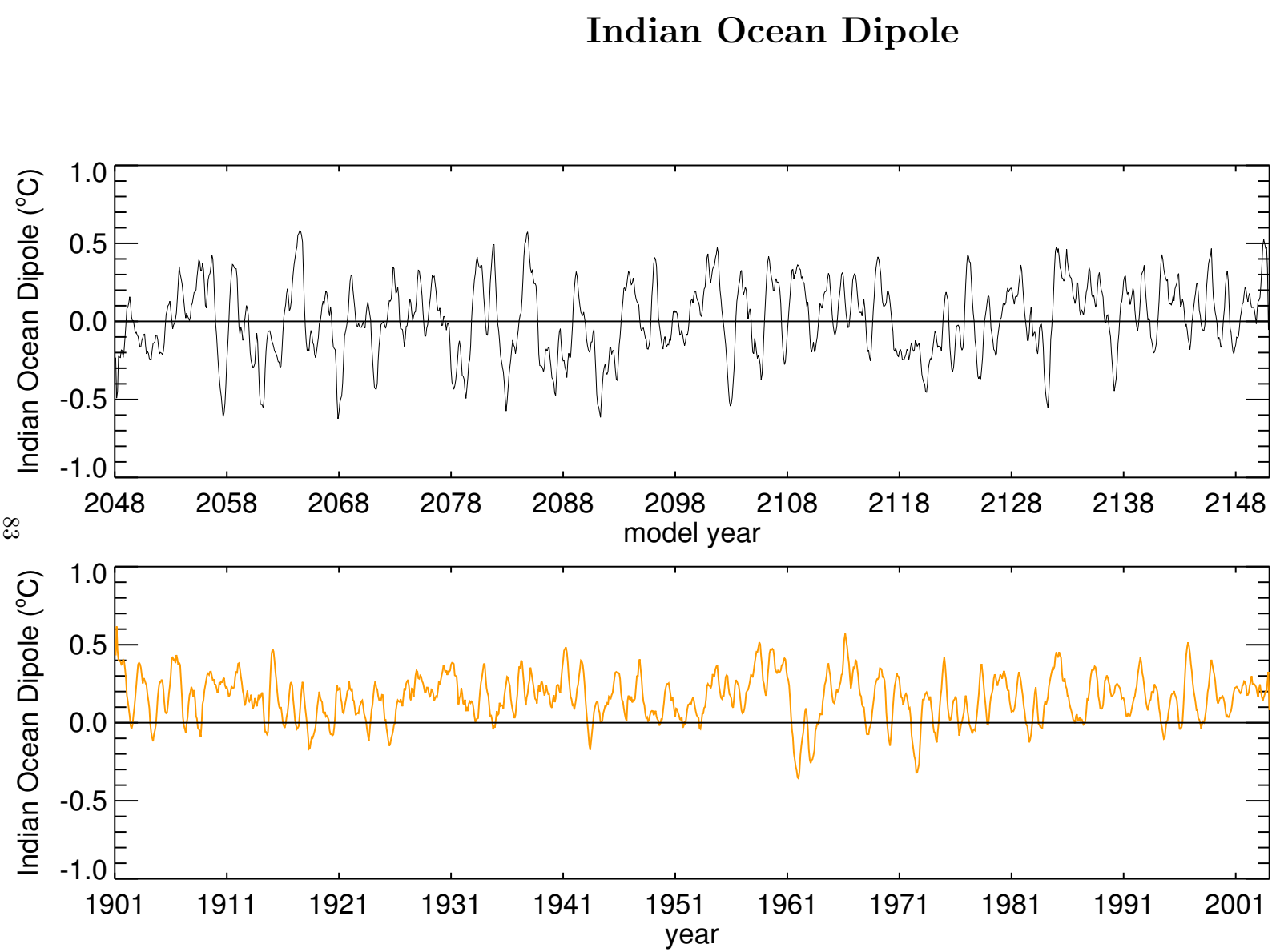

Figure 40: Indian Ocean dipole of sea surface temperature anomaly.Black line: model; Orange line: SST data from the Hadley Centre. The Indian Ocean dipole is defined as the difference between the SSTA over a western region and eastern region. The western region extends from the Equator to 10°N and from 90°E to 110°E. The eastern region extends from 10°S to 10°N and from 50°E to 70°E.

Atlantic Ocean Dipole

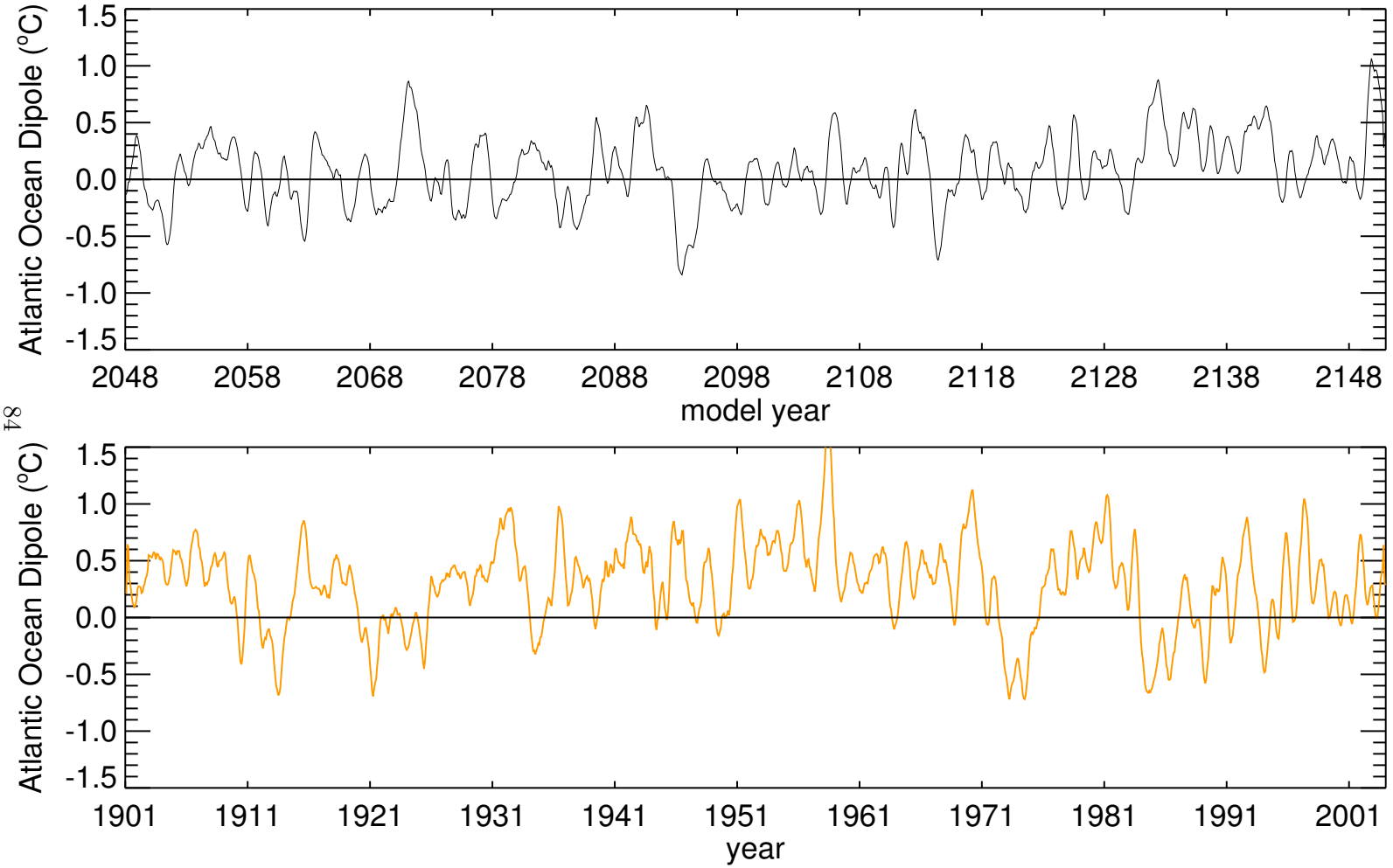

Figure 41: Atlantic Ocean dipole of sea surface temperature anomaly.Black line: model; Orange line: SST data from the Hadley Centre. The Atlantic Ocean dipole is defined as the difference between the SSTA over a northern region and southern region. The northern region extends from the 50°N to 20°N and from 60°W to 30°W. The southern region extends from 20°S to the Equator and from 30°W to 10°E.

EOF1 of North Atlantic Sea Level Pressure Anomaly

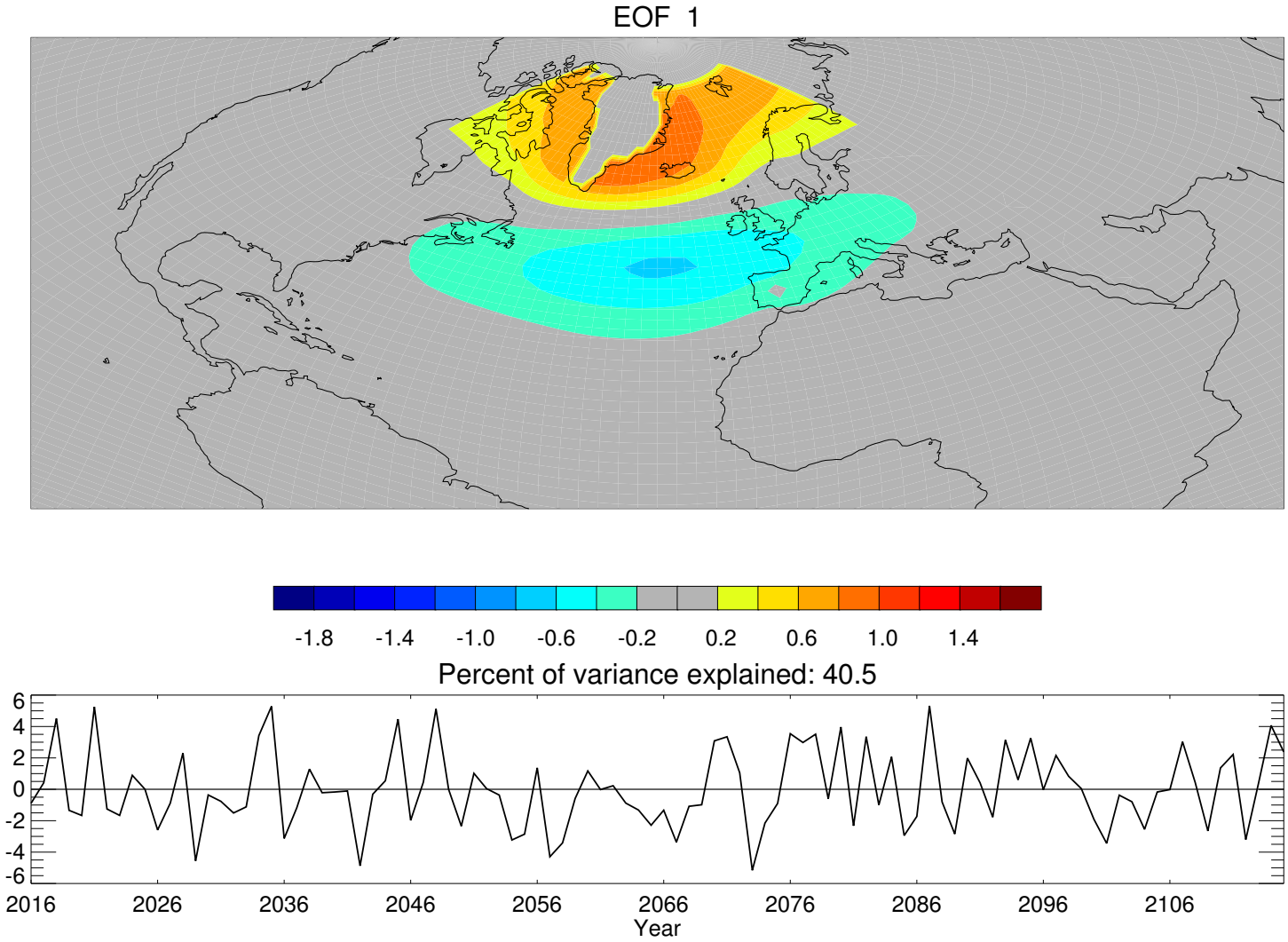

Figure 42a: North Atlantic Oscillation.First EOF of the annual mean SLP anomaly over the Atlantic sector (20°N to 80°N and 90°W to 40°E). This EOF represents 40.5% of the total variance in SLP anomaly in this sector. The associated principal component time series is plotted below the EOF pattern.

EOF1 of Observed North Atlantic Sea Level Pressure Anomaly

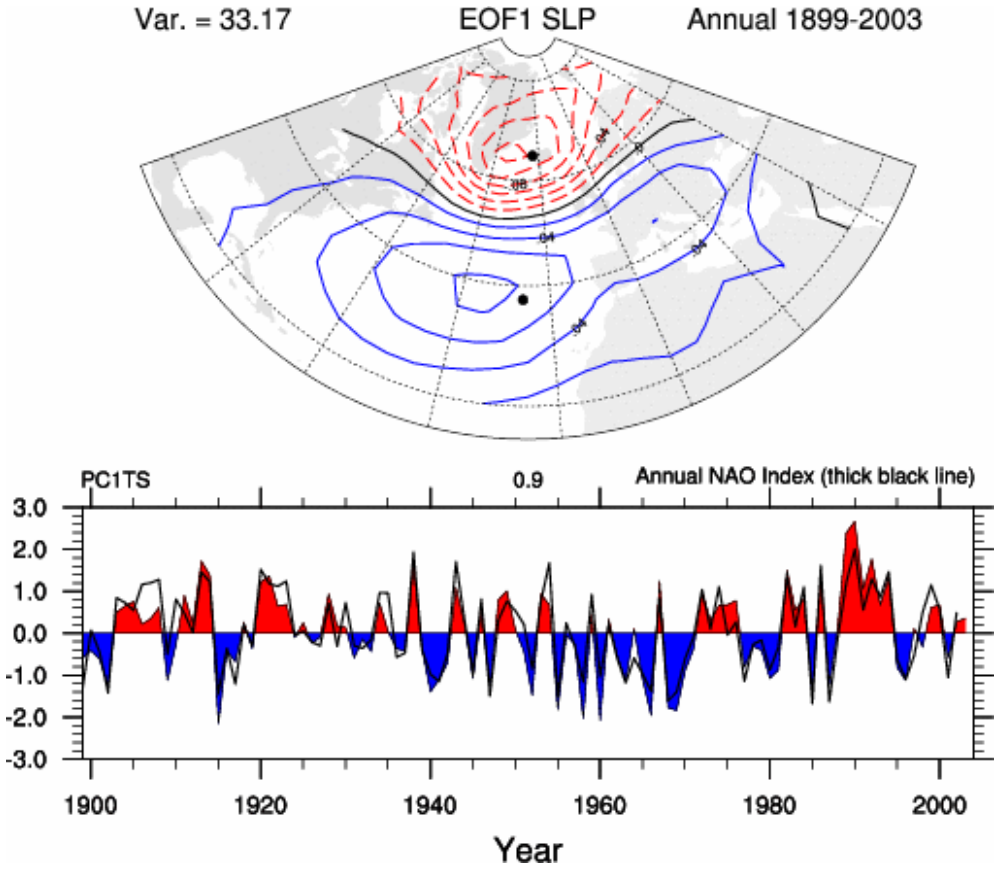

Figure 42b: North Atlantic Oscillation from observations.First EOF of the annual mean SLP anomaly over the Atlantic sector (20°N to 80°N and 90°W to 40°E). This EOF represents 33.87% of the total variance in SLP anomaly in this sector. The associated principal component time series is shaded below the EOF pattern; the thick black line represents the NAO index as computed from the station

MODEL COMPARISON

Figures from 1° CGCM Experiment

Figures from CGCM experiments

Annual Mean Sea Surface Temperature

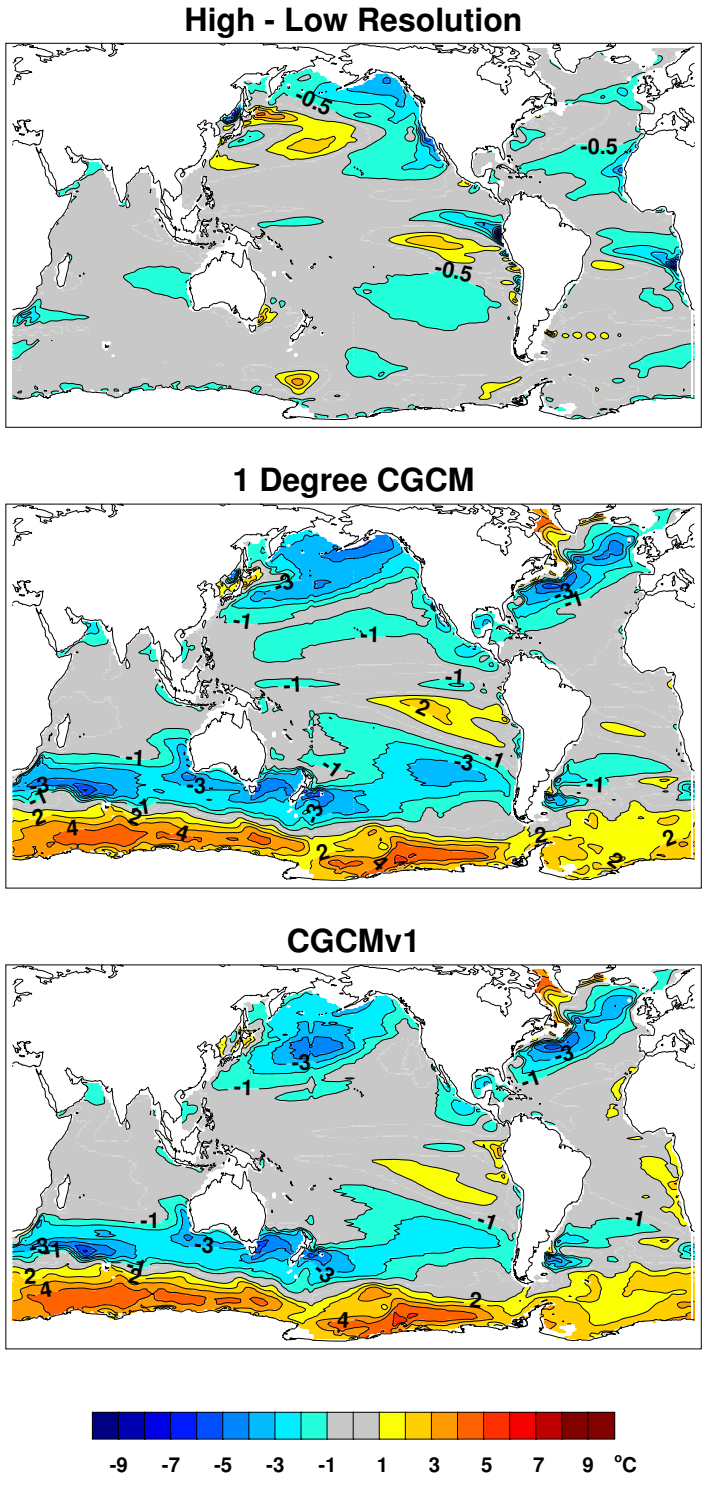

Figure 43: Sea surface temperature (°C).Top: difference in bias between the regular CGCMv1 and the 1° CGCM (0.5°C contour interval); Middle: annual mean SST bias for the 1 ° CGCM (1.0°C contour interval); Bottom: annual mean SST bias for CGCMv1 (1.0°C contour interval).

Sea Surface Temperature Standard Deviation

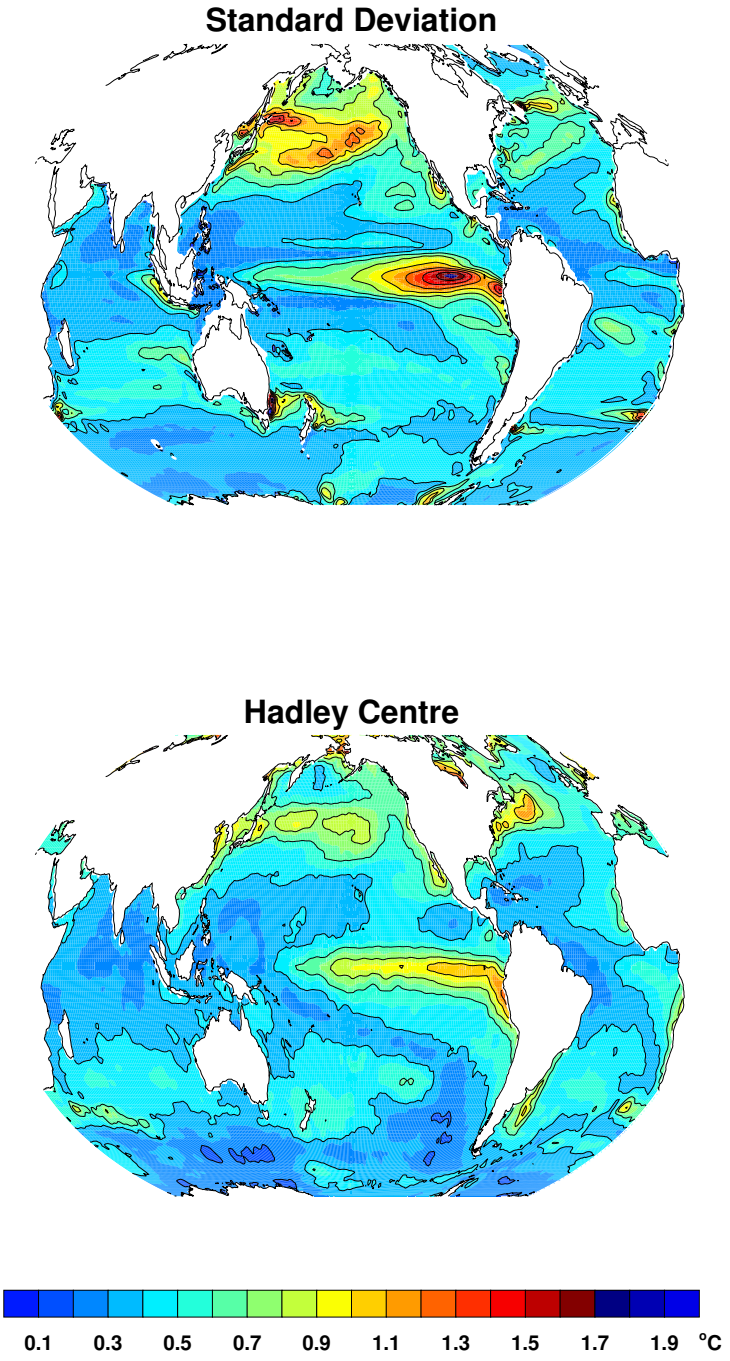

Figure 44: Standard deviation of sea surface temperature (°C).Top: 1° CGCM, Bottom: observations from Hadley Centre. Contour interval is 0.1°C.

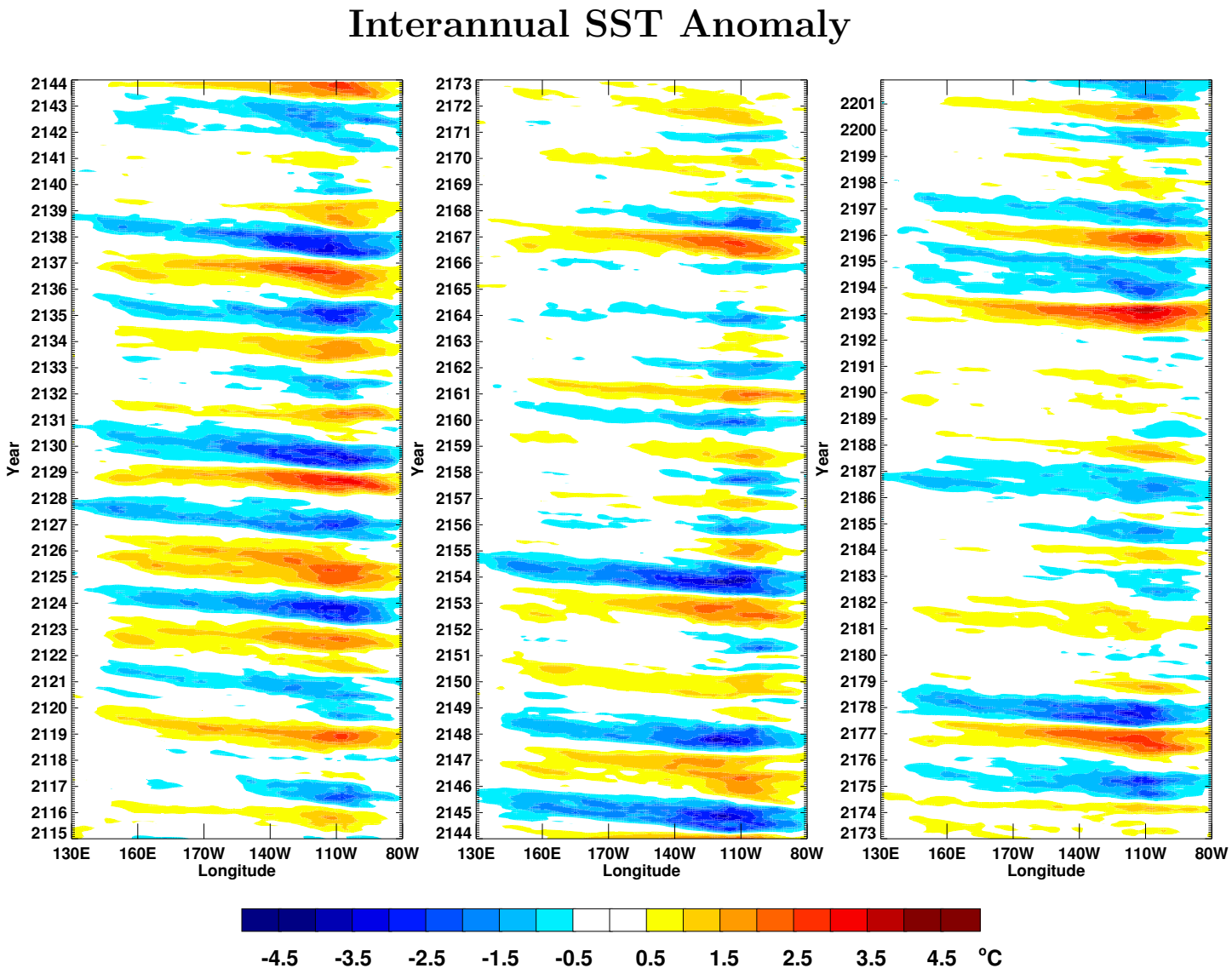

Figure 45: Interannual anomaly of Equatorial Pacific sea surface temperature (SST).Hovmuller diagram of SST anomaly for 87 years of the 1° CGCM. Years progress from bottom to top and left to right. Contour interval is 0.5°C.

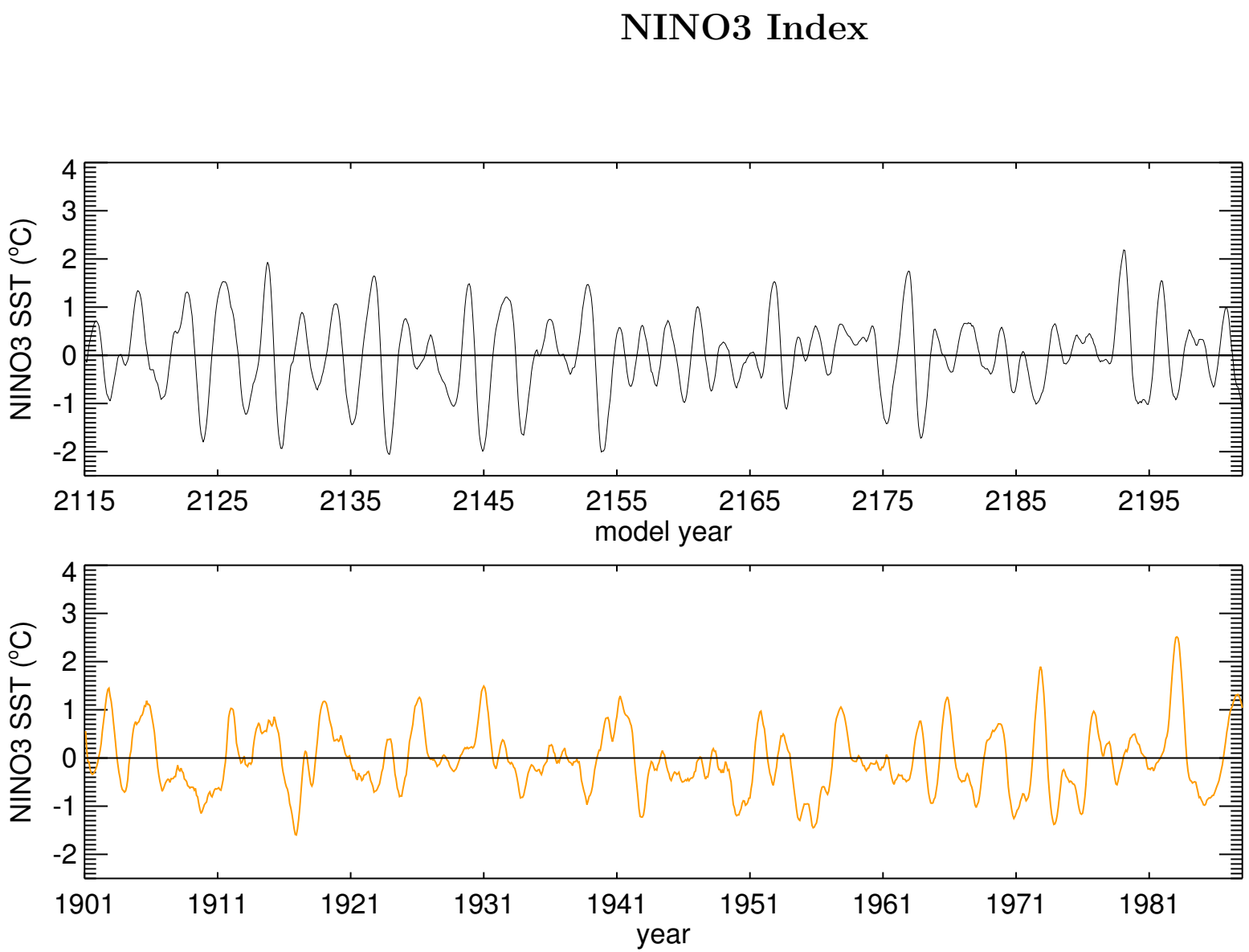

Figure 46: NINO3 Sea Surface Temperature Index.Black line: 1 ° CGCM; Orange line: SST data from the Hadley Centre. The NINO3 index box extends from 5°S to 5°N and from 90°W to 150°W.

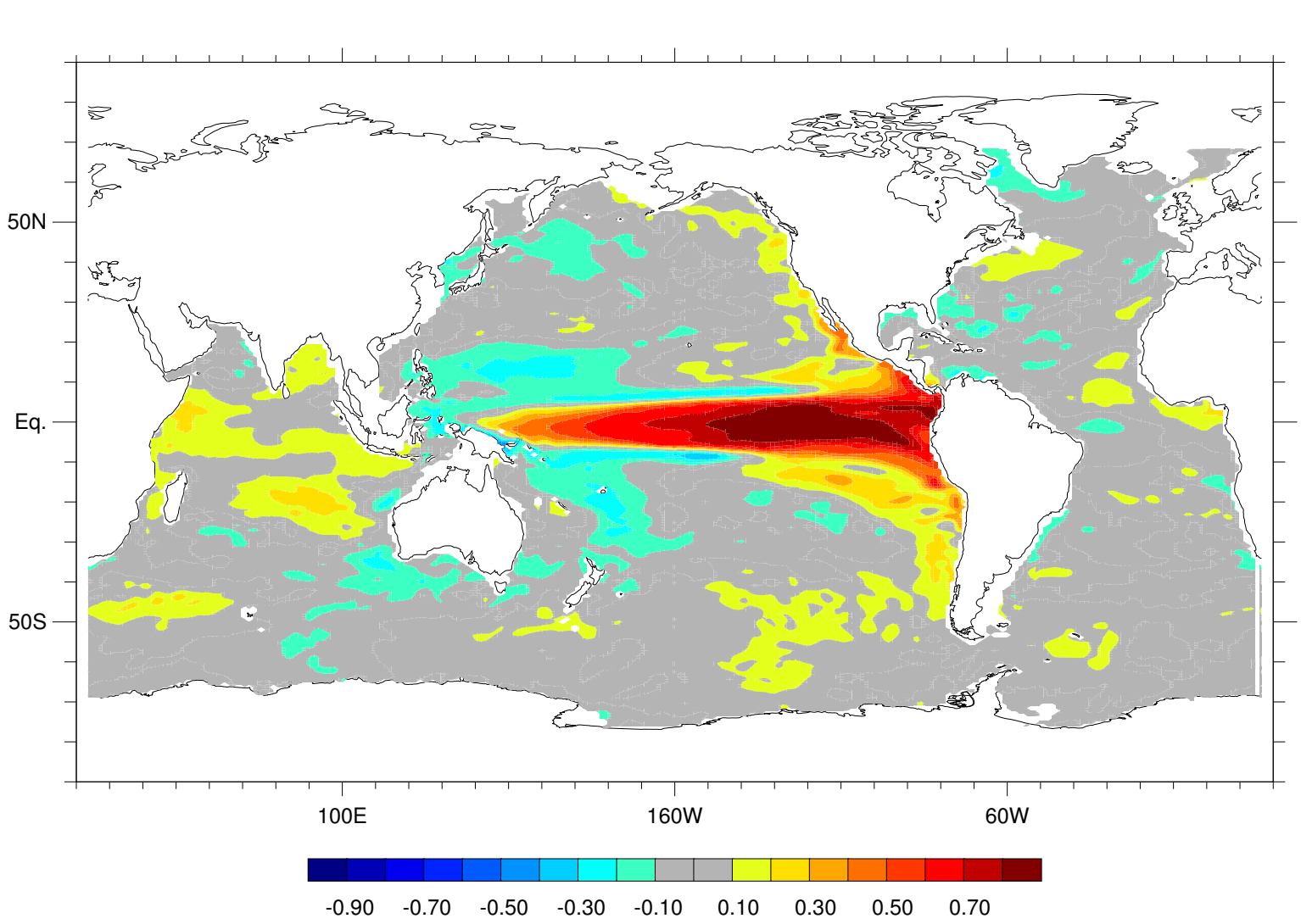

Figure 47: Pointwise correlation of NINO3 index and sea surface temperature.Contour interval is 0.1.

Correlation of NINO3 and 200mb Heights

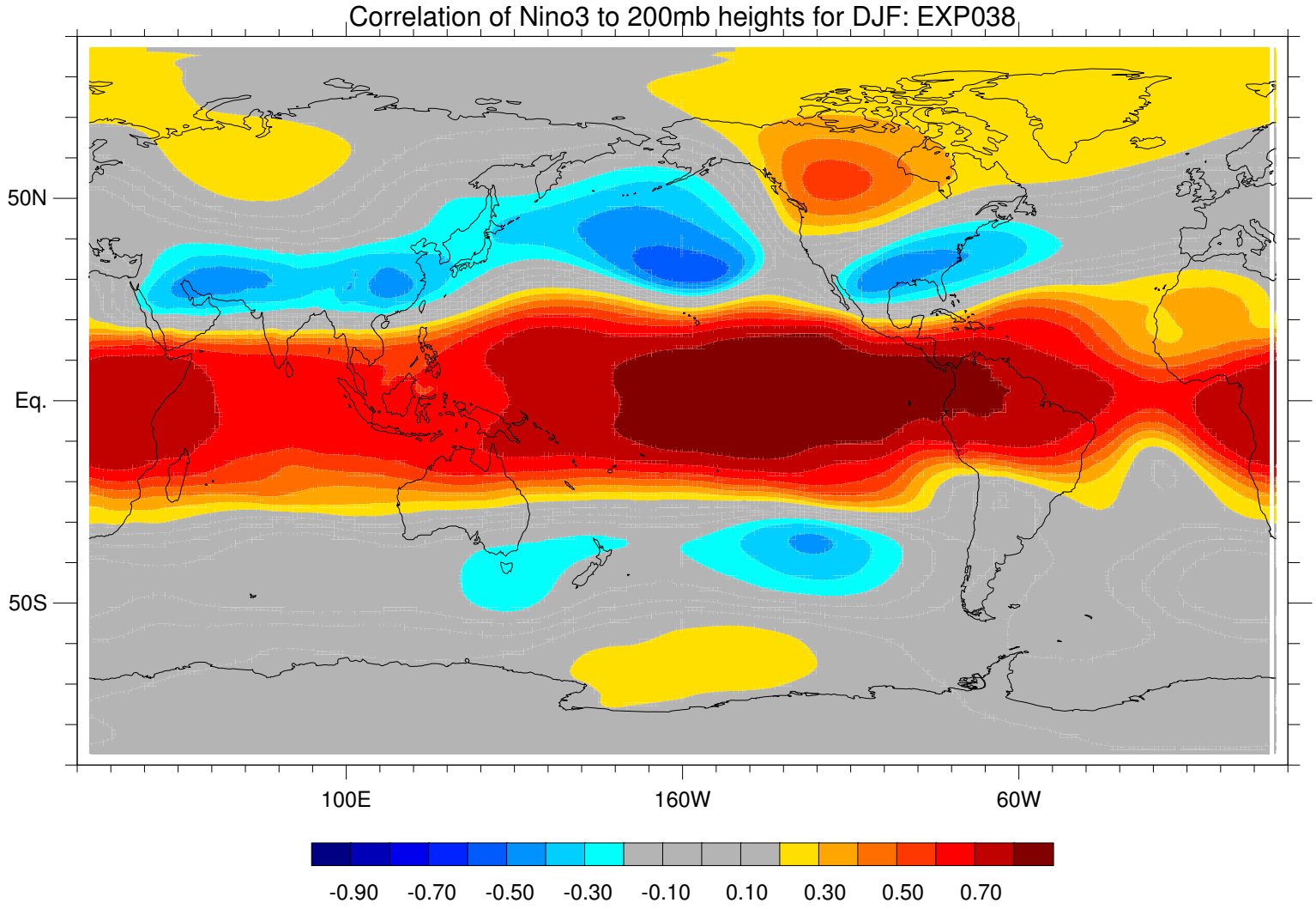

Figure 48: Pointwise correlation of NINO3 index and 200mb geopotential height.Contour interval is 0.1.

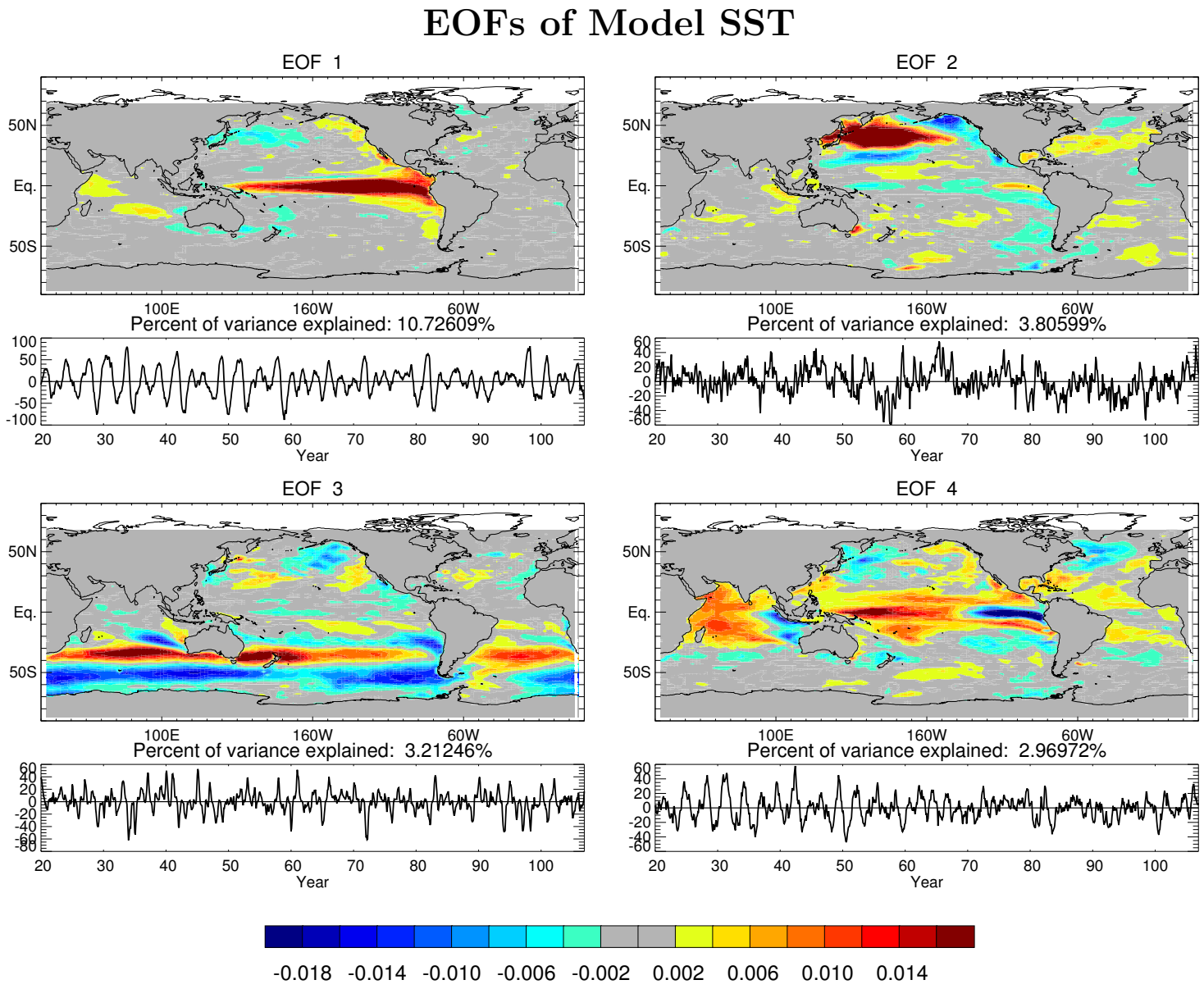

Figure 49: Empirical orthogonal function (EOF) of model sea surface temperature.Only the first four rotated EOFs are shown. The associated principal component timeseries is plotted below each EOF.

Ice Fraction

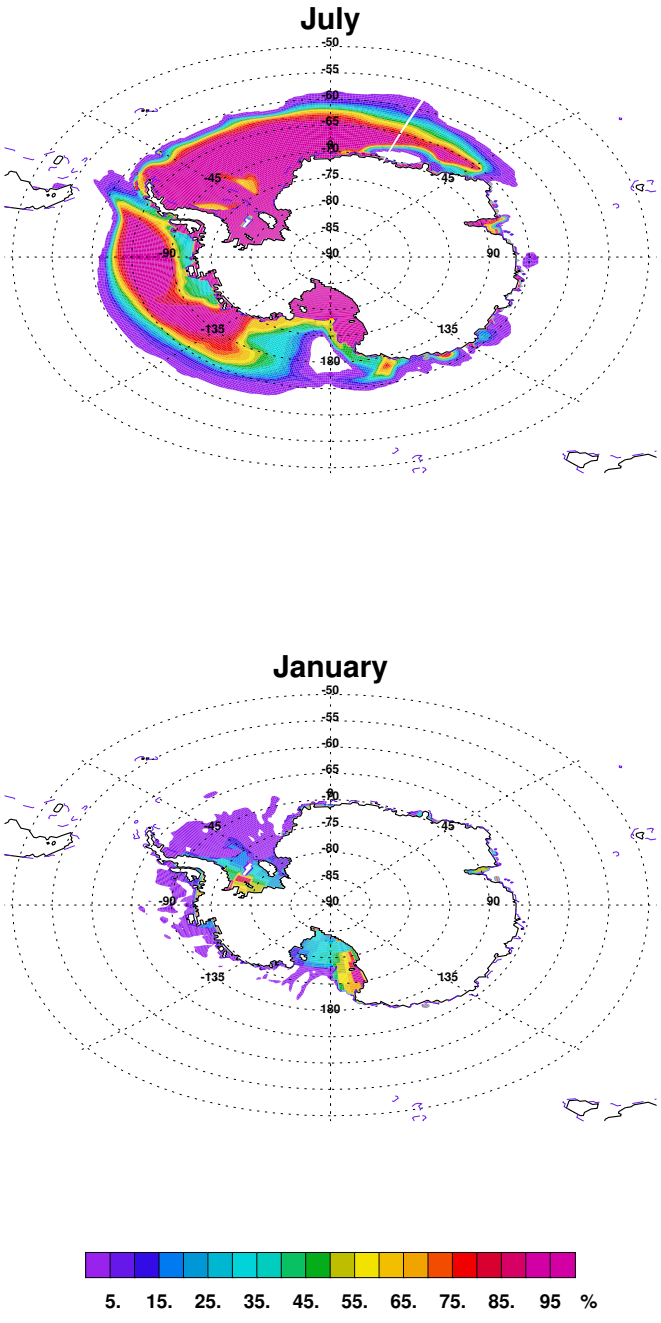

Figure 50: Ice Fraction in the Antarctic Ocean from an experiment with more realistic abyssal temperature and salinity values in the Antarctic.Top: July, Bottom: January. Contour interval is 5%.